Lappeenranta
University of Technology

Anastasia Sklyarova

HYPERFINE INTERACTIONS IN THE NEW Fe-BASED SUPERCONDUCTING STRUCTURES AND RELATED MAGNETIC PHASES

Thesis for the degree of Doctor of Science (Technology) to be presented with due permission for public examination and criticism in Auditorium 1382 at Lappeenranta University of Technology, Lappeenranta, Finland on the 13th of March, 2015, at noon.

Acta Universitatis
Lappeenrantaensis **628**

Supervisors Professor Erkki Lähderanta
School of Engineering Science
Department of Mathematics and Physics
Lappeenranta University of Technology
Finland

Docent Johan Lindén
Faculty of Natural Science
Department of Physics
Åbo Akademi University
Finland

Reviewers Professor Lennart Häggström
Department of Physics
Uppsala University
Sweden

Professor Valentin P. Filippov
Department of Applied Nuclear Physics
National Research Nuclear University "MEPHI"
Russia

Opponent Associate Professor Kim Lefmann
Niels Bohr Institute
University of Copenhagen
Denmark

ISBN 978-952-265-749-7
ISBN 978-952-265-750-3 (PDF)
ISSN-L 1456-4491
ISSN 1456-4491

Lappeenrannan teknillinen yliopisto
Yliopistopaino 2015

Abstract

Anastasia Sklyarova
HYPERFINE INTERACTIONS IN THE NEW Fe-BASED SUPERCONDUCTING STRUCTURES AND RELATED MAGNETIC PHASES
Lappeenranta, 2015
72 p.
Acta Universitatis Lappeenrantaensis 628
Diss. Lappeenranta University of Technology
ISBN 978-952-265-749-7, ISBN 978-952-265-750-3 (PDF), ISSN-L 1456-4491, ISSN 1456-4491

This thesis is devoted to the study of the hyperfine properties in iron-based superconductors and the synthesis of these compounds and related phases. During this work polycrystalline chalcogenide samples with stoichiometry 1:1 ($FeTe_{1-x}S_x$, $FeSe_{1-x}$) and pnictide samples with stoichiometry 1:2:2 ($BaFe_2(As_{1-x}P_x)_2$, $EuFe_2(As_{1-x}P_x)_2$) were synthesized by solid-state reaction methods in vacuum and in a protecting Ar atmosphere. In several cases post-annealing in oxygen atmosphere was employed. The purity and superconducting properties of the obtained samples were checked with X-ray diffraction, SQUID and resistivity measurements. For studies of the magnetic properties of the investigated samples Mössbauer spectroscopy was used. Using low-temperature measurements around T_c and various values of the source velocity the hyperfine interactions were obtained and the magnetic and structural properties in the normal and superconducting states could be studied. Mössbauer measurements together with XRD characterization were also used for the detection of impurity phases. DFT calculations were used for the theoretical study of Mössbauer parameters for pnictide-based samples $BaFe_2(As_{1-x}P_x)_2$ and $EuFe_2(As_{1-x}P_x)_2$.

Keywords: superconductivity, magnetism, Mössbauer spectroscopy

Acknowledgments

This research work was carried out at the Physics Department of Åbo Akademi University (Mössbauer research group) and at the Department of Chemistry at Aalto University with financial support from Lappeenranta University of Technology.

First of all, I want to thank my supervisors Docent Johan Lindén for help with the planning and realizing the experimental work, scientific discussions and writing of articles, and Prof. Erkki Lähderanta for the support for my work, and opportunities to present the obtained experimental results on international conferences.

I also want to thank my colleagues and co-authors Prof. Maarit Karppinen, Prof. Hisao Yamauchi, D. Sc. Eeeva-Leena Rautama, M. Sc. Otto Mustonen from Aalto University, Ph. D. Girish C. Tewari from Weizmann Institute of Science (Israel) .

I express my gratitude to Sören Fröjdö, Tommy Abrahamsson, Paul Ek (Åbo Akademi University), and Jussi Kauppila (Turku University) for help with the samples synthesis, and Alexander Lashkul (Lappeenranta University of Technology) for the help with measurements.

And I want to thank especially my reviewers Prof. Valentin P. Filippov (National Research Nuclear University MEPhI, Russia) and Prof. Lennart Häggström (Uppsala University, Sweden) for their work and invaluable comments.

Lappeenranta, January 2015

Anastasia Sklyarova

LIST OF THE ORIGINAL ARTICLES AND THE AUTHOR'S CONTRIBUTION

This thesis consists of an introductory part and five original refereed articles in scientific journals. The articles and the author's contributions in them are summarized below.

I **A. Sklyarova, J. Lindén, E.-L. Rautama, and M. Karppinen**, A ^{57}Fe Mössbauer study of $FeTe_{1-x}S_x$, *J. Magn. Magn. Matter.*, 329, 129, 2013.

II **A. Sklyarova, G. C. Tewari, J. Lindén, H. Yamauchi, and M. Karppinen**, Evidence of magnetic broadening in Mössbauer spectra of superconducting $FeTe_{0.8}S_{0.2}$, *Hyperfine Interact.*, 221, 15, 2013.

III **A. Sklyarova, G. C. Tewari, J. Lindén, E.-L. Rautama, and M. Karppinen**, Evolution of the internal magnetic field in chalcogenide superconductors $FeTe_{1-x}S_x$ for various x values, *J. Magn. Magn. Matter.*, 357, 82, 2014.

IV **A. Sklyarova, J. Lindén, G. C. Tewari, E.-L. Rautama, and M. Karppinen**, ^{57}Fe Mössbauer study of a secondary phase in $FeSe_{1-x}$ with a large quadrupole splitting, *Hyperfine Interact.*, 226, 341, 2014.

V **A. Sklyarova, G. C. Tewari, J. Lindén, O. Mustonen, E.-L. Rautama, and M. Karppinen**, Mössbauer study of hyperfine interactions in $EuFe_2(As_{1-x}P_x)_2$ and $BaFe_2(As_{1-x}P_x)_2$, *J. Magn. Magn. Matter.*, 378, 327, 2015.

The author of this thesis planned all experiments, participated in the samples synthesis, in the measurements of the superconducting properties and purity checking, carried out the Mössbauer measurements, the author analyzed all data, and is the principal author in all papers.

A	Area
A	Unspecified chemical element
a, b, c	Lattice parameters
BCS theory	Bardeen, Cooper and Schrieffer theory for superconductivity
B	Internal magnetic field
B_{eff}	Effective magnetic field
DFT	Density Functional Theory
EFG	Electric Field Gradient
IS	Isomer Shift
I	Intensity
FC	Field Cooling
RT	Room Temperature
SDW	Spin Density Wave
SQUID	Superconducting Quantum Interference Device
T	Temperature
T_c	Critical temperature
T_m	Critical temperature for magnetic transition
XRD	X-Ray Diffractometry
ZFC	Zero-Field Cooling
Γ	Line width
ΔB	Mean value of an internal magnetic field
ΔE_Q	Quadrupole-splitting parameter
δ	Isomer shift
eQV_{zz}/2	Quadrupole splitting constant
QS	Quadrupole Splitting constant
Θ_D	Debye temperature

Sample labels (Chapter 3)	target stoichiometry
S1	$FeTe_{0.8}S_{0.2}$
S2	$FeTe_{0.8}S_{0.2}$
S3	$FeTe_{0.8}S_{0.2}$
S4	$FeTe_{0.8}S_{0.2}$
S5	$FeTe_{0.8}S_{0.2}$
S6	$FeTe_{0.9}S_{0.1}$
S7	$FeTe_{0.95}S_{0.05}$

PART I: OVERVIEW OF THE THESIS

CHAPTER I

Introduction

1.1 Short review

Fe-based superconductors are a new class of superconducting materials [1, 2]. The discovery was unexpected because iron is a strong magnetic material and, according superconductivity theory, magnetism and superconductivity should be mutually exclusive. Thanks to intensive studies of iron-based superconductors, several groups of these materials are known up to this moment. Pnictide and chalcogenide superconductors are the most significant ones. Superconducting compounds belonging to these groups have rather simple crystal structures with Fe tetrahedrally coordinated to four pnictide or chalcogenide atoms. The simplest one is FeSe, which has a T_c of 8 K [3, 4]. Until the discovery of these iron-based compounds the phenomenon of high-temperature superconductivity was limited to the cuprate superconductors. Currently the highest T_c values in the Fe-pnictides exceed 50 K [5], i.e. the limit of 40 K predicted by the BCS theory. It is not known whether the mechanism behind the high-T_c superconductivity in the cuprates and the pnictides/chalcogenides has the same origin. There are many similarities between the two families of superconductors, e.g. a layered structure, possible interplay between magnetism and superconductivity etc., but also important differences, e.g. the metallic conductivity of the pnictides and an antiferromagnetic insulating ground state for the parent phases of the cuprates. Interaction between magnetism and superconductivity has been studied for the last 25 years. Due to the fact that the "parent" cuprates have an antiferromagnetic structure with a simple collinear order of magnetic moments, a theory of antiferromagnetic spin fluctuation related to the Cooper pairing and emergence of superconductivity was developed [6]. It is known that in the undoped situation "parent" compounds for the cuprates are insulators and host one fermion with 1/2 spin value for each atom. That leads to strong electron correlations and localization of the magnetic moments. Superconductivity emerges after injection of charge carriers, which suppresses the antiferromagnetic state. But some of the cuprates show coexistence of superconductivity and magnetism [7, 8]. And also in copper-based superconducting systems with added Fe this coexistence was found [9, 10]. Following these experimental works, the discovery of such type of coexistence in iron-based superconductors was not very surprising.

Fe-based superconductors are interesting and promising objects for investigation thanks to their physical properties and potential applications. The presence of Fe offers also the possibility to characterize the pnictide samples using Mössbauer spectroscopy. This method of study gives information about phase composition and hyperfine interactions that can be studied using the parameters

of the experimental spectra. Furthermore, ^{57}Fe is the most frequently used nucleus for Mössbauer spectroscopy measurements.

Important issues related to Fe-based superconductors are e. g. the increase of critical temperature, critical field and critical current values. These are accordingly the most investigated fields. Increasing these values can be achieved by adding new elements, application of special synthesis conditions (inert atmosphere, heating and cooling rates, etc.), adjusting ambient conditions (application of an external pressure), etc. [11, 12].

The nature of superconductivity and, perhaps, related to this question of coexistence of magnetism and superconductivity is the cross-cutting issue of this materials and magnetic-properties study. Iron-based superconductors that have a magnetic ordering along with the superconductivity properties are intensively studied nowadays [13–16]. Central questions are the cooperative way (coexistence or competition) of magnetism and superconductivity, and related to this, the study of new superconductors showing presence of magnetic ordering below the superconductivity transition temperature.

1.2 Objectives

The goal of this work is to study the hyperfine interactions in iron-based superconductors and related compounds at temperatures below and above superconductivity transition temperature, and to study the evolution of magnetic properties in all temperature ranges. As Mössbauer spectroscopy readily detects the appearance and vanishing of magnetic ordering, this method was a good choice for this study.

The simplest chalcogenide and pnictide superconductors were chosen as the objects for investigation. Compounds belonging to the 1:1 and 1:2:2 (stoichiometric ratio of the constituent elements) groups were synthesized and their properties were studied. The description of the synthesis process, phase purity, superconductivity and magnetic properties are presented in this thesis.

1.3 Summary of publications

This thesis is based on the following original publications:

1. A. Sklyarova, J. Lindén, E.-L. Rautama, and M. Karppinen: A ^{57}Fe Mössbauer study of $FeTe_{1-x}S_x$. *J. Magn. Magn. Matter.*, **329**, 129 (2013).

In this paper a polycrystalline sample with formula $FeTe_{1-x}S_x$ was studied. The synthesis process, phase content and physical properties studied by various methods are described. Using magnetization measurements a superconductivity transition value of $T_c \approx 10$ K was found and magnetic ordering below this temperature was observed by Mössbauer spectroscopy. Unusual behavior of the hyperfine field for one of the magnetic components was observed and conclusions about possible competition between antiferromagnetism and superconductivity were drawn.

2. A. Sklyarova, G. C. Tewari, J. Lindén, H. Yamauchi, and M. Karppinen: Evidence of magnetic broadening in Mössbauer spectra of superconducting $FeTe_{0.8}S_{0.2}$. *Hyperfine Interact.*, **221**, 15 (2013).

In this paper further studies of the properties of sulphur-substituted $FeTe_{1-x}S_x$ materials are presented. A sample with the $FeTe_{0.8}S_{0.2}$ stoichiometry, which is optimal for the emergence of bulk

superconductivity, was synthesized. An extended synthesis process with a high annealing temperature and an additional annealing step in a pure oxygen atmosphere were applied. The low-velocity Mössbauer measurements in the temperature range of 5.7 – 300 K enabled studies of the broadening, due to magnetic ordering, seen in the spectral lines above and below T_c. A new fit model of the Mössbauer spectra indicated behavior compatible with a competition between magnetism and superconductivity.

3. A. Sklyarova, G. C. Tewari, J. Lindén, E.-L. Rautama, and M. Karppinen: Evolution of the internal magnetic field in chalcogenide superconductors $FeTe_{1-x}S_x$ for various x values. *J. Magn. Magn. Matter.*, **357**, 82 (2014).

The evolution of the internal magnetic field in $FeTe_{1-x}S_x$ with different values of x is presented in this paper. Mössbauer spectra in the 6.8 –300 K temperature range were recorded using high and low Doppler velocities for the sample with x = 0.05, 0.10 and 0.20. SQUID and resistivity measurements revealed a non-superconductive state (x = 0.05), filamentary superconductivity (x = 0.10) and bulk superconductivity (x = 0.20) for the investigated samples. The evolution of the magnetic hyperfine field with various x values was studied by Mössbauer spectroscopy. The temperature dependencies of the internal field for the non-superconducting sample and the samples that show a superconducting transition were obtained. A sharp drop of the magnetic field value below the superconducting transition temperature suggests a suppression of the magnetic ordering by the emerging superconductivity.

4. A. Sklyarova, J. Lindén, G. C. Tewari, E.-L. Rautama, and M. Karppinen: ^{57}Fe Mössbauer study of a secondary phase in $FeSe_{1-x}$ with a large quadrupole splitting. *Hyperfine Interact.*, **226**, 341 (2014).

The hyperfine interactions in samples belonging to the Fe-Se system are presented in this work. Several samples with various concentrations of selenium were synthesized and investigated and the presence of an additional phase with a large quadrupole splitting was observed. The special synthesis conditions needed for obtaining this secondary phase are described. The objective was to find synthesis conditions increasing the concentration of the secondary Fe-Se phase which has a large quadrupole splitting of ∼1.7 mm/s. At $T_m \approx 104\ K$ this secondary phase undergoes a magnetic ordering. It was found that in the investigated samples the secondary-phase Fe has valence 2+ and resides is a high-spin state while the main phase Fe atoms are in a divalent low-spin state.

5. A. Sklyarova, G. C. Tewari, J. Lindén, O. Mustonen, E.-L. Rautama, and M. Karppinen: Mössbauer study of hyperfine interactions in $EuFe_2(As_{1-x}P_x)_2$ and $BaFe_2(As_{1-x}P_x)_2$. *Submitted to JMMM*.

In this paper the hyperfine properties of pnictide superconductors with the $BaFe_2(As_{0.68}P_{0.32})_2$ and $EuFe_2(As_{0.8}P_{0.2})_2$ compositions were studied by ^{57}Fe Mössbauer spectroscopy. A superconducting transition at 30 K was detected and coexistence of magnetism and superconductivity at low temperatures was observed. The Mössbauer spectra show two different iron atoms surroundings, which are attributed to unsubstituted AFe_2As_2 and substituted $AFe_2(As_{1-x}P_x)_2$, with at least one phosphorus atoms in the tetragonal iron environment, (A = Ba or Eu). DFT calculations were used for theoretical evaluation of the quadrupole splitting for different iron surroundings.

CHAPTER II

Materials and Methods

2.1 Synthesis methods and Materials

During this work polycrystalline samples were synthesized and investigated. The samples were grown using solid-state reaction schemes. There are several reasons for choosing this method of preparation. Sample synthesis methods are important because they influence on obtained crystal structure and its stability, presence of impurity phase, appearance of superconductivity, superconductivity transition temperature etc. Obtaining polycrystalline materials (grain size $\sim$1 – 10 μm) or single crystals (grain size from $\sim$0.1 mm to 1 cm) is also dependent on the synthesis method and the synthesis conditions [17]. Even in successfully synthesized samples small defects and traces of impurity phases can be observed, the presence of which influence on the physical properties of these samples [18]. From the superconductivity-properties point of view, the combination of crystal structure and chemical composition influences on the values of critical temperature, critical fields and critical current of superconducting materials.

For the synthesis process of iron-based superconductors safety issues are also important: several of the elements are toxic or sensitive to reactions with air. So, special conditions during the synthesis process should be applied such as using an inert gas atmosphere during the powder mixing and grinding processes.

Three common synthesis methods of iron-based superconductors are used: flux-growth from a solution, Bridgman method of crystal growth and solid-state reactions [19–23]. For obtaining polycrystalline samples the solid-state reaction is simpler and does not require special laboratory equipment. Hence, it was chosen for this work.

For the preparation of chalcogenide and pnictide samples commercial iron powder and pieces, tellur, selenium, and sulphur powders, barium, europium, and arsenic pieces, and phosphorus powder were used. A list of elements, suppliers and chemical purities are presented in Table 2.1.

2.2 Analytical methods

The study of synthesized sample purity and characterization of the powders were carried out by the following analytical methods: Cu $K\alpha 1$ X-ray powder diffractometry, and ^{57}Fe and ^{151}Eu Mössbauer spectroscopy were used for phase composition study; SQUID measurements and resistivity

Table 2.1: Description of chemical elements

Chemical element	Formula	Supplier	Purity, %
Iron (pieces)	Fe	Bureau of Analysed Samples, Ltd	99.95
Iron (powder)	Fe	unspecified	99.99
Tellur	Te	ALDRICH Chemistry	99.8
Tellur	Te	unspecified	99.999
Sulphur	S	MERCK	DAB 6
Sulphur	S	unspecified	99.99
Barium	Ba	SIGMA-ALDRICH	99.9
Europium	Eu	unspecified	99.9
Arsenic	As	ALDRICH	99.999
Phosphorus	P	MERCK	$\geq$97

measurements gave information about superconducting properties; Mössbauer spectroscopy, as the main investigation method in this work, allowed us to obtain information on the hyperfine interactions of the synthesized samples. A short description of the methods used are presented below.

2.2.1 X-ray powder diffractometry

The purity and phase composition of produced polycrystalline samples were checked in this work by X-ray powder diffraction (PanAnalytical X'Pert Pro MPD diffractometer). The measurements were made in the θ - 2θ geometry using Cu $K\alpha 1$ (λ = 154.051 pm) radiation. Powder diffraction patterns were registered at room temperature in the beam-angle range of 2θ = 5 – 220°.

The experimental equipment allows measurement of diffraction patterns from 10 mg (lower limit) of sample, which is important when only small quantities of investigated materials are available.

For phase identification the FullProf software [24] and PDF4 database were used. The crystal-structure refinement was made using the Rietveld method and a March-Dollase function was included due to the presence of preferred orientation of crystallites.

2.2.2 SQUID measurements

The temperature dependencies of magnetic susceptibilities were obtained using a commercial magnetometer (Quantum Design MPMS-XL). The magnetometer operates within the temperature range of 1.7 – 400 K and the largest possible value of external magnetic field is 50 kOe. The maximal sensitivity of the magnetometer is in the range of 10^{-9} emu. The smallest experimentally used sample mass was $\sim$24 mg.

For carrying out of measurements the samples were placed into a gelatine capsule or wrapped in a weighing paper and placed inside a straw, and then fixed in the holder. The external magnetic field (in field-cooling measurements) was 10 – 20 Oe.

The obtained experimental results (output data) were fitted using the ORIGIN software.

2.2.3 Resistivity measurements

Resistivity measurements of the synthesized samples were carried out using a home-built four-probe setup (Aalto University, Chemical Department). The samples plates ($\sim$3$\times$4 mm) were placed and fixed at the holder surface. Copper conducting wires were fixed to the sample by silver paste. The resistivity measurements were made in the temperature range of 4 – 300 K. Starting from room temperature the sample temperature was changed by sinking the holder slowly by hand into a liquid helium dewar. The visualization of obtained results was made during the measurement process on the screen. The output data were fitted by the ORIGIN program.

2.2.4 Seebeck measurements

Seebeck measurements of the investigated samples were made using a home-built setup (Aalto University, Chemical Department). Under microscope the sample plate was attached between cooper plates using silver paste. Gold wires were used as conducting parts between sample and the Cu plate. Seebeck-coefficient measurements were made in the temperature range of 4 – 300 K gradually the lowering temperature from room temperature to 4 K by slowly sinking the holder with

the sample into a dewar with liquid He. The SRLWin software was used for the data collection. The visualization of obtained results was made during the measurement process on the screen. The output data were fitted by the ORIGIN program.

2.2.5 Mössbauer spectroscopy

Mössbauer spectroscopy was used for the study of the hyperfine interactions in our samples and for the refinement of the phase compositions together with X-ray powder diffraction. The Mösbauer measurements were done using the equipment of the Mössbauer research group at Åbo Akademi University, with a Cyclotron Company ^{57}Co:Rh gamma source in transmission geometry and an LND inc. proportional counter (model 45431). An Engelhard NaI scintillator (model 2007P), for detecting the γ-quanta of a ^{151}Sm:Sm_2O_3 source, was used.

For the absorber preparation about 50 mg of sample powder was put in crater of 2.1 cm diameter pressed into an aluminium foil, and thoroughly mixed with a two-component resin (LOCTITE Power Epoxy Universal). The distribution of the powder in the glue was as homogeneous as possible, and presence of air bubbles in the absorber were avoided. The solidified absorber was covered by a protective plastic film.

The Mössbauer measurements were carried out in the temperature range of 4.8 –315 K. The low-temperature measurements were made using an Oxford CF506 continuous-flow cryostat with liquid He as a coolant below 77 K and liquid N_2 at and above 77 K. The temperature stability was controlled by an Oxford Intelligent Controller (ITC 4). The obtained spectra were visualized on a computer screen using the MCDWIN program which was also responsible for the gathering of data. The obtained experimental data were fitted using home-made software.

CHAPTER III

Iron-chalcogenide compounds $FeTe_{1-x}S_x$: synthesis and study

3.1 Motivation

The substituted 1:1 material $FeTe_{1-x}S_x$ belongs to the chalcogenide superconductor group. The stability of the prepared material and the simplicity of the structure make this material attractive for investigations. Although the critical temperature value T_c∼8 K is not high [25–28] this compound has a number of interesting properties which justify further studies. The parent FeTe compound of the investigated $FeTe_{1-x}S_x$ material has an $anti-PbO$ type layered crystal structure with a tetragonal symmetry (space group $P4/nmmm$) [29], Fig. 3.1. The simple structure allows for inclusion

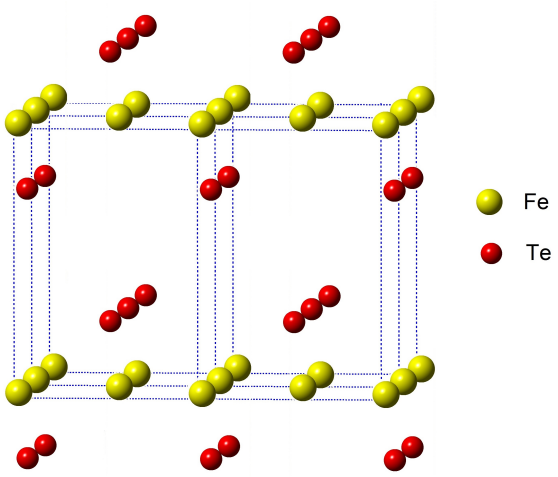

Figure 3.1: FeTe crystal structure.

of ions between the Fe_2Te_2 layers [30] and in this way change the properties of the material. The crystal structure of the chalcogenide superconductors is dependent on the chemical elements in the superconducting compound, and on the method for the synthesizing superconductor, and on the synthesis conditions like temperature, pressure etc. [31]. It is important to obtain samples with a

stable structure. The parent FeTe is a stable compound, and substituted compounds based on it, can be easily produced by solid-state reaction methods.

In the parent FeTe phase structural and magnetic transitions occur at $\sim$70 K. Below the transition temperature this compound shows antiferromagnetic ordering and the wave vector of the antiferromagnetic fluctuations is not favorable for superconductivity, like it is for FeSe, where authors connected these fluctuations with the appearing superconductivity properties [32–40]. The usual method for inducing superconductivity – an applied hydrostatic pressure – does not work, excluding the case of FeTe thin films, in which a tensile stress induces a superconductivity transition at $\sim$13 K [41]. This superconductivity in FeTe thin films under tensile stress is accompanied by a softening of the first-order magnetic and structural phase transition. Under high pressure pure bulk FeTe remains antiferromagnetic even at the lowest temperatures [42, 43].

Superconductivity in the parent FeTe can be achieved only through a substitution process [28, 44–46]. A large number of research papers devoted to the most usual chalcogenide $FeTe_{1-x}Se_x$ phase exists [47–49]. The popularity of the $FeTe_{1-x}Se_x$ material is due to an easy synthesis process of this compound. In the case of the sulphur-substituted compound $FeTe_{1-x}S_x$ the synthesis process is more difficult because the large difference in ionic radii of Te and S. The less known properties of $FeTe_{1-x}S_x$ make this material attractive for investigations.

3.2 Synthesis procedures of sulphur-substituted samples

Polycrystalline sample with the chemical formula of $FeTe_{1-x}S_x$ were synthesized by solid-state reaction methods using various temperature regimes and special synthesis steps as immersing into ethanol and oxygen-annealing. A search for optimal synthesis conditions for achieving superconducting properties in $FeTe_{1-x}S_x$ was made.

Five polycrystalline samples were synthesized using two-steps and three-steps reactions (with and without ethanol immersing and powder pelletization) and three-steps reaction with powder pelletization and O_2-annealing; these obtained samples were denoted S1, S2, S3, S4 and S5, respectively. For all samples S1 – S5 the target stoichiometry was $FeTe_{0.8}S_{0.2}$ because the $FeTe_{1-x}S_x$ compound with this stoichiometry shows the best superconductivity properties [25].

The following synthesis program for sample S1 was used: A TeS precursor was synthesized. Stoichiometric quantities of Te (ALDRICH, 99.8%) and S (MERK, DAB6) powders were mixed, sealed inside an evacuated quartz tube and annealed at 400°C for 12 h. The obtained TeS precursor was reground in an agate mortar, mixed with Fe (99.5%) and Te powders for achieving the $FeTe_{0.8}S_{0.2}$ stoichiometry, sealed into an evacuated quartz tube and annealed again at 600°C for 12 h. A furnace cooling from 600°C to room temperature was made by turning off the furnace. The natural cooling rate of the furnace is shown in Fig. 3.2.

For sample S2 the same synthesis program was used, but after two synthesis steps the obtained material was reground, pressed into a pellet and a third annealing at 600°C for 12 h was made. And sample S4 was produced using the same scheme but a third annealing step was made at 200°C for 2 h in an oxygen atmosphere inside a quartz ampule with the sample. Immersing in ethanol at 100°C for 15 h was used as a third synthesis step for sample S3 although the first two steps were the same as for samples S1 and S2.

Different conditions for the synthesis of sample S5 were used. Synthesis of sample S5 was made at higher temperatures and the reaction time was extended. The appropriate Fe, Te and S powder

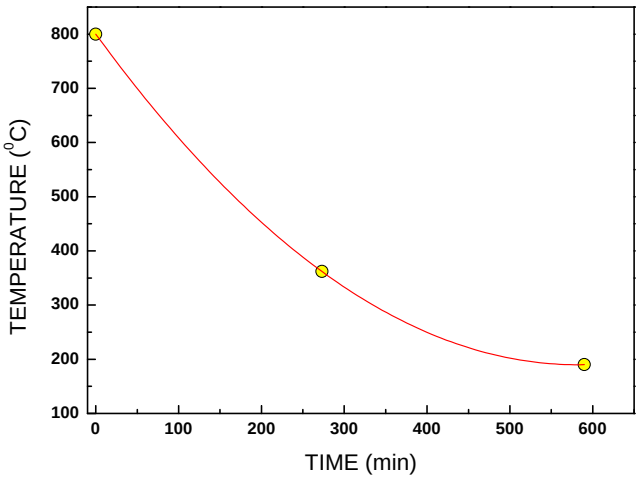

Figure 3.2: Natural cooling rate of turned off furnace.

mixture was pelletized, sealed in an evacuated quartz tube, slowly heated up to 1050°C and annealed at this temperature for 30 h. The obtained sample was reground, pressed, sealed in a quartz tube, and annealed again in vacuum at 800°C for 20 h and, finally, the obtained sample was annealed at 200°C for 12 h in an oxygen atmosphere inside an ampule.

The synthesis programs used for all samples S1 – S5 are given in Table 3.1.

A preliminary quick analysis of the phase content in the obtained samples was done using Mössbauer spectroscopy. Due to the chemical composition of the synthesized samples the most likely impurities should contain iron and, thus, Mössbauer spectroscopy would give information about the phase contents and their percentage in the samples. The phase amount is directly proportional to the intensity of the subspectrum, assuming the recoil free-fraction is the same. Using the experimental data the relative intensities of the subspectra from different phases were found.

Mössbauer spectra were recorded at 300 K using a Doppler velocity of $\sim$8 mm/s that allows for detection of probable magnetic iron-oxide impurities.

The recorded 300 K Mössbauer spectra of samples S1, S2 and S5 are shown in Fig. 3.3.

Obtained spectra were fitted using one paramagnetic doublet and one magnetic sextet. The hyperfine field for magnetic components, quadrupole splitting, relative intensity and isomer shift relative to α-Fe were used as fit parameters. The obtained Mössbauer parameters are given in Table 3.2 (sample S1, S3 and S4), Table 3.3 (sample S2) and Table 3.4 (sample S5).The paramagnetic doublet and magnetic sextet were assigned to the main $FeTe_{1-x}S_x$ phase and to the impurity FeS phase, respectively. The difference in the FeS isomer shift values is, probably, due to the some variation in this phase stoichiometry ($FeS_{1\pm x}$).

The room temperature spectrum of sample S1 shows the presence of an impurity phase that occupies 29% of the main spectral area, Fig. 3.3 (upper picture). According to the synthesis theory [50, 51], the solid-state reaction rate depends on the ion diffusion through the reaction product layer, which forms on the phase boundary. Sample grinding, mixing and pressing improve homogeneity of the mixture, reduce the grain size, improve the contact between particles and reduce the voids. An additional annealing step at low temperature (600°C) promotes impurity reduction from 29% to 18%

Table 3.1: The synthesis program of the $FeTe_{0.8}S_{0.2}$ materials

Sample label	Reaction	Temperature program
S1	1^{st} reaction (TeS)	RT-3.3h-400 °C/12h-RT(natural cooling)
	2^{nd} reaction (TeS+Fe)	RT-3h-600 °C/12h-RT(natural cooling)
S2	1^{st} reaction (TeS)	RT-3.3h-400 °C/12h-RT(natural cooling)
	2^{nd} reaction (TeS+Fe)	RT-3h-600 °C/12h-RT(natural cooling)
	3^{rd} reaction (pellet)	RT-3h-600 °C/12h-RT(natural cooling)
S3	1^{st} reaction (TeS)	RT-3.3h-400 °C/12h-RT(natural cooling)
	2^{nd} reaction (TeS+Fe)	RT-3h-600 °C/12h-RT(natural cooling)
	3^{rd} step (ethanol exposure)	100 °C/15h-RT(natural cooling)
S4	1^{st} reaction (TeS)	RT-3.3h-400 °C/12h-RT(natural cooling)
	2^{nd} reaction (TeS+Fe)	RT-3h-600 °C/12h-RT(natural cooling)
	3^{rd} reaction (pellet, O_2)	RT-1h-200 °C/2h-RT(natural cooling)
S5	1^{st} reaction ($FeTe_{0.8}S_{0.2}$) (pellet)	RT-20h-1050 °C/30h-5h-RT
	2^{nd} reaction (pellet)	RT-800 °C/20h-RT
	3^{rd} reaction (pellet, O_2)	RT-200 °C/12h-RT

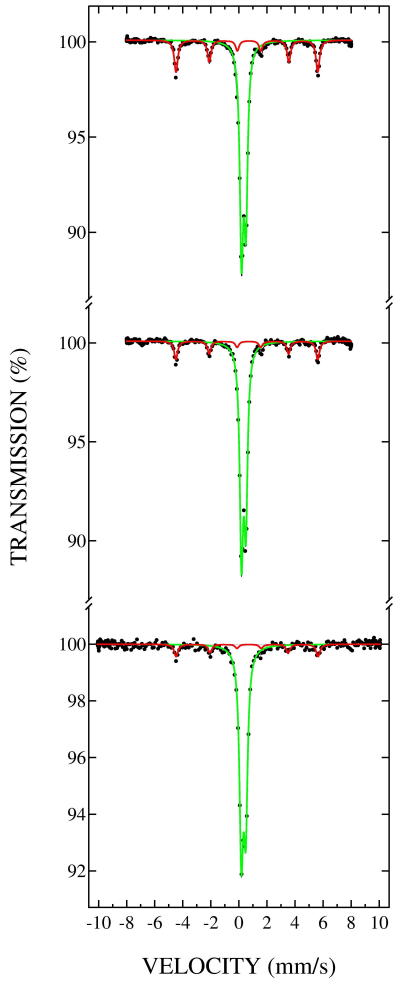

Figure 3.3: RT Mössbauer spectra of samples S1 (upper), S2 (middle), and S5 (lower) with the formal stoichiometry of $FeTe_{0.8}S_{0.2}$. Components due to a paramagnetic doublet (green), and the FeS (red) impurity are indicated.

Table 3.2: RT Mössbauer parameters of samples S1, S3 and S4 with the formal stoichiometry of $FeTe_{0.8}S_{0.2}$

Sample	Component	Assignment	IS, mm/s	eQV_{zz}, mm/s	B, T
S1	Doublet	$FeTe_{1-x}S_x$	0.487(9)	-0.62(3)	–
	Sextet	FeS	0.890(1)	-1.46(8)	31.5(9)
S3	Doublet	$FeTe_{1-x}S_x$	0.455(5)	-0.62(5)	–
	Sextet	FeS	0.791(6)	-1.49(7)	32.6(6)
S4	Doublet	$FeTe_{1-x}S_x$	0.450(3)	-0.70(2)	–
	Sextet	FeS	0.902(2)	-1.46(9)	31.7(4)

(according Mössbauer data) for sample S2, Fig. 3.3 (middle picture) but the remaining impurity portion is still large. It was experimentally found that, for our samples, increasing the synthesis temperature and reaction time with additional annealing steps reduce the impurity content to 1% (sample S5 [**Publication 2**, **Publication 3**], Fig. 3.3 (lower picture).

The superconductivity properties, that our obtained samples have, depend on the used synthesis program. The evolution of superconductivity in samples S1 – S5 was checked by SQUID measurements of the magnetic susceptibility, Fig. 3.4.

SQUID data for the samples S1 – S4 revealed only filamentary superconductivity in these samples. For the first synthesized sample S1, magnetic susceptibility temperature behavior obtained in ZFC regime indicates an onset superconductivity at 8 – 10 K, Fig. 3.4 (a). Sample pelletization and one additional annealing at 600°C for 12 h weakly influence on the susceptibility shape, Fig. 3.4 (b). Although the nature of the following is not understood yet [52], additional procedures of oxygen annealing and ethanol exposure slightly improve the superconducting transition: the down turn of the susceptibility curves becomes more clearly defined and the values of the magnetic susceptibility reach negative values, Fig. 3.4 (c). There are two possibilities for the influence of oxygen atoms: some S atoms are substituted by oxygen, or oxygen atoms occupy interstitial positions. The magnetic-susceptibility behavior of sample S5 shows a clear transition to the superconductivity state at T_c = 9 K, Fig. 3.4 (d). The influence of the oxygen annealing on the superconductivity transition is presented in Fig. 3.5. The oxygen-annealed sample S5 shows a more clear and sharp superconductivity transition with zero-resistivity below T_c.

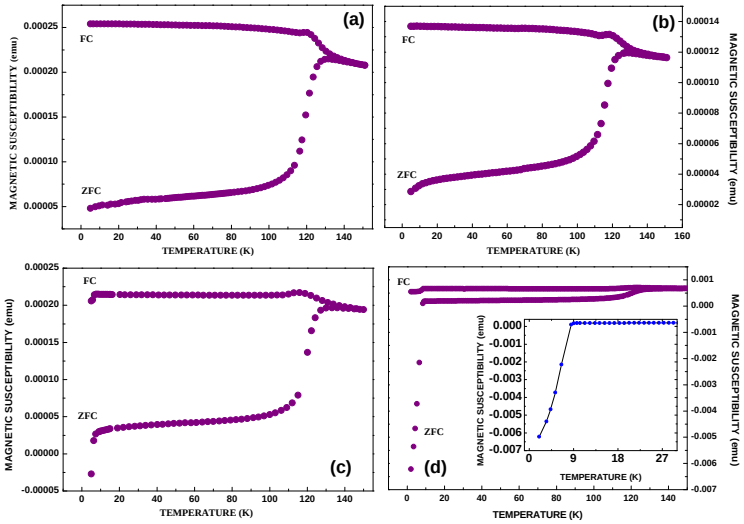

Figure 3.4: Magnetic susceptibility vs. temperature of samples S1 (a), S2(b), S3 (c) and S5 (d) with formal stoichiometry of $FeTe_{0.8}S_{0.2}$, recorded in zero-field-cooling (ZFC) and field-cooling (FC, 20 Oe) regimes.

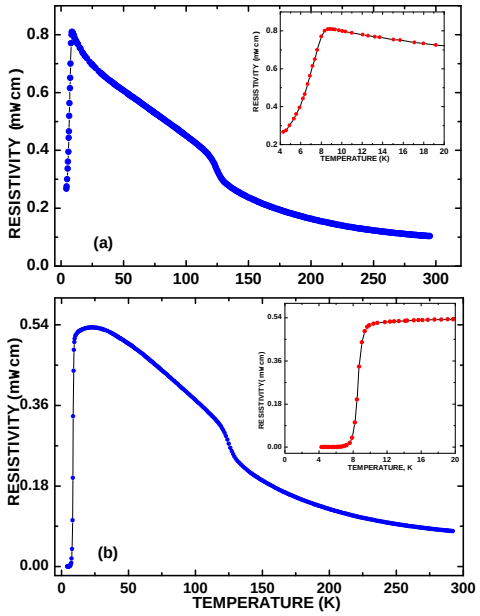

Figure 3.5: Resistivity vs. temperature of sample $FeTe_{0.8}S_{0.2}$ (S5) before O_2-annealing (a) and after O_2-annealing (b). Insets show the transition region in more detail.

3.3 Characterization of $FeTe_{1-x}S_x$ compounds

The polycrystalline $FeTe_{1-x}S_x$ sample (marked S2) with the nominal composition x = 0.2 was synthesized using the solid-state reaction method described in Section 3.2 and Table 3.2. The purity of the obtained sample was checked using two methods: X-ray powder diffractometry (PanAnalytical X'Pert Pro MPD diffractometer) and Mössbauer spectroscopy. Superconductivity properties were investigated by SQUID measurements (Quantum Design, MPMS-XL) in zero-field cooling and field-cooling at a 10-Oe external magnetic field, and magnetic properties of the sample were studied by ^{57}Fe Mössbauer spectroscopy.

Mössbauer spectra were recorded in the temperature range of 5.4 – 300 K with a 15 K temperature step in transmission geometry. The maximum Doppler velocity value was 8.00 mm/s, which is enough for detection of magnetic impurity phases. A three component model was used for the experimental data fit: two magnetic (C_1 and C_2) and one paramagnetic (C_3) component. The usual Mössbauer parameters of a magnetic hyperfine field for magnetic components, quadrupole splitting, relative intensity and isomer shift relative to α-Fe were used as fit parameters. The full hamiltonian was used in the fit program. The asymmetry parameter η was fixed at zero due to the tetragonal crystal symmetry of the phase and the local tetrahedral symmetry of Fe atoms surrounding suggesting that $V_{xx} = V_{yy}$. The angle between V_{zz} and B_{eff} was also fixed to zero. Phase composition in the obtained sample was checked by XRD and, 2% of FeS along with 5% of paramagnetic $FeTe_2$ was detected, Fig. 3.6. The FeS impurity quantities obtained by XRD (2%) and by Mössbauer spectroscopy (18%) differ possibly due to poor or uneven crystallinity for FeS, although some of the FeS lines seem to be rather sharp. The thickness effect for Mössbauer absorber can also influence the obtained FeS content: the absorption area of the main paramagnetic doublet saturates faster than the area of the magnetic sextet for the FeS impurity, which is more spread out. Hence, in reality the portion of FeS could be a few %-units smaller than the obtained 18%. Nevertheless, a certain discrepancy remains.

The XRD pattern shows presence of grain orientation along to the $00l$ direction. One of the reasons for this effect to arise is powder sedimentation during the sample preparation for the XRD measurement, another reason is the internal texture of the crystallite structure. This preferred orientation was taken into account in the fitting by the March-Dollase function [53]. The preferred orientation factor:

$$T_{hkl} = \frac{1}{N}\sum_{i=1}^{N}\left(G^2 cos^2\phi^i_{hkl} + \frac{1}{G}sin^2\phi^i_{hkl}\right)^{-3/2}, \tag{3.1}$$

where N is the number of symmetry-equivalent reflections, G is a numerical refinable parameter, $cos\phi_{hkl} = \frac{\mathbf{d_{hkl}}\cdot\mathbf{d^T}}{d_{hkl}d^T}$, $\mathbf{d_{hkl}}$ is an inter-planar spacing between crystallographic planes belonging to the same family (h,k,l), and $\mathbf{d^T}$ the texture axis direction.

In accordance with the literature, sample S2 belongs to the tetragonal P4/nmm space group. The obtained XRD data, which was fitted using the commercial FullProf program package [24], gives the values 2% and 5% for the FeS and $FeTe_2$ impurity contents, respectively, and 93% for the main $FeTe_{1-x}S_x$ phase. The c lattice parameter of the main phase was found to be 6.275 Å. In earlier studies of $FeTe_{1-x}S_x$ a relation between the c lattice parameter value and the sulphur concentration was observed: the c value is decreasing with increasing sulphur concentration x up to x = 0.25 and, at $x > 0.25$ the c parameter saturates [54]. Using this relation the content of sulfur in our sample was found to be 3.9%. This estimated sulfur concentration indicates that the synthesis conditions

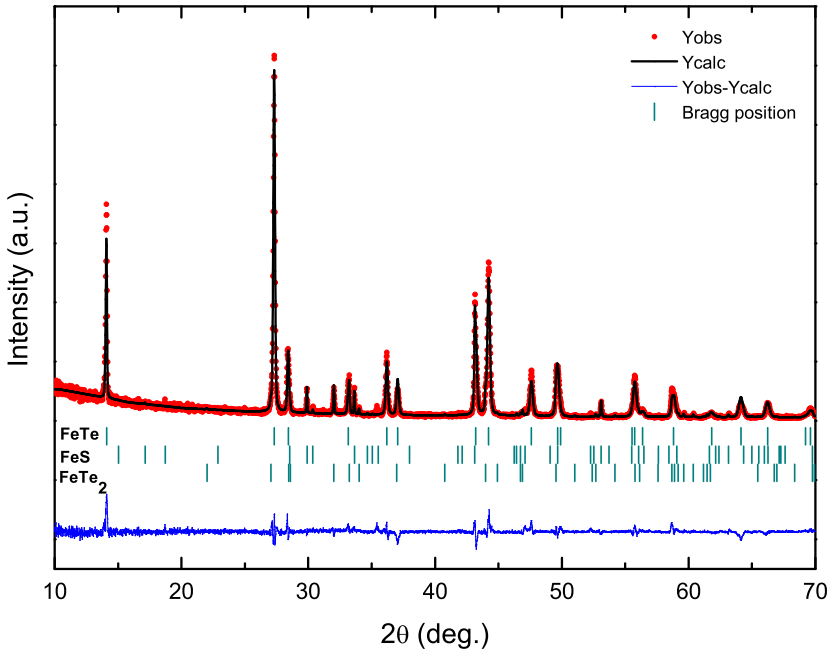

Figure 3.6: X-ray powder diffraction pattern and Rietveld refinement profile of $FeTe_{1-x}S_x$ (S2). Minority phases are indicated below the main phase (FeTe on the pattern). Tetragonal P4/nmm space group was used in the refinement for the main phase. This picture was taken from **Publication 1**.

(annealing duration and temperature) were not optimal for the preparation of the sample. The same result was obtained by other authors that used flux-growing method for $FeTe_{1-x}S_x$ material preparation, where a nominal $x = 0.2$ was coincided with an $x = 0.11$ value obtained from electron-probe microanalysis measurements [54]. In our case we also had a FeS impurity so the concentration of S would be smallish.

SQUID measurements, Fig. 3.4 (b), show only the beginning of a down turn of the ZFC magnetization curve and negative values are not reached. This suggests the presence of mere filamentary-type superconductivity in our sample, i. e. the case when in a non-superconducting sample superconducting "paths" have formed. Then only a weak and broad susceptibility signal is observed. This filamentary-type superconductivity in our sample agrees with the experimentally observed sulphur concentration. The onset of T_c was found to be 10 K, where the ZFC curve of the magnetic moment begins turn towards negative values.

The magnetic properties were investigated by ^{57}Fe Mössbauer spectroscopy. As mentioned earlier, the paramagnetic state in the parent FeTe compound undergoes an antiferromagnetic ordering at temperatures below $\sim$70 K and a Mössbauer study of this material shows a well-resolved sextet below the magnetic transition temperature [29]. Upon substituting a part of Te by another chalcogenide element this ordering is suppressed [25, 28, 55]. The obtained Mössbauer spectra of our $FeTe_{1-x}S_x$ sample show a partial magnetic ordering, observed as a broadening of the main para-

magnetic doublet, Fig. 3.7. For obtaining and analyzing of the hyperfine parameters a fit model, consisting of two subspectra at high temperatures and three subspectra at temperatures below 77 K, was used. At room temperature two components suffice to describe the Mössbauer spectrum: an intensive paramagnetic doublet (C_3) associated with the main paramagnetic $FeTe_{1-x}S_x$ phase and a sextet (C_1) that can be attributed to the magnetic FeS impurity. In contrast to the XRD results, Mössbauer parameters values of $FeTe_2$ are close to the parameters values of the main phase, and it may be a reason that this paramagnetic impurity is not visible in the spectra: the paramagnetic doublet from the $FeTe_2$ is masked by the more intensive paramagnetic doublet from the main $FeTe_{1-x}S_x$ phase.

The Mössbauer spectra have identical shapes at all temperatures down to ∼77 K. The broadening of the main component due to magnetic ordering appears at temperatures below ∼77 K and, in accordance with a low-temperature Mössbauer study of the parent compound, an unresolved magnetic sextet (C_2) was entered in to the fit model [56]. A reasonable explanation of the nature of this unresolved sextet is the antiferromagnetic "sea" surrounding of the paramagnetic "islands" that are distributed through the sample volume [**Publication 1**]. This "sea" is characterized by lower concentration of S close to Fe, and opposite in "islands" Fe atoms have more neighboring S atoms. The concentration of S atom neighbors varies continuosly and, therefore, areas poor in S atoms order magnetically at higher temperatures, than areas rich in S atoms. The size of these paramagnetic "islands" decrease with decreasing temperature while the antiferromagnetically ordered part of the samples grows. This process continues with decreasing temperature down to T_c and then an opposite trend sets in. The magnetic component C_2 remains visible in the spectra down to the lowest temperature of 5.4 K even when the superconductivity state below 10 K appears. These two, magnetically ordered (C_2) and superconducting (C_3), phases are intertwined. Parameter values of the fitted spectra are presented in Table 3.3.

Table 3.3: Mössbauer parameters of sample $FeTe_{1-x}S_x$ (S2)

	Component					
		Component C_3		Component C_2		
T, K	Γ, mm/s	IS, mm/s	eQV_{zz}, mm/s	IS, mm/s	QS, mm/s	B, T
300 K	0.334(2)	0.481(1)	-0.62(6)	–	–	–
125 K	0.321(9)	0.553(1)	-0.74(4)	–	–	–
77 K	0.310(6)	0.571(3)	-0.73(6)	–	–	–
66 K	0.302(4)	0.572(4)	-0.72(1)	0.53(1)	0.23(5)	7.7(5)
5.4 K	0.277(1)	0.570(1)	-0.96(5)	0.54(3)	0.25(8)	9.0(8)

A competition between magnetism and superconductivity was found by studying the Mössbauer parameters of C_2 and C_3 components. The behavior of two parameters: internal magnetic field value of the C_2 spectral component and the C_2/C_3 intensity ratio, were studied in the temperature range

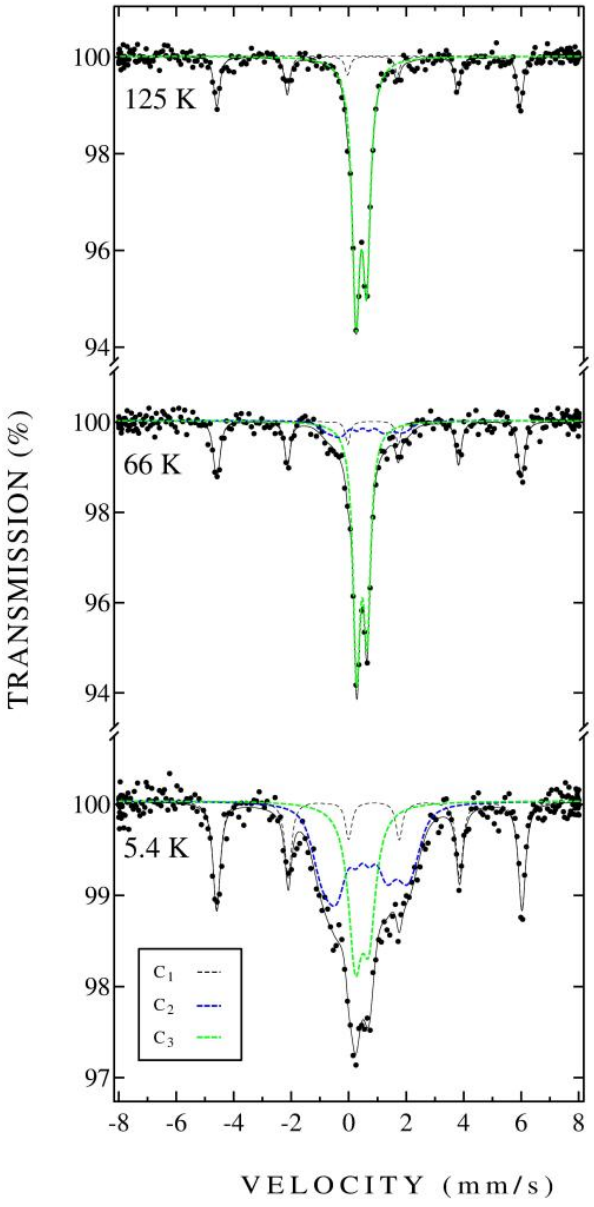

Figure 3.7: ^{57}Fe Mössbauer spectra of $FeTe_{0.8}S_{0.2}$ (sample S2) recorded at 5.4 K, 66 K and 125 K. The two main components: paramagnetic doublet (C3, dashed green line) and magnetic sextet (C2, dashed blue line), and the FeS impurity (C1, dashed black line) are indicated. This picture was taken from **Publication 1.**

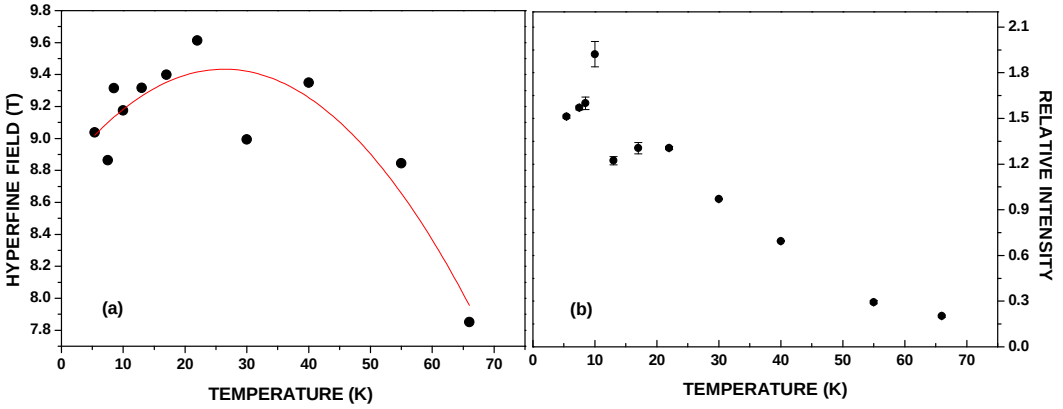

Figure 3.8: Internal field vs. temperature for component C_2 (a) and intensity ratio between the magnetic component C_2 and the paramagnetic doublet C_3 vs. temperature (b) for the sample S2 ($FeTe_{0.8}S_{0.2}$). The line is a guide for the eye. This figures were taken from **Publication 1.**

of 77 – 5.4 K, Fig. 3.8. The internal magnetic field value decreases at low temperatures (Fig. 3.8 (a)) and the peak-like kink in the intensity ratio at 10 K (Fig. 3.8 (b)), indicates the presence of a competition between superconductivity and low-temperature magnetic ordering in our sample.

Further studies of the relation between low-temperature magnetism and superconductivity has been conducted on $FeTe_{1-x}S_x$ samples with x = 0.20, 0.10 and 0.05 (S5, S6 and S7). Investigated materials were synthesized by solid-state reaction, as described earlier for sample S5 (see Section 3.2 and Table 3.1). All samples were subjected to oxygen annealing as a final synthesis step. The phase purity of the produced polycrystalline samples was checked by XRD and the obtained patterns are shown in Fig. 3.9. According to the XRD results the substitution of tellur by sulphur was successful: the XRD pattern for the sample with x = 0.20 shows only a 1% presence of the FeS impurity, and for the two other samples the XRD patterns do not show any traces of FeS. The sulphur solubility limit may be a reason for the presence of FeS in the compound with the largest S concentration. The behavior of the c lattice parameter, which decreases with increasing x, also suggests a success of the substitution processes. The presence of two paramagnetic $FeTe_2$ and $Fe_{0.67}Te$ impurities and their percentage in the investigated samples are also indicated on the XRD patterns. Observation of trace of impurities with concentrations below 2%, i. e. close to the detection limit of XRD, was possible by comparing all three XRD patterns with each other.

The superconductivity properties of the obtained samples coincide with those reported in literature: the sample with x = 0.05 doesn't show superconductivity down to the lowest temperature of 4 K. SQUID and resistivity measurements of $FeTe_{0.9}S_{0.1}$ and $FeTe_{0.8}S_{0.2}$ samples show the presence of filamentary and bulk superconductivity, respectively, Fig. 3.10 (b) and (d). The different scale for the magnetic susceptibility is due to the two reasons: : one of them is the simple scaling between max and min values and the second is the presence of a ferrimagnetic Fe_3O_4 impurity, that gives a positive background in Fig. 3.10 (b). The Verwey transition in Fe_3O_4 causes a hump in the FC data at $\sim$120 K, and a divergence between the FC and ZFC lines is observed. The SQUID data for $FeTe_{0.8}S_{0.2}$ suggests some presence of this impurity as well, but approximately five times smaller

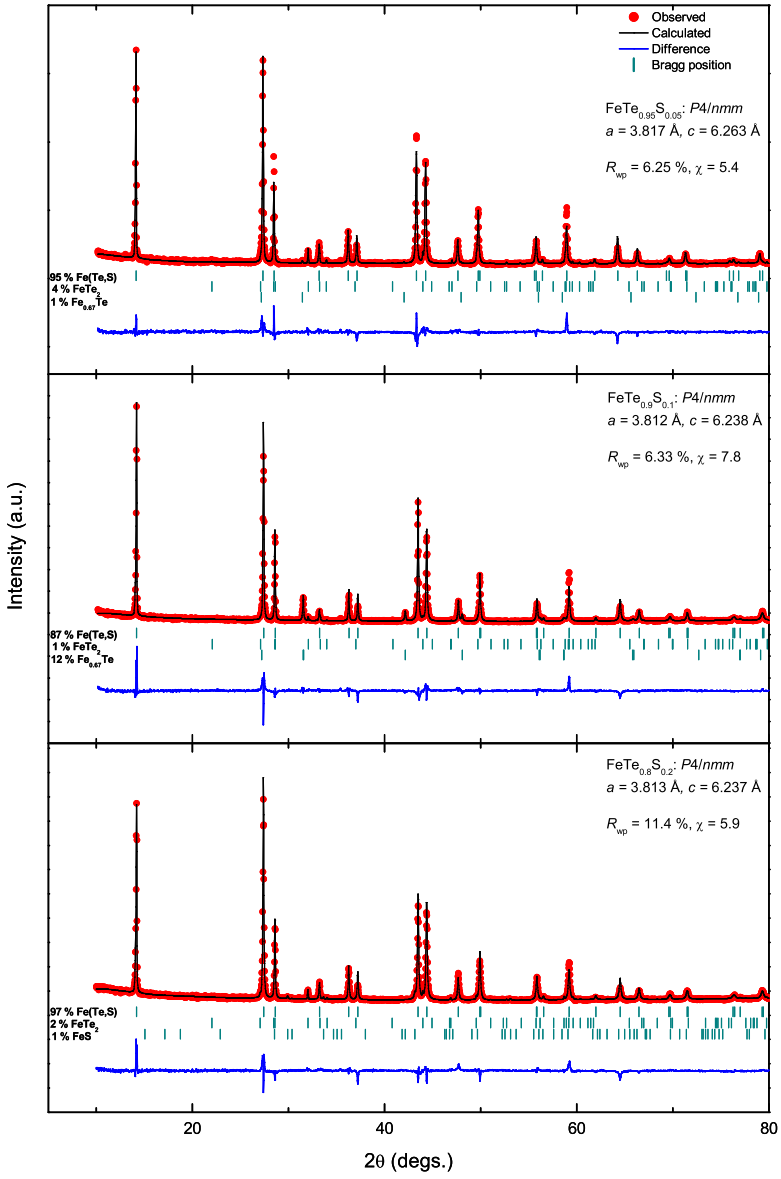

Figure 3.9: X-ray powder diffraction patterns for the samples $FeTe_{0.95}S_{0.05}$ (S7), $FeTe_{0.9}S_{0.1}$ (S6) and $FeTe_{0.8}S_{0.2}$ (S5). This picture was taken from **Publication 3.**

than in $FeTe_{0.9}S_{0.1}$, and therefore not observable by Mössbauer spectroscopy. Resistivity measurements were also done for our samples and the resistivity vs. temperature curve of $FeTe_{0.8}S_{0.2}$ shows a transition to zero resistivity at around 9 K, Fig. 3.10 (c).

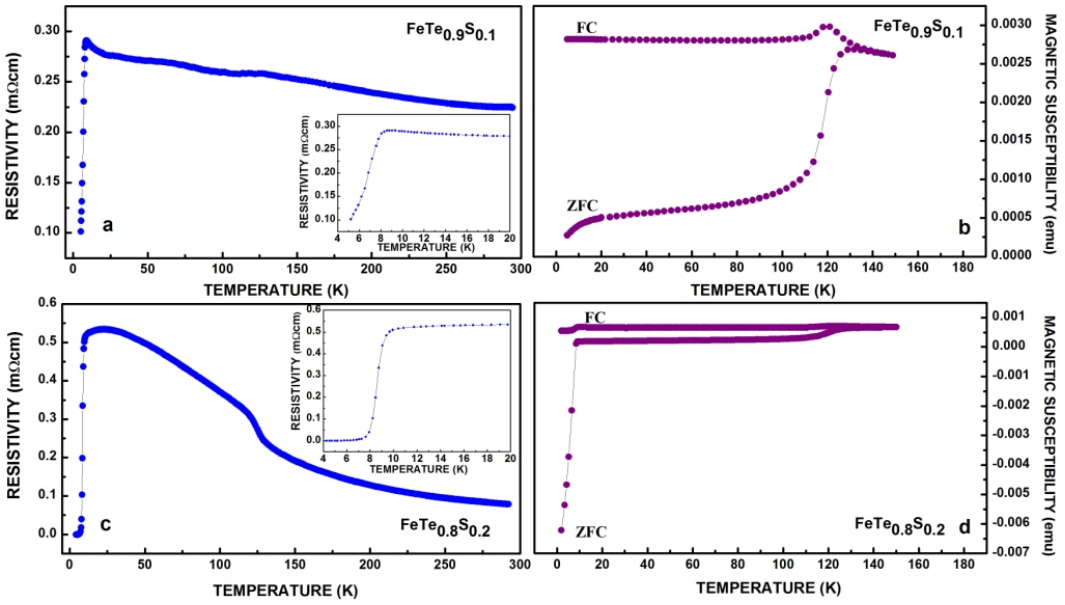

Figure 3.10: Resistivity vs. temperature for samples $FeTe_{0.9}S_{0.1}$ (S6) (a) and $FeTe_{0.8}S_{0.2}$ (S5) (c), respectively. The insets show the transition regions in more detail. Magnetic susceptibility vs. temperature for samples $FeTe_{0.9}S_{0.1}$ (S6) (b) and $FeTe_{0.8}S_{0.2}$ (S5) (d) obtained in field-cooling (FC) and zero-field-cooling (ZFC) regimes of the SQUID measurements. This picture was taken from **Publication 3.**

Transition-temperature values of T_c = 10 K and T_c = 9 K were found for $FeTe_{0.9}S_{0.1}$ and $FeTe_{0.8}S_{0.2}$ samples, respectively.

Mössbauer spectra of all samples were recorded in the temperature range of 5.7 – 300 K in transmission geometry. Maximum Doppler velocity values of 10 mm/s and 1.70 mm/s were used. The high velocity measurements exhibit the presence of magnetic impurities due to the Fe_3O_4 phase in $FeTe_{0.9}S_{0.1}$ (S6). This impurity phase was not observed using XRD, which can be explained by the 2% detection limit of XRD and probably the poor crystallinity of Fe_3O_4. But the paramagnetic $FeTe_2$ and $Fe_{0.67}Te$ impurities were not visible on the Mössbauer spectra due to the fact that the more intensive main doublet masks these two phases, as both these impurities are paramagnetic at room temperature [57–59].

The low-velocity Mössbauer spectra allow for extracting information of the hyperfine interactions of the main phase. The combined pictures of RT, high-velocity and low-velocity Mössbauer spectra at indicated temperatures are shown in Figs. 3.11 and 3.12.

A modified fit model was used for analyzing the spectra: instead of introducing a third phase with a magnetic ordering temperature below 77 K (spectral component C_2 described above) an internal

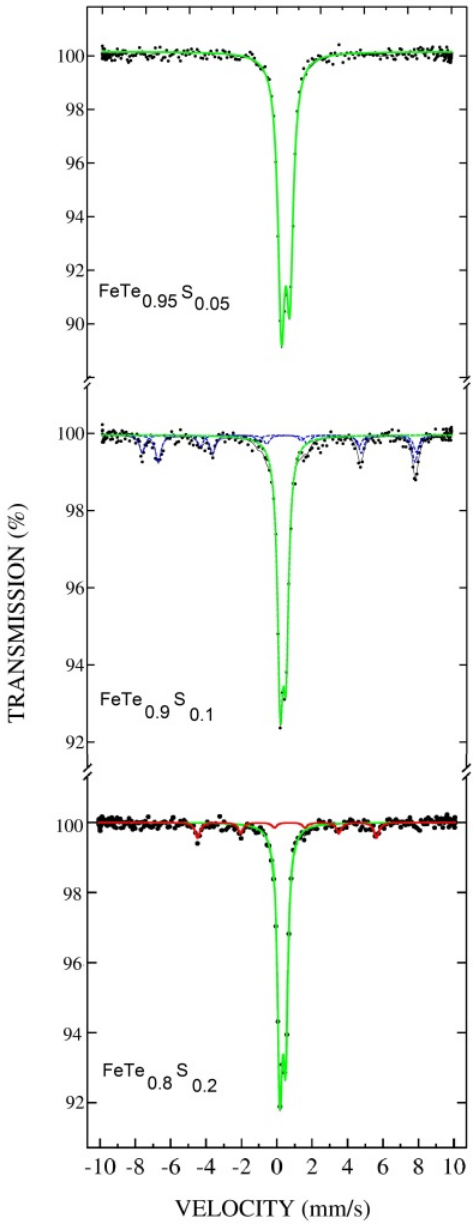

Figure 3.11: ^{57}Fe high-velocity Mössbauer spectra of $FeTe_{0.95}S_{0.05}$ (S7) (upper panel), $FeTe_{0.9}S_{0.1}$ (S6) (middle panel), and $FeTe_{0.8}S_{0.2}$ (S5) (lower panel) recorded at room temperature. Components due to the paramagnetic doublet (green), and the magnetic Fe_3O_4 (blue) and FeS (red) impurities are indicated.

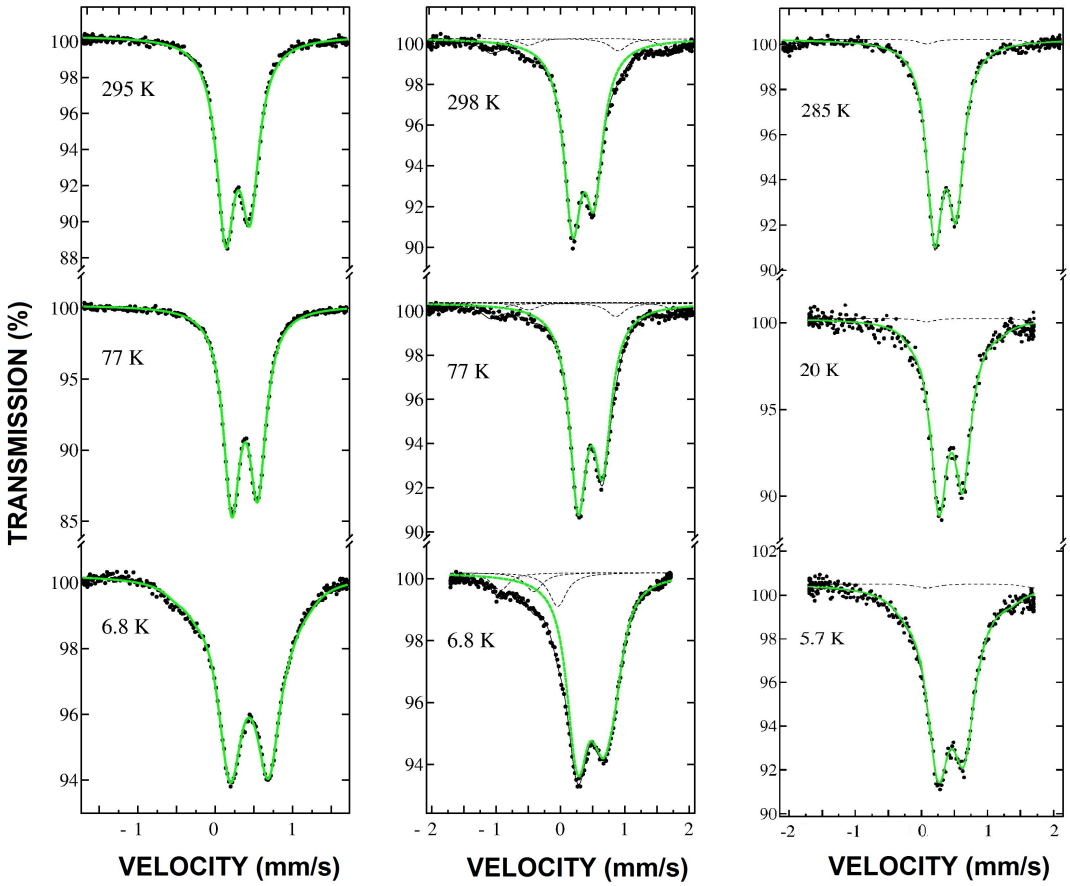

Figure 3.12: Left panel: ^{57}Fe Mössbauer spectra of $FeTe_{0.95}S_{0.05}$ (S7) recorded at indicated temperatures. Middle panel: ^{57}Fe Mössbauer spectra of $FeTe_{0.9}S_{0.1}$ (S6) recorded at indicated temperatures. Right panel: ^{57}Fe Mössbauer spectra of $FeTe_{0.8}S_{0.2}$ (S5) recorded at indicated temperatures. Components due to the broadened paramagnetic doublet (green), the Fe_3O_4 and FeS impurities central lines (gray dashed) are indicated. These pictures were taken from **Publications 2 and 3.**

magnetic field with a distribution was added to the paramagnetic doublet of the main phase. All components (impurities and main components) had the same linewidth. As texture was observed at 300 K, the angle between the wave vector and the z-axis of the electric field gradient (due to the sample texture) was fixed to the 300 K value. The main component was then fitted using relative intensity, isomer shift relative to α-Fe and eQV_{zz} as free parameters (η was fixed at 0). The magnetic broadening was included by fitting a histogram of 20 field values between 0 and 10 T, so that their relative intensities add up to 1. One may think of this as having 20 components with identical values for V_{zz}, isomer shift, eta and line width, but various values for the internal field and again the angle between V_{zz} and B_{eff} was fixed at 0 degrees and with total intensity adding up to the value specified (but fitted) for the main component. For the FeS all parameters were fixed to the 77 K values, as these were not expected to change at low temperatures. Furthermore these parameters could not be reliably fitted in low-velocity spectra, as only lines 3 and 4 occur in the velocity interval.

The low-velocity Mössbauer spectra show an asymmetric quadrupole doublet, that was assigned to the superconducting $FeTe_{1-x}S_x$ phase, and lines 3 and 4 of the magnetic impurities. Combining the found preferred orientation of the XRD patterns and the Mössbauer data, the asymmetry of the doublet is due to crystalline texture and the angle between wave vector and z-axis of the main component of the electric field gradient was found to be $\sim$ 39.5°C between 77 K and 300 K. It was fixed at this value when fitting the spectra recorded below 77 K. The isomer shift of the paramagnetic main phase doublet is compatible with intermediate spin (S = 1) Fe^{2+}.

In the spectra recorded above 77 K purely paramagnetic behavior is observed for the main component. Below 77 K all spectra display a distinct broadening of the asymmetric doublet. This broadening changes with the temperature, reaching a maximum around T_c for the $FeTe_{0.9}S_{0.1}$ (S6) and $FeTe_{0.8}S_{0.2}$ (S5) samples. For $FeTe_{0.95}S_{0.05}$ (S7) the main doublet broadening is increased up to the lowest measuring temperature of 6.8 K. The broadened doublets were fitted with a histogram distribution of hyperfine magnetic fields, Fig. 3.13. The arithmetic weight ΔB gives the integrated mean value of the internal magnetic field is obtained.

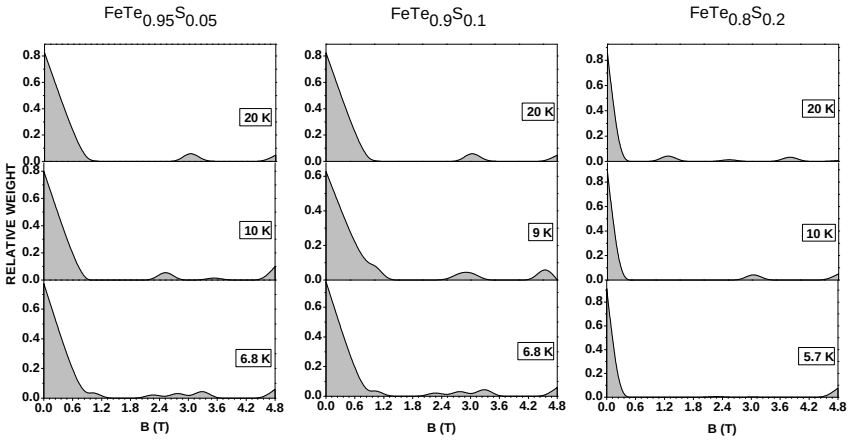

Figure 3.13: Internal field distribution histograms of $FeTe_{0.95}S_{0.05}$ (S7), $FeTe_{0.9}S_{0.1}$ (S6), and $FeTe_{0.8}S_{0.2}$ (S5) obtained at indicated temperatures.

The parameters of the fitted spectra are presented in Table 3.4.

Table 3.4: Mössbauer parameters of samples $FeTe_{0.95}S_{0.05}$ (S7), $FeTe_{0.9}S_{0.1}$ (S6) and $FeTe_{0.8}S_{0.2}$ (S5).

T, K	Γ, mm/s	IS, mm/s	eQV_{zz}, mm/s	ΔB, T
$FeTe_{0.95}S_{0.05}$				
295	0.340(4)	0.512(3)	-0.76(3)	–
77	0.341(1)	0.515(5)	-0.83(4)	–
20	0.350(1)	0.556(9)	-0.95(4)	0.74(8)
10	0.373(1)	0.559(8)	-1.00(4)	0.83(9)
6.8	0.362(4)	0.558(8)	-1.00(1)	0.88(2)
$FeTe_{0.9}S_{0.1}$				
298	0.320(6)	0.515(1)	-0.65(5)	–
77	0.321(2)	0.552(6)	-0.78(1)	–
20	0.333(2)	0.580(1)	-0.78(2)	0.45(1)
9	0.326(9)	0.587(5)	-0.80(4)	0.83(1)
6.8	0.321(1)	0.593(2)	-0.79(7)	0.74(4)
$FeTe_{0.8}S_{0.2}$				
285	0.290(5)	0.431(3)	-0.62(6)	–
77	0.272(2)	0.554(2)	-0.71(1)	–
20	0.280(7)	0.552(8)	-0.72(2)	0.08(1)
10	0.361(3)	0.564(1)	-0.75(2)	0.21(7)
5.7	0.413(2)	0.564(1)	-0.78(2)	0.13(2)

The temperature dependencies of the average hyperfine field are shown in Fig 3.14. The average

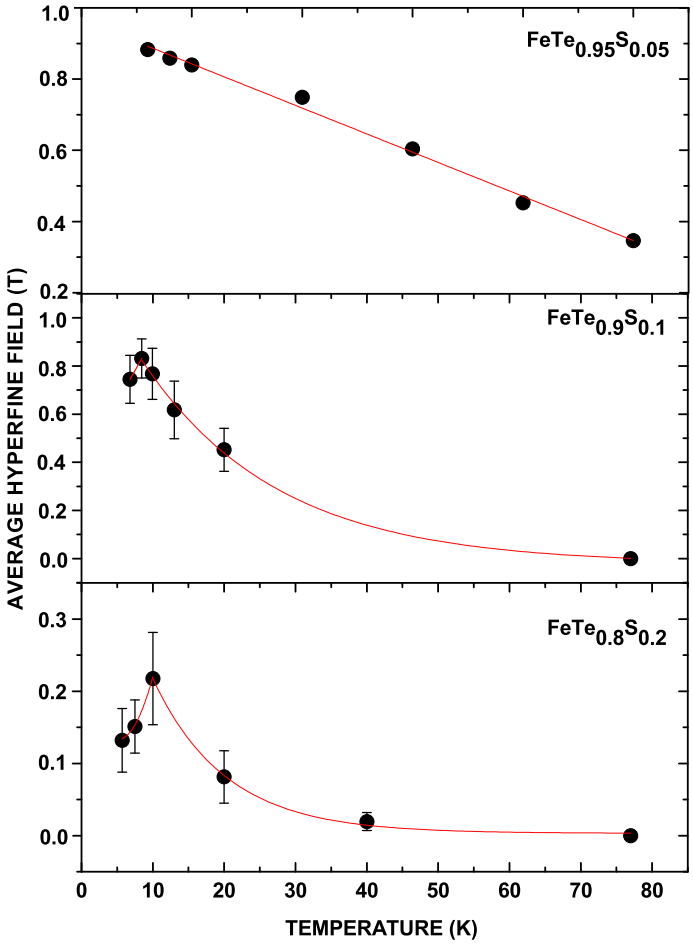

Figure 3.14: Average internal fields vs. temperature for $FeTe_{0.95}S_{0.05}$ (S7) (upper panel), $FeTe_{0.9}S_{0.1}$ (S6) (middle panel), and $FeTe_{0.8}S_{0.2}$ (S5) (lower panel).The lines are guides for the eye. This picture was taken from **Publication 3.**

fields peak at T_c for the superconducting samples, declining upon further cooling. The declining section coincides with the onset of superconductivity and the observed temperature behavior agrees with the hypothesis of coexistence of magnetism and superconductivity in our samples, **Publications 1, 2 and 3**. The overall portion of magnetically-ordered Fe in the earlier measured $FeTe_{0.8}S_{0.2}$ sample decreases below T_c, Fig. 3.15, that is also in agreement with the competition scenario.

The temperature dependencies of the center shift and the quadrupole splitting constant (eQV_{zz}) were studied in our best superconducting sample with $x = 0.20$. The quadrupole splitting of the main component has a negative sign, obtained owing to the sample texture, and equals $eQV_{zz} = -0.71$ mm/s at 77 K. The temperature dependence of the quadrupole splitting follows a $(1 - aT^{3/2})$ dependence [60], Fig. 3.16. The a value was found to be $3.2 \cdot 10^{-5}$ $K^{-3/2}$. Below $\sim$ 20 K the quadrupole splitting

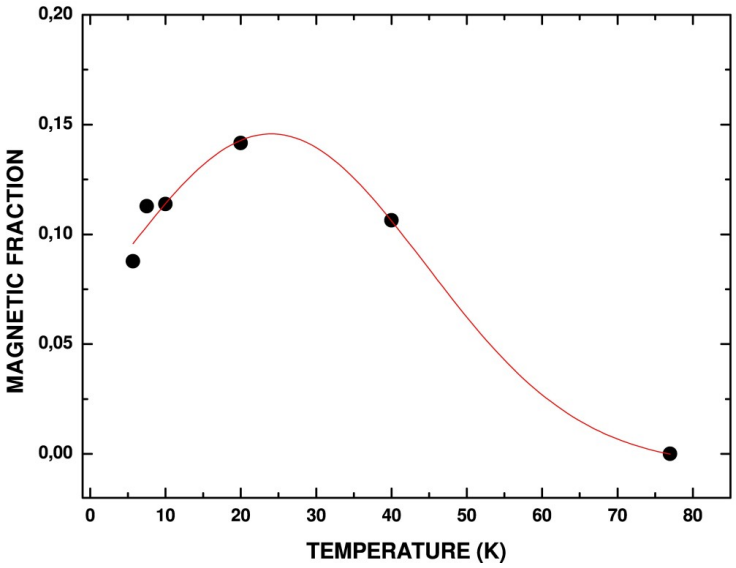

Figure 3.15: The fraction of magnetically ordered Fe vs. temperatures for sample $FeTe_{0.8}S_{0.2}$ (S5). The line is a guide for the eye. This picture was taken from **Publication 2.**

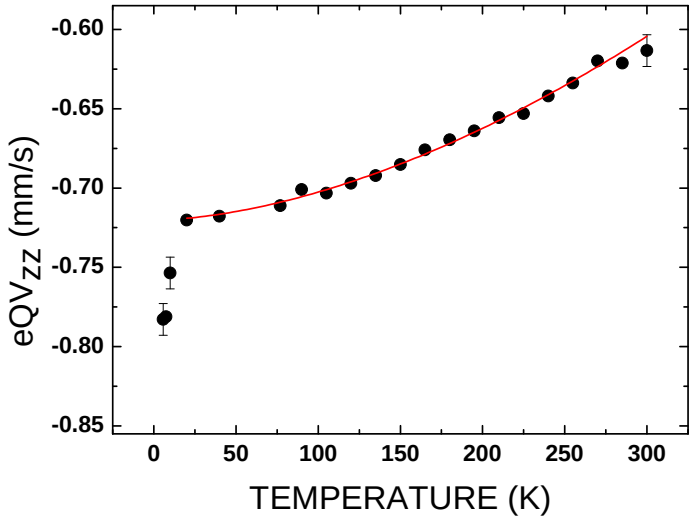

Figure 3.16: Quadrupole coupling constant eQV_{zz} vs. temperature for $FeTe_{0.8}S_{0.2}$ (sample S5) with a power law fitting, at temperatures above 20 K. This picture was taken from **Publication 2**.

value undergoes a sharp drop which roughly coincides with the decline of the internal field. The fast decline could be associated with a minor change in the non-spherical electronic structure of the observed Fe^{2+} state.

The temperature dependence of the center shift also shows a deviation from a simple Debye-behavior at temperatures below $\sim$ 77 K, Fig. 3.17. The high temperature part can be fitted using the

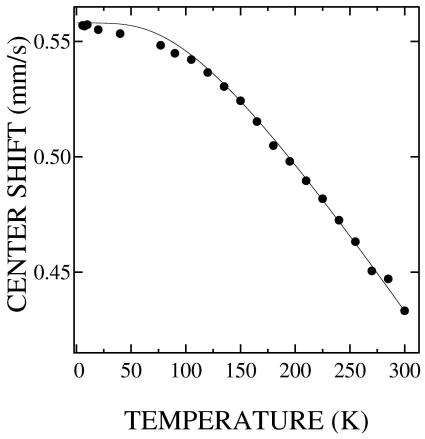

Figure 3.17: Temperature dependence of center shift for $FeTe_{0.8}S_{0.2}$ (sample S5), with the high-temperature part fitted with the Debye model.

Debye model with a Debye temperature of Θ_D = 405 K.

Also Seebeck measurements were done for obtaining information of the charge-carrier type in $FeTe_{0.8}S_{0.2}$, Fig. 3.18. The negative Seebeck coefficient indicates a conductivity of n-type with electrons as the charge carriers in the chalcogenide $FeTe_{1-x}S_x$ superconductors.

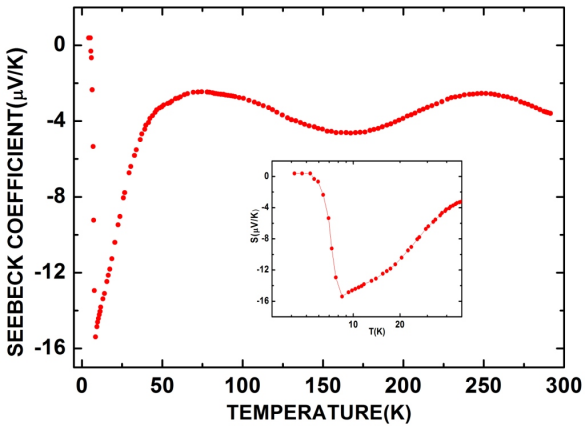

Figure 3.18: Seebeck measurement for $FeTe_{0.8}S_{0.2}$ (sample S5).

CHAPTER IV

Iron-chalcogenide compounds $FeSe_{1-x}$: synthesis and analysis

4.1 Motivation

Before the discovery of iron-based superconductors FeSe was a well known as a commercially available material and the structure of this material was thoroughly studied [61, 62]. Similar to FeTe this material has a layered structure with Fe_2Se_2 layers [30, 63] allowing a third type of atoms to be intercalated to the interlayer spaces. Among the new superconductors FeSe has the simplest structure and exhibits superconducting properties at an optimal 1:1 stoichiometric composition of Fe and Se even without doping [3]. The superconductivity transition temperature in FeSe is below $\sim$8 K [3, 67]. One of the routes for increasing the transition temperature is application of an external pressure [64, 65]. Several phases can form during the FeSe synthesis: α-FeSe, β-FeSe and γ-FeSe [3, 66], that are dependent on the stoichiometry and the temperature of the synthesis [62, 67]. These phases have different structures, but only the tetragonal (β) phase shows superconductivity properties below $T_c \approx 8$ K [3, 67]. The tetragonal phase is in the paramagnetic state at room temperature. This phase undergoes a tetragonal-to-orthorhombic structural transition at 70 – 90 K but this transition is not accompanied by a magnetic transition as it is for FeTe. In case of selenium deficiency non-stoichiometric superconducting $FeSe_{1-x}$ material show a magnetic ordering under an applied hydrostatic pressure [4, 68]. Other non-superconducting phases of FeSe show a magnetically ordered structure at normal conditions.

Paramagnetic FeSe phase should exhibit a single paramagnetic doublet in the Mössbauer spectrum at room temperature. Due to observations in earlier experimental works [69, 70] of a "strange" additional paramagnetic doublet in the Mössbauer spectra, we decided to examine more closely the properties of non-stoichiometric FeSe and its synthesis conditions. In other words, we tried to optimize the conditions for obtaining the strange phase and then characterize its properties. The binary composition $Fe_{1-x}Se_x$ has a very rich phase diagram, Fig. 4.1. Therefore, the existence of hitherto undescribed phases is perhaps not very astonishing.

4.2 Preparation of samples

For the investigation of polycrystalline $FeSe_{1-x}$ phases samples with x = 0.1, 0.18, 0.25 and 0.4 were produced using a solid-state reaction method. The appearance of the secondary phase was

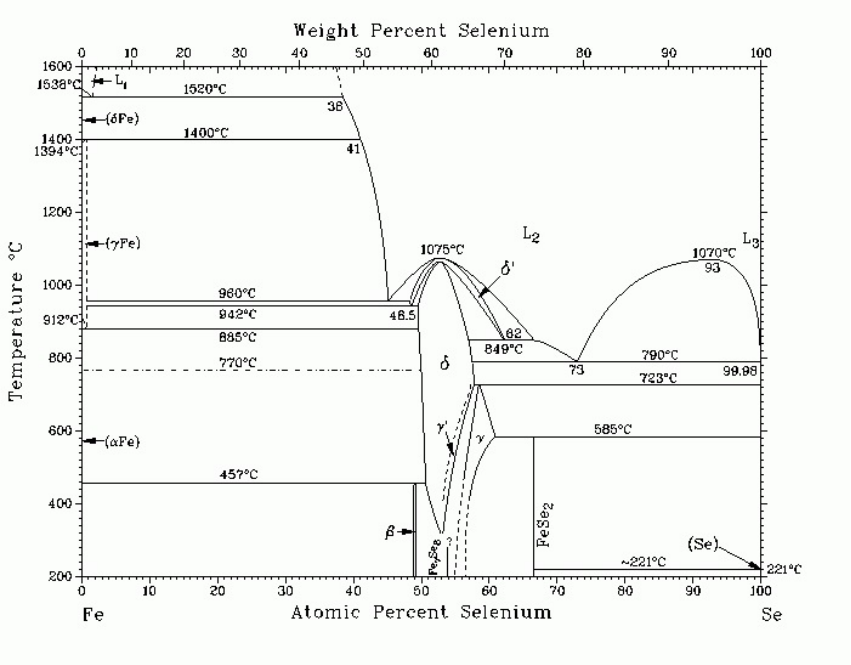

Figure 4.1: FeSe phase diagram [62].

found to require a second synthesis step. A two-step solid-state reaction at temperatures of 650 °C and 750 °C was used for the preparation of the samples. One of the synthesis-temperature values (650 °C) was taken from literature [69, 71].

Stoichiometric ratios 1:(1-x) of iron (99.99%) and selenium (99.99%) powders were mixed, sealed in evacuated quartz tubes, annealed at 650°C for 20 h, and quenched into cold water. The obtained samples were denoted series I. Thereafter, the samples were reground in a mortar, pressed into pellets and sintered again at the same synthesis conditions. After 20 h the samples were quickly taken out of the furnace and quenched into cold water. These samples were denoted series II. Polycrystalline $FeSe_{1-x}$ samples series III and IV were synthesized by the same scheme but using a higher synthesis temperature of 750°C. Samples which were obtained after the first 750°C-synthesis step were marked series III, and samples which were obtained after second 750°C-synthesis step were marked series IV.

4.3 Characterization of $FeSe_{1-x}$

Mössbauer spectroscopy was used for observation of the secondary phase arising in the obtained samples. ^{57}Fe Mössbauer spectra were recorded in transmission geometry with Doppler velocities of $\sim$8.00 mm/s and 2.5 mm/s. High-velocity spectra reveals the presence of impurity phases and low-velocity spectra give information about the interesting paramagnetic secondary phase. Mössbauer spectra were recorded in the temperature interval of 77 - 300 K using an Oxford CF506 continuous-flow cryostat for low-temperatures measurements and a year-old Cyclotron Co, ^{57}Co:Rh source. The following fit parameters were used: line width (Γ), quadrupole splitting ($QS = eQV_{zz}/2$), iso-

mer shift (δ), component intensities (I), and magnetic hyperfine field (B_{eff}) for magnetically-split components. Isomer shift values are quoted relative to α-Fe at room temperature.

Samples from series I and III do not show presence of the additional paramagnetic doublet, whereas samples which were obtained using two synthesis steps followed by quenches show the presence of this secondary phase. Room temperature Mössbauer spectra of series II samples synthesized at 650 °C are shown in Fig. 4.2. Using the spectral parameters, the percentage of the additional phase

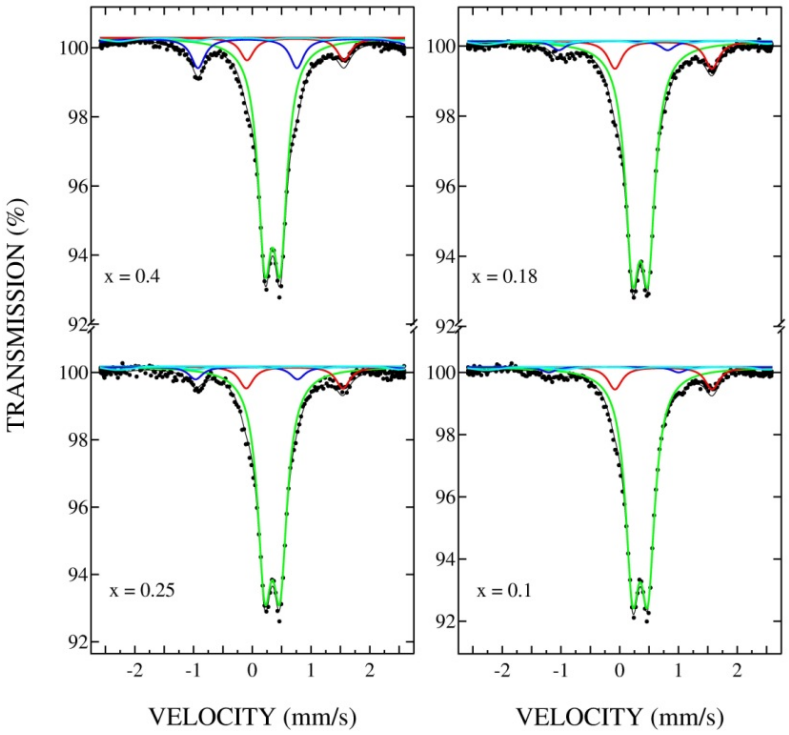

Figure 4.2: RT Mössbauer spectra of $FeSe_{1-x}$ (x = 0.4, 0.25, 0.18, 0.1) series II samples synthesized at 650 °C. Green, blue, cyan and red lines indicate the paramagnetic main doublet, elementary iron, Fe_7Se_8 and secondary phase, respectively.

was ∼12.4%, 7.6%, 9.9%, and 9% from the total spectral area for series II samples with x = 0.4, 0.25, 0.18, 0.1, respectively. By increasing the synthesis temperature to 750°C the secondary phase percentage increased to ∼18%. The samples from series III, obtained at the highest temperature (750 °C), did not show presence of the secondary paramagnetic phase, whereas in the spectra of series IV the additional paramagnetic doublet was visible for the all samples, Fig. 4.3. The secondary phase content was found to be ∼18% of the total spectral area of the sample $FeSe_{0.75}$ (series IV). Obtained Mössbauer parameters for all spectra of series IV samples are presented in Table 4.1.

Due to the sample stoichiometry with excess iron a magnetically split component of metallic Fe was observed in all Mössbauer spectra starting from RT, Fig. 4.4. This impurity component is most intense in the $FeSe_{0.6}$ compound (33% of total spectral area) and is only 3% for $FeSe_{0.9}$ sample, see Table 4.1 and Fig. 4.4. Magnetic separation can be used for removing of this iron impurity, as

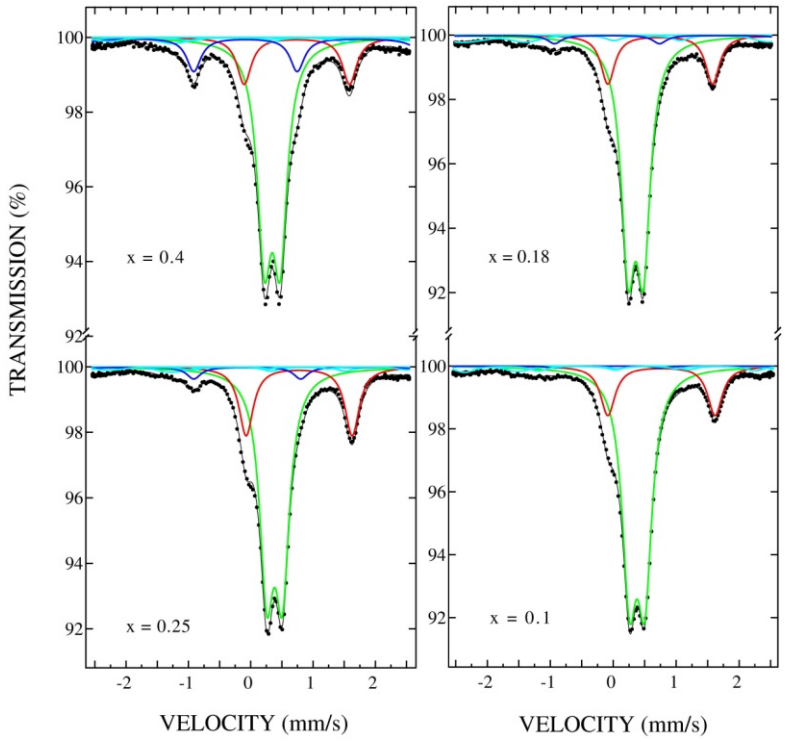

Figure 4.3: Mössbauer spectra of $FeSe_{1-x}$ (x = 0.4, 0.25, 0.18, 0.1) series IV samples at room temperature. Green, blue and red lines indicate the paramagnetic main doublet, elementary iron and secondary phase, respectively. Lines (cyan) due to magnetic Fe_7Se_8 are visible in the background. This picture was taken from **Publication 4**.

Table 4.1: Parameters of the $FeSe_{1-x}$ Mössbauer spectra at RT and around magnetic transition temperature (T_m). For the secondary component P denotes paramagnetic and M magnetic. The table was taken from **Publication 4**.

origin	T, K	Γ, mm/s	δ, mm/s	QS, mm/s	B_{eff}, T	A^1, %	T_m, K
$FeSe_{0.6}$							
FeSe	298	0.276(5)	0.458(5)	0.25(5)	–	42(2)	101
2^{nd} (P)		0.276(5)	0.853(5)	1.69(5)	–	12(2)	
FeSe	102	0.298(5)	0.549(5)	0.29(5)	–	43(2)	
2^{nd} (P)		0.298(5)	0.884(5)	1.61(5)	–	4(2)	
2^{nd} (M)		0.517(9)	0.90(9)	0.19(9)	12.3(7)	10(2)	
FeSe	98	0.311(5)	0.551(5)	0.30(5)	–	42(2)	
2^{nd} (P)		–	–	–	–		
2^{nd} (M)		0.811(7)	0.90(5)	0.08(8)	11.9(9)	13(2)	
$FeSe_{0.75}$							
FeSe	298	0.301(5)	0.495(5)	0.25(5)	–	53(2)	101.5
2^{nd} (P)		0.301(5)	0.886(5)	1.71(5)	–	18(2)	
FeSe	102	0.291(5)	0.555(5)	0.28(5)	–	50(2)	
2^{nd} (P)		0.291(5)	0.982(5)	1.71(5)	–	8(2)	
2^{nd} (M)		0.605(9)	0.812(7)	0.056(9)	10.1(8)	10(2)	
FeSe	101	0.298(5)	0.548(5)	0.29(5)	–	49(2)	
2^{nd} (M)		1.03(9)	0.841(9)	-0.27(7)	9.8(9)	23(2)	
$FeSe_{0.82}$							
FeSe	298	0.361(5)	0.491(5)	0.24(5)	–	64(2)	103
2^{nd} (P)		0.361(5)	0.901(5)	1.72(5)	–	15(2)	
FeSe	104	0.316(5)	0.548(5)	0.29(5)	–	63(2)	
2^{nd} (P)		0.316(5)	0.951(5)	1.80(5)	–	14(2)	
FeSe	102	0.299(5)	0.541(5)	0.291(5)	–	56(2)	
2^{nd} (M)		0.697(8)	0.955(9)	0.12(9)	7.5(9)	17(2)	
$FeSe_{0.9}$							
FeSe	298	0.278(5)	0.445(5)	0.25(5)	–	67(2)	104
2^{nd} (P)		0.278(5)	0.851(5)	1.71(5)	–	17(2)	
FeSe	106	0.291(5)	0.547(5)	0.29(5)	–	63(2)	
2^{nd} (P)		0.291(5)	0.957(5)	1.74(5)	–	18(2)	
FeSe	102	0.290(5)	0.551(5)	0.29(5)	–	63(2)	
2^{nd} (P)		0.290(5)	0.953(5)	1.76(5)	–	6(2)	
2^{nd} (M)		0.688(9)	0.719(9)	0.063(8)	10.7(7)	16(2)	
FeSe	77	0.323(5)	0.554(5)	0.30(5)	–	62(2)	
2^{nd} (M)		0.441(7)	0.935(7)	0.058(9)	16.3(8)	21(2)	

1 Metallic Fe portions of $\sim$33 %, $\sim$17 %, $\sim$12 % and $\sim$3 % at all indicated temperatures were found for samples with x = 0.4, 0.25. 0.18 and 0.1, respectively. Fe_7Se_8 portions of $\sim$12 %, $\sim$13 %, $\sim$16 % and $\sim$14 % at all indicated temperatures were found for samples with x = 0.4, 0.25. 0.18 and 0.1, respectively.

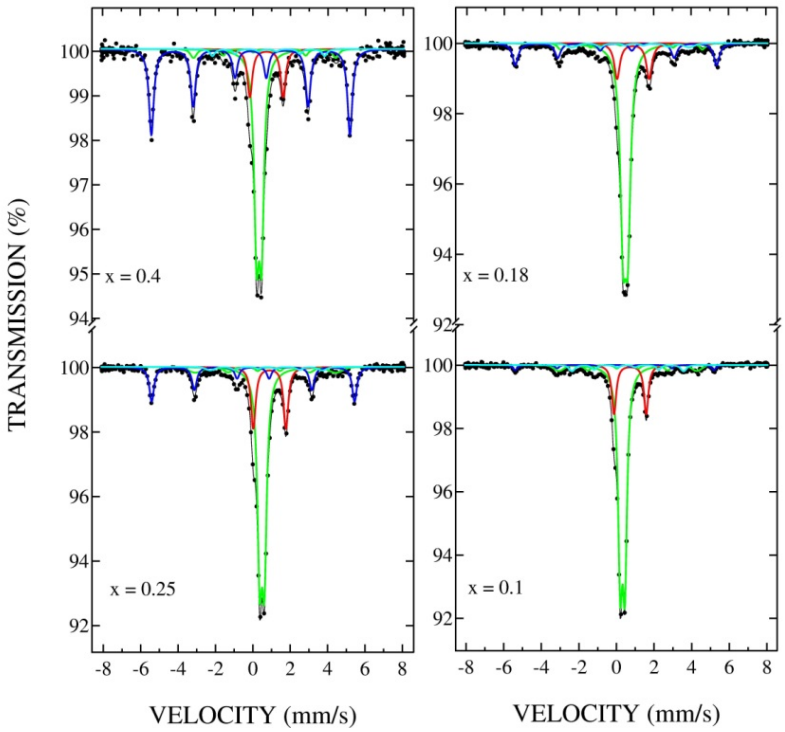

Figure 4.4: High-velocity Mössbauer spectra of $FeSe_{1-x}$ (x = 0.4, 0.25, 0.18, 0.1) series IV samples at room temperature. Green, blue, cyan and red lines indicate the main paramagnetic doublet, elementary iron, Fe_7Se_8 and secondary phase, respectively.

pure iron is ferromagnetically ordered at room temperature. The $FeSe_{0.6}$ sample with the largest iron content was cleaned using this method. The sample powder was collected on the magnet surface and the non-ferromagnetic part was separated by shaking the magnet handle. The result of the magnetic separation is shown in Fig. 4.5. Only a small trace of pure iron is visible in the $FeSe_{0.6}$ spectrum

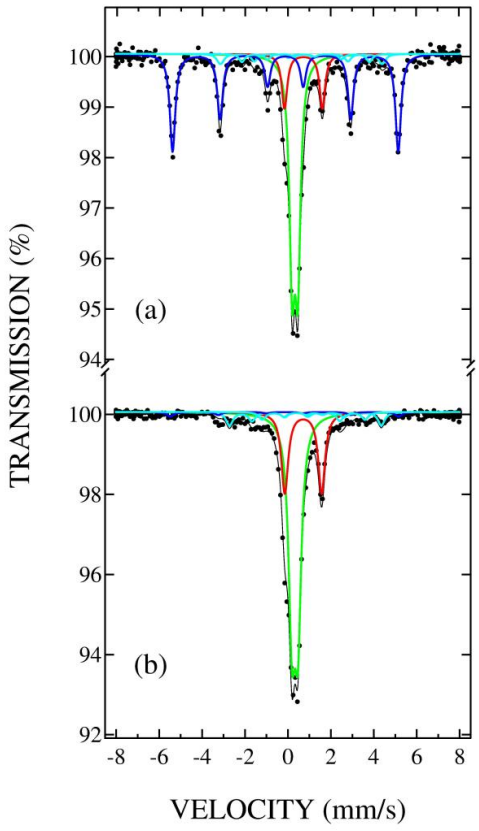

Figure 4.5: High-velocity RT ^{57}Fe Mössbauer spectra of $FeSe_{0.6}$: as-synthesized (a) and after removing of metallic Fe with a magnet (b).

after removing of metallic Fe, which means that in the future the magnet treatment can be used for processing $FeSe_{1-x}$ samples.

A Mössbauer study of the secondary phase in $FeSe_{1-x}$ samples of series IV was made. The exact phase content was studied by X-ray powder diffraction and a comparison of series III and IV samples was made. Obtained XRD patterns for $FeSe_{0.6}$ and $FeSe_{0.9}$ samples are shown in Figs. 4.6 and 4.7.

XRD patterns were fitted using the Rietveld method. Fit results revealed the presence of the FeSe main phase, an unknown Fe-Se phase, Fe_7Se_8, and elementary Fe. The peaks from the unknown Fe-Se phase are noticeably sharper than the peaks from main phase and their intensity increases after the second sintering. The PDF-4 database does not contain this secondary phase. Peaks of this phase were already observed on XRD patterns in several works but were not identified by the

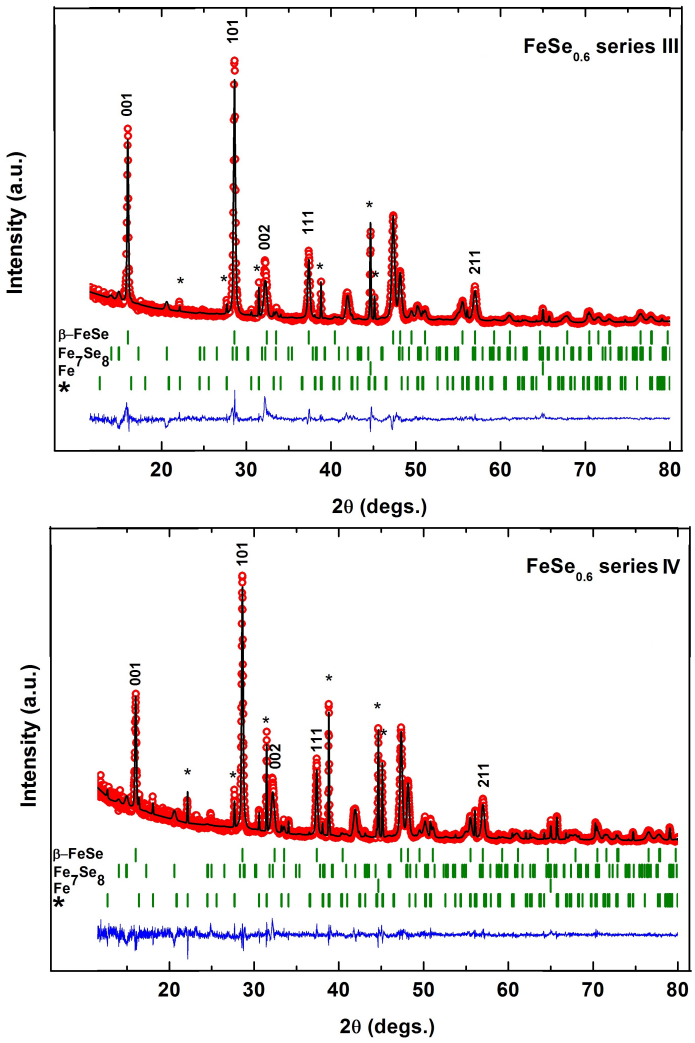

Figure 4.6: X-ray powder diffraction patterns for series III and series IV $FeSe_{0.6}$ samples. Main peaks of the secondary phase component are denoted by asterisks. Indices concern the main β-FeSe phase. This figure was taken from **Publication 4**.

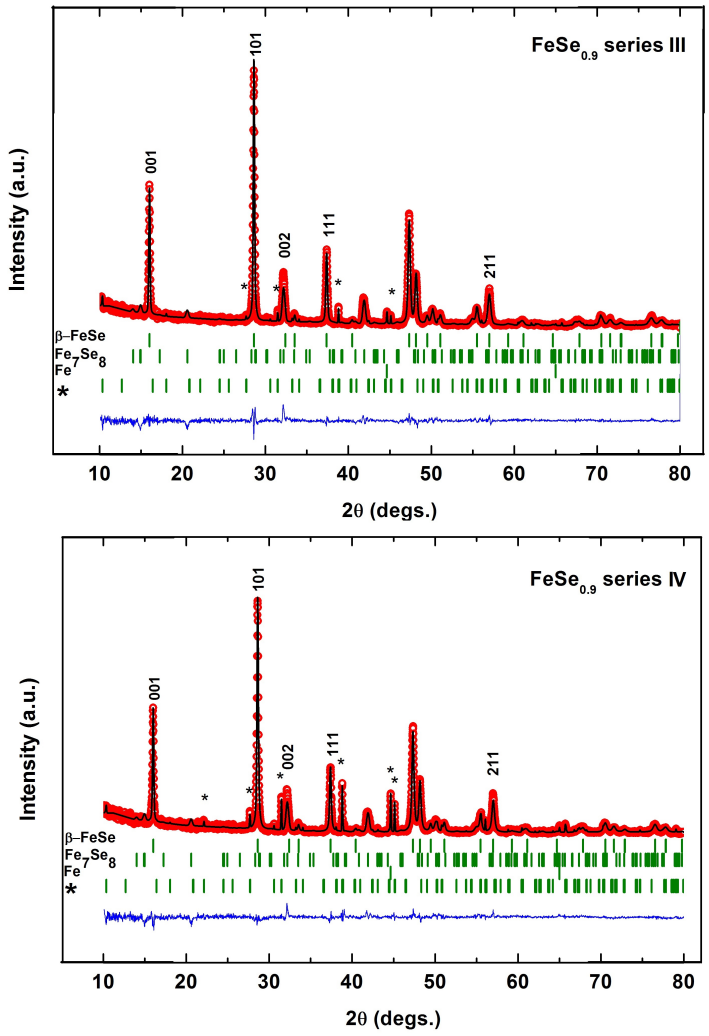

Figure 4.7: X-ray powder diffraction patterns for series III and series IV $FeSe_{0.9}$ samples. Main peaks of the secondary phase component are denoted by asterisks. Indices concern the main β-FeSe phase. This figure was taken from **Publication 4**.

authors [3, 72]. Using the FullProf software approximate unit cell parameter of this unknown phase were found. The orthorhombic phase with lattice parameters a ≈ 8.52 Å b ≈ 6.96 Å, and c ≈ 4.90 Å describes all reflections of the secondary phase. The most intensive reflections are marked by asterisks on the XRD patterns, Fig. 4.6 and Fig. 4.7.

Superconducting properties were studied for the series IV samples with $FeSe_{0.82}$ and $FeSe_{0.9}$ stoichiometry. Magnetic susceptibility versus temperature curves are given in Fig. 4.8. Both curves

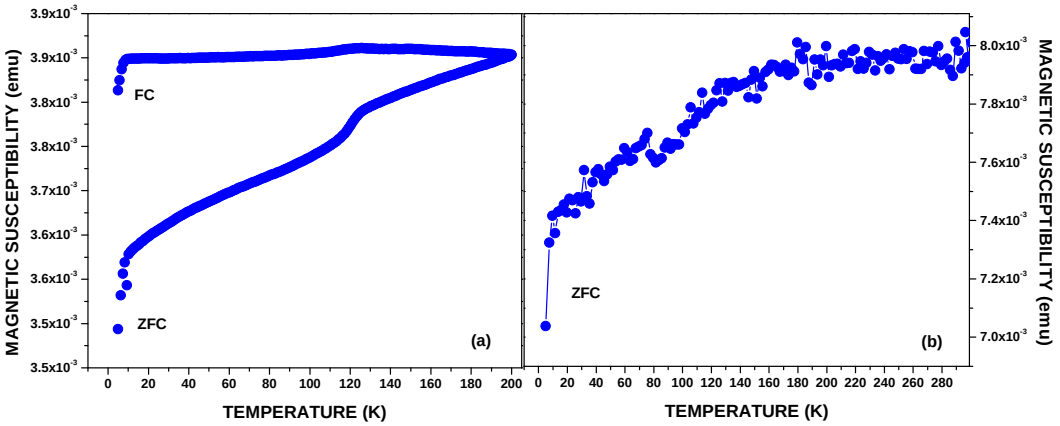

Figure 4.8: Magnetic susceptibility vs. temperature for $FeSe_{0.82}$ (a) and $FeSe_{0.9}$ (b) series IV samples obtained in field-cooling (FC) and zero-field-cooling (ZFC) regimes of the SQUID measurements.

show a down turn of the magnetic susceptibility at ∼8 K, that coincides with the literature value for the superconducting transition for the main phase [3, 67].

Mössbauer spectra of the series IV samples were recorded in the temperature interval of 77–300 K. At room temperature these spectra contain two paramagnetic doublets and several magnetic sextets, Fig. 4.4. Magnetic sextets are attributed to metallic iron and Fe_7Se_8 impurities. One of the paramagnetic doublets with δ = 0.44 mm/s and $eQV_{zz}/2 \approx 0.25$ mm/s can be assigned to the main FeSe phase, which probably remains stoichiometric, whereas variation of x was done only to promote the formation of the secondary phase, even on the expense of obtaining more Fe_7Se_8 and metallic Fe. The isomer shift and quadrupole splitting values for the paramagnetic doublet from FeSe phase coincide with the tetragonal β-FeSe and the isomer shift is compatible with the low-spin state of divalent iron [73]. The second doublet with the quadrupole splitting value of ∼1.7 mm/s and $\delta \approx 0.9$ mm/s is due to the unknown phase. The isomer shift value of the second paramagnetic doublet is compatible with high-spin Fe^{2+} [70].

Upon decreasing temperature the secondary phase undergoes a magnetic transition below ∼106 K, Fig. 4.9. Mössbauer measurements using small temperature steps of 0.5–1 K were made around transition temperature. For $FeSe_{0.9}$ sample the magnetic transition temperature (T_m) was found to be ∼105 K. The main component does not show any changes around T_m, indicating that the main phase and the secondary phase are well separated. The parameter values at temperatures around T_m are presented in Table 4.1. For all samples Mössbauer spectra at temperatures below 77 K were recorded. No significant changes in the spectral shapes were observed, Fig. 4.10.

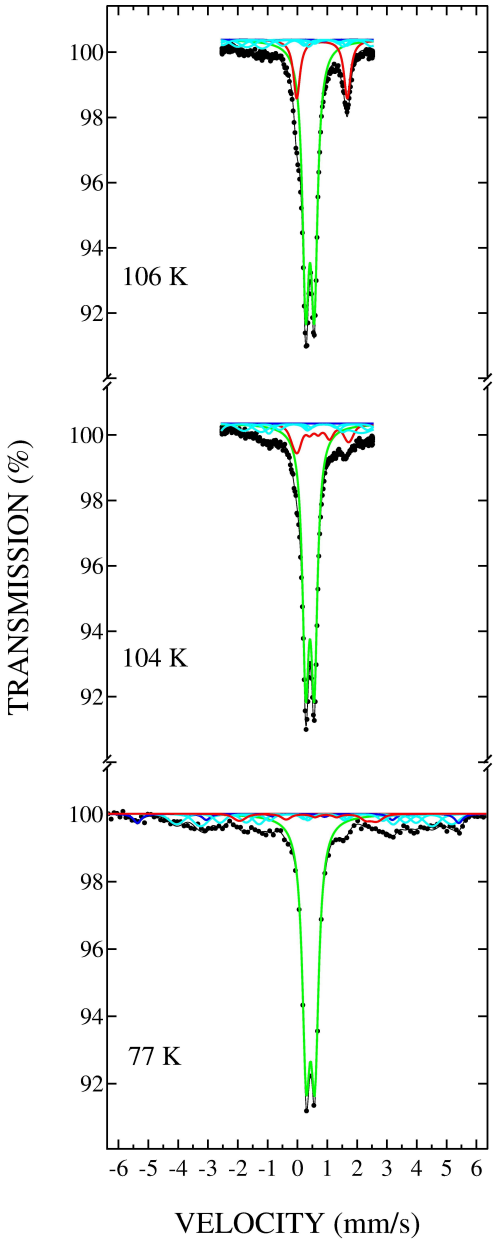

Figure 4.9: Mössbauer spectra of the $FeSe_{0.9}$ series IV sample recorded at temperatures around the magnetic transition temperature of the secondary phase. Green and red lines are due to the main phase and secondary phase, respectively. Weak lines due to metallic Fe (blue) and magnetic Fe_7Se_8 (cyan) are visible in the background.

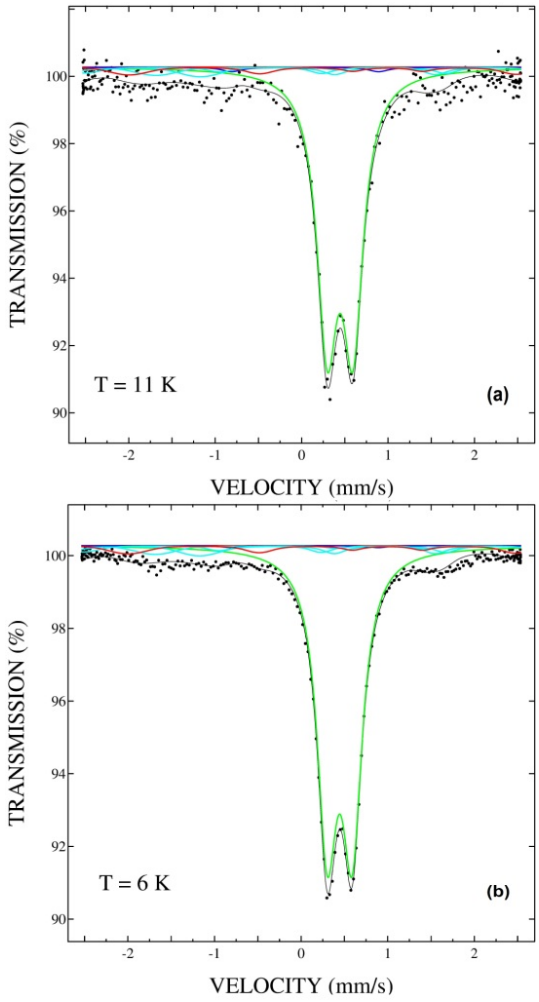

Figure 4.10: Mössbauer spectra of the $FeSe_{0.82}$ (a) and $FeSe_{0.9}$ (b) series IV samples recorded at indicated temperatures. Green and red lines are due to the main phase and secondary phase, respectively. Weak lines due to metallic Fe and magnetic Fe_7Se_8 are visible in the background.

CHAPTER V

Iron-pnictide compounds $A\mathrm{Fe}_2(\mathrm{As}_{1-x}\mathrm{P}_x)_2$: synthesis and study

5.1 Motivation

Pnictide superconductors show a variety of physical and chemical properties. One of these properties is coexistence between magnetism and superconductivity that several of these compounds have in the superconducting state [16, 74, 75]. Some of the phosphorus-doped materials $A\mathrm{Fe}_2(\mathrm{As}_{1-x}\mathrm{P}_x)_2$ also show this coexistence and Ba/EuFe$_2$(As$_{1-x}$P$_x$)$_2$ compounds were chosen for Mössbauer spectroscopy studies, as detection of magnetic ordering is easy.

The parent AFe$_2$As$_2$ compounds of our investigated objects have the same ThCr$_2$Si$_2$-type crystal structure with tetragonal $I4/mmm$ arrangement at room temperature, Fig. 5.1.

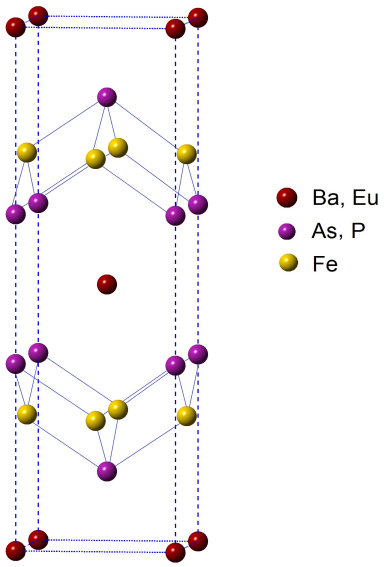

Figure 5.1: Ba/EuFe$_2$As$_2$ crystal structure.

In the 140 K – 200 K temperature interval the tetragonal lattice undergoes a structural transition to

orthorhombic $Fmmm$ that is accompanied by spin density wave effect [76–80]. Although the parent $\mathrm{BaFe_2As_2}$ and $\mathrm{EuFe_2As_2}$ materials do not show a superconducting transition at any temperatures down to 4 K, superconductivity in both compounds can be induced by replacing a part of the arsenic atoms by phosphorus atoms. Such substitution does not change the compounds charge but creates an internal pressure due to the difference in atomic radii of As and P atoms and gives rise to a superconducting volume fraction [81–83]. Superconductivity in $A\mathrm{Fe_2(As_{1-x}P_x)_2}$ appears in the narrow phosphorus concentration range of x = 0.2 – 0.6 for A = Ba and x = 0.14 – 0.23 for A = Eu [83–85]. The narrowness of the optimal concentration range may partially explain the coexistence between magnetism and superconductivity mentioned above [74, 75].

It was interesting to study the hyperfine interactions in Ba/$\mathrm{EuFe_2(As_{1-x}P_x)_2}$ compounds by Mössbauer spectroscopy and obtain the information about local iron atoms environment over the samples volume. For the study stoichiometries with x = 0.32 for the Ba-sample and x = 0.20 for the Eu-sample were chosen and, thanks to the presence of Eu, the europium sample was also studied by ^{151}Eu along with ^{57}Fe Mössbauer spectroscopy.

5.2 Sample preparation

The solid-state synthesis reaction method was used for the preparation of samples with the nominal compositions of $\mathrm{BaFe_2(As_{0.68}P_{0.32})_2}$ and $\mathrm{EuFe_2(As_{0.8}P_{0.2})_2}$. For both the samples stoichiometric ratios of iron powder (99.99%), barium pieces (99.9%) (or europium pieces), arsenic pieces (99.999%), and phosphorus powder were mixed, placed inside an alumina crucible and sealed into an evacuated quartz tube. Two reaction steps were used. For the Ba-sample, in the first annealing step, the powder mixture was slowly heated up to 600 °C for 18 h, annealed at this temperature at 3 h for prevention of phosphorus evaporation outside the mixture. After that the reaction temperature was increased up to 850 ° and the mixture was annealed at this temperature for 10 h, and slowly cooled down to room temperature. For the Eu-sample the heating time from room temperature up to 1050 °C was 10 h and the annealing time was 36 h with natural cooling to room temperature inside the furnace. In the second synthesis step the obtained samples were reground, pressed into pellets, and sintered again at 950 °C for 25 h. Both the preparation of the mixtures and the grinding processes were made inside a glove box with an inert Ar atmosphere.

5.3 Characterization of the Ba/$\mathrm{EuFe_2(As_{1-x}P_x)_2}$ samples

For the characterization of the obtained samples X-ray powder diffractometry (PanAnalytical X'pert Pro MPD, Cu $K\alpha 1$ radiation) and SQUID measurements (Quantum Design, MPMS-XL) were used, which gave information of phase purity and superconducting properties.

The XRD patterns of the obtained polycrystalline samples are presented in Fig. 5.2. According to the obtained results both samples have a tetragonal $\mathrm{ThCr_2Si_2}$-type crystal structure ($I4/mmm$) of the main $A\mathrm{Fe_2(As_{1-x}P_x)_2}$ phase. The presence of preferred orientation along the $00l$ direction was also seen on the XRD patterns and this effect due to powder sedimenting was taken into account during the fit by the Rietveld method. The fitting was carried out using the FullProf software program. From the data analysis the following lattice parameters were found: a = 3.928 Å and c = 12.824 Å for the Ba-sample, and a = 3.901 Å and c = 11.934 Å for the Eu-sample. A shrinkage of the lattice parameters in comparison with undoped samples was observed and this is typical for substituted materials [86].

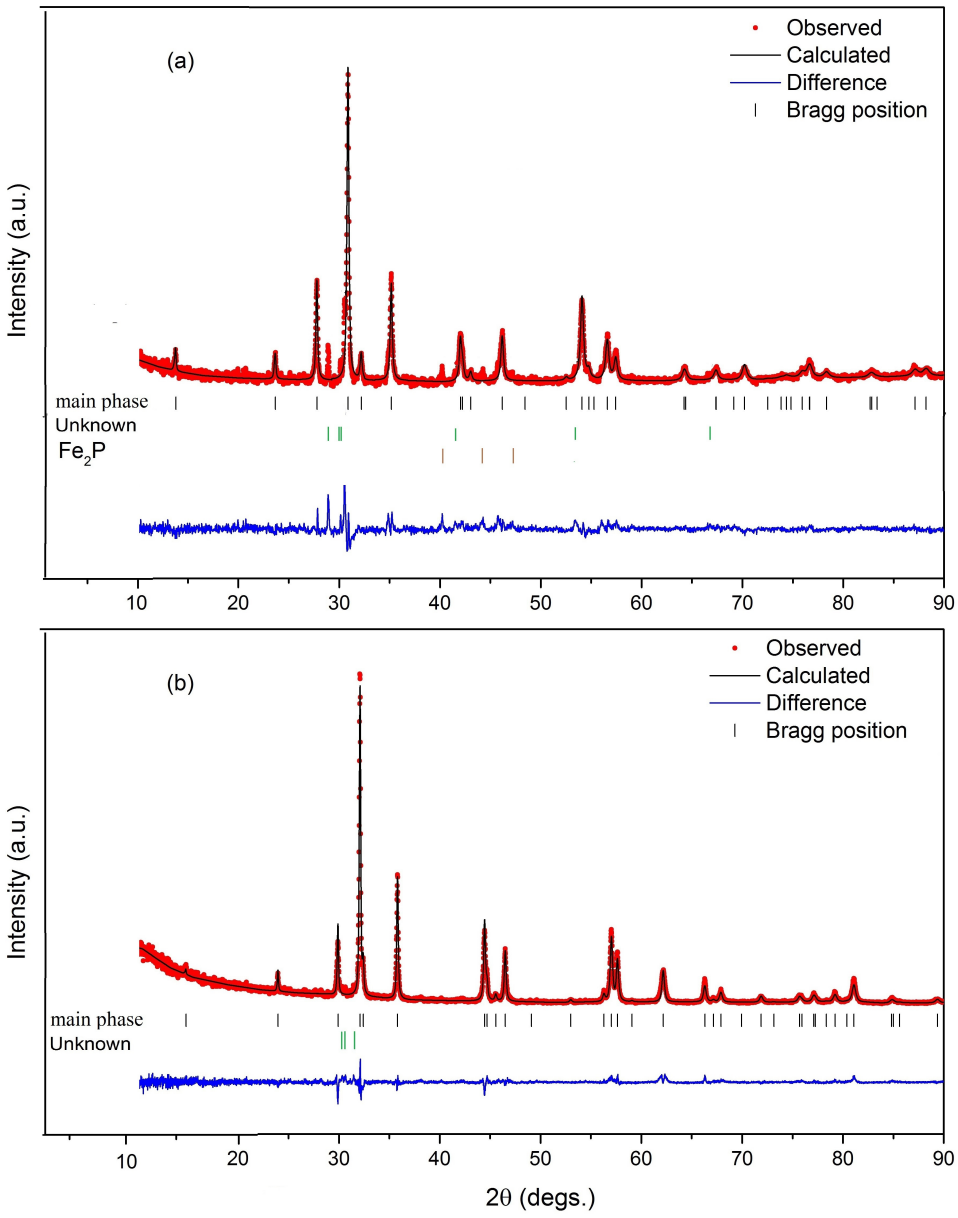

Figure 5.2: X-ray powder diffraction pattern for the $BaFe_2(As_{0.68}P_{0.32})_2$ (a) and $EuFe_2(As_{0.8}P_{0.2})_2$ (b) samples. The peaks from the Fe_2P and an unknown impurity are indicated. This picture was taken from **Publication 5**.

From Fig. 5.2 it can be seen that the XRD pattern of the Ba-sample shows, besides the main phase, presence of a Fe_2P impurity and some quantity of an unknown phase, the recognition of which failed in an earlier study [87]. The XRD pattern of the Eu-sample consists of the main phase and a small quantity of an unknown phase.

Superconductivity properties were studied by SQUID measurements (Quantum Design, MPMS-XL) in zero-field-cooled (ZFC) and field cool (FC) regimes. SQUID data of the Eu-sample shows the typical, for this material, increase of the magnetic susceptibility at low temperatures due to the magnetic ordering of the Eu^{2+} atoms at 19 K [82] (Fig. 5.3(b)). The Ba-sample shows a sharp drop to negative values of the magnetic susceptibility at 30 K indicating the superconducting transition at this temperature, Fig. 5.3(a). Due to the high-T_c value the estimated phosphorus concentration is

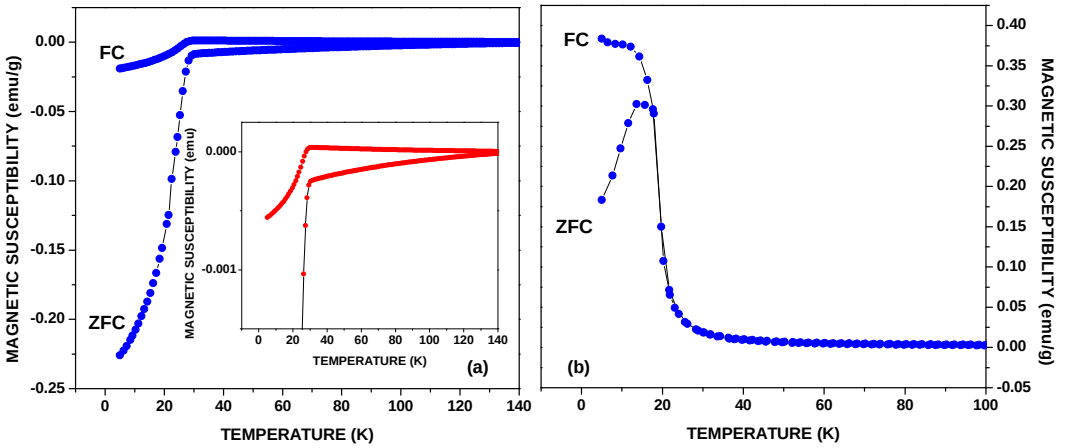

Figure 5.3: Magnetic susceptibility vs. temperature for $BaFe_2(As_{0.68}P_{0.32})_2$ (a) and $EuFe_2(As_{0.8}P_{0.2})_2$ (b) samples obtained in 10 Oe field-cooling (FC) and zero-field-cooling (ZFC) regimes of the SQUID measurements. This picture was taken from **Publication 5**.

$x \approx 0.3$ [81]. The positive background from the ferromagnetic Fe_2P impurity was removed from the SQUID data of the Ba-sample. An attempt of removing this ferromagnetic impurity out of the Ba-sample by a third annealing step at 1050 ° for 25 h was made. The comparative SQUID picture for the Ba-samples after the second and the third annealing step is shown in Fig. 5.4. After the third reaction a three-fold reduction of the positive background was observed in the SQUID data, but, according to XRD, new impurity phases emerge instead. That is why we used the Ba-sample obtained after two synthesis for further studies.

The hyperfine interactions in the samples were studied by Mössbauer spectroscopy using ^{57}Fe and ^{151}Eu resonances in transmission geometry with Doppler velocities of 4.50 mm/s and 2.50 mm/s for ^{57}Fe measurements and 16.53 mm/s for ^{151}Eu measurements. The Ba-sample was studied by ^{57}Fe Mössbauer spectroscopy in the temperature range from 6.1 K up to 310 K with an Oxford continuous-flow cryostat and coolants of liquid He and liquid N_2 for achieving the temperatures below and above 77 K, respectively. For the Eu-sample ^{57}Fe Mössbauer spectra in the temperature range from 77 K up to 310 K were obtained while the ^{151}Eu Mössbauer spectrum was recorded at room temperature.

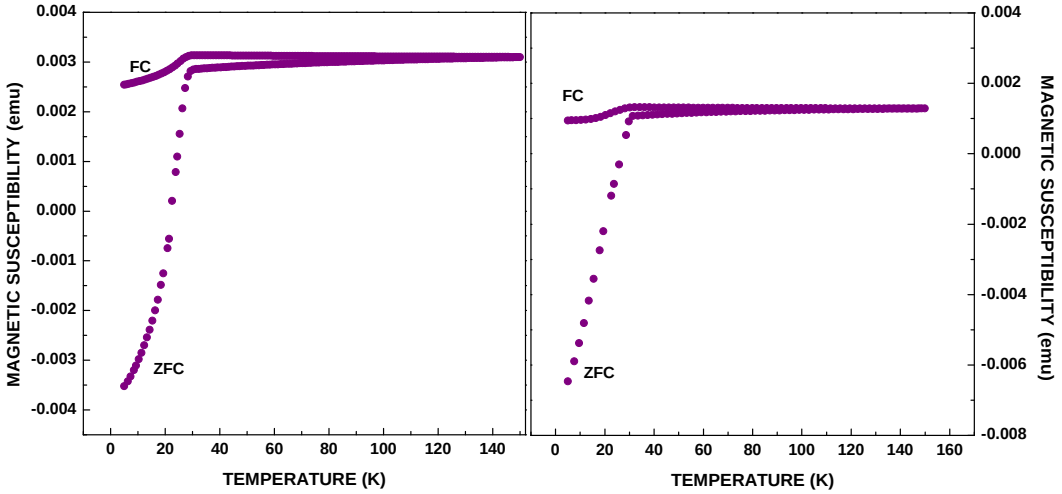

Figure 5.4: Magnetic susceptibility vs. temperature for BaFe$_2$(As$_{0.68}$P$_{0.32}$)$_2$ samples synthesized by a two-step (a) and three-step (b) reaction. 10 Oe field-cooling (FC) and zero-field-cooling (ZFC) regimes are indicated on the pictures.

The room temperature ^{151}Eu Mössbauer spectrum of the Eu-sample is shown in Fig. 5.5. The spectrum shows the presence of one paramagnetic component. For fitting this spectrum an eight-line model was used for the unresolved quadrupole interaction. The obtained isomer-shift value $IS \approx$ -12 mm/s indicates that the Eu atoms occupy the +2 valence state.

The ^{57}Fe Mössbauer spectra of both the Eu- and Ba-samples recorded at room temperature consist of one asymmetric doublet due to the main AFe$_2$(As$_{1-x}$P$_x$)$_2$ phase, Fig. 5.6 (a) and (b). One possible origin of this asymmetry is the texture effect. For excluding of this possibility room temperature ^{57}Fe Mössbauer spectra were recorded in the magic angle (54.74°) between the normal of the sample's plane and the gamma-quanta propagation direction, Fig. 5.6 (c) and (d). As can be noticed, no significant changes in the spectral shapes are observed.

For the fit procedure of the Eu-sample, inclusion of two components gives a good description of this asymmetric doublet. The fitting resulted in the isomer-shift (IS) values of 0.33 mm/s and 0.56 mm/s, and quadrupole-splitting (QS) values of 0.119 mm/s and 0.06 mm/s for the first (more intensive) and the second component, respectively. Similarly, the asymmetric doublet of the Ba-sample spectrum consists two doublets with IS = 0.34 mm/s and 0.44 mm/s, and QS = 0.216 mm/s and 0.003 mm/s for the first (more intensive) and the second component, respectively, Fig. 5.6 (b). The values of the isomer shift are compatible with the low-spin state (S = 0) of Fe^{2+}. The literature values for the hyperfine parameters of the two extremes AFe$_2$As$_2$ and AFe$_2$P$_2$ are IS = 0.31/0.41 mm/s, QS = -0.03/0.07 mm/s, and IS = 0.28/0.28 mm/s, QS = 0.22/0.16 mm/s for compounds with A = Ba/Eu, respectively [77, 86, 88–90]. Comparing the obtained parameters for our two subspectra with the literature data the two components of the asymmetric doublets look very similar to these extreme cases.

Assuming both components originate from the main phase, the following prediction about the ori-

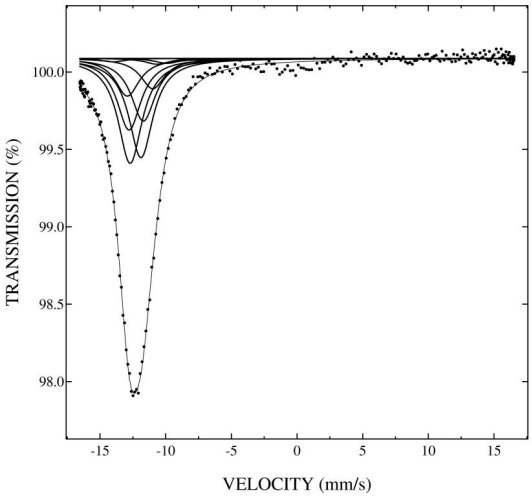

Figure 5.5: ^{151}Eu Mössbauer spectra of the $EuFe_2(As_{0.8}P_{0.2})_2$ sample recorded at room temperature. The eight lines are due to the unresolved quadrupole interaction, completely determined (i.e. position and intensity) by the value of V_{zz}.

gin of these components can be done: one of them (with the large quadrupole splitting) is due to the $AFe_2(As_{1-x}P_x)_2$ phase, and the second (with the small quadrupole splitting) is due to the pure AFe_2As_2 structure. In the AFe_2As_2 structure one iron atom is tetragonally coordinated by four nearest neighboring arsenic atoms. Simple calculations using the binomial distribution of phosphorus atoms in substituted compounds indicate that the most likely number of nearest phosphorus atoms, tetrahedrally coordinated to Fe, is 0 or 1 (see Table 5.1). This could explain the observed complex structure of the RT Mössbauer spectra: two paramagnetic doublets with a larger and a smaller quadrupole splitting originate from the two possible Fe atom surroundings containing one or zero phosphorus atoms, respectively.

Table 5.1: Isomer shift- and quadrupole splitting values. Experimental and calculated (binomial model) values of line intensities of Ba/$EuFe_2(As_{1-x}P_x)_2$ Mössbauer spectra recorded at RT. This Table was taken from **Publication 5**.

	$EuFe_2(As_{0.8}P_{0.2})_2$		$BaFe_2(As_{0.68}P_{0.32})_2$	
	1^{st} component	2^{nd} component	1^{st} component	2^{nd} component
IS, mm/s	0.33	0.56	0.34	0.44
QS, mm/s	0.119	0.060	0.216	0.003
I(exp), %	76	24	79	21
I(binomial), %	59	41	76	24
Assignment	1P3As*	4As	1P3As*	4As

* includes surroundings 2P2As, 3P1As and 4P.

Low-temperature ^{57}Fe Mössbauer spectra were also measured. Spectra of the Ba- and Eu-samples

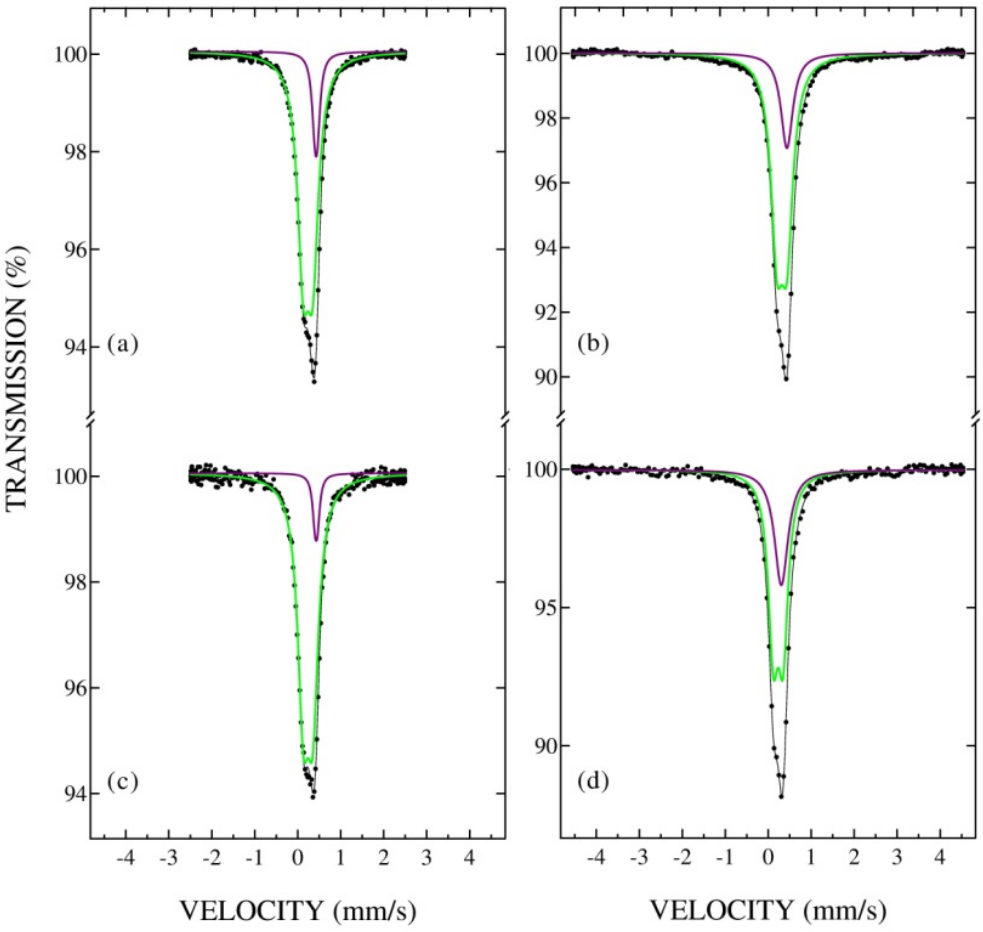

Figure 5.6: Room temperature Mössbauer spectra of EuFe$_2$(As$_{0.8}$P$_{0.2}$)$_2$ (a, c) and BaFe$_2$(As$_{0.68}$P$_{0.32}$)$_2$ (b, d) with γ-ray beam parallel to sample normal (a, b), and in the magic angle (c, d). Components used in the fit were a paramagnetic doublet (green) and an unresolved doublet (violet). This picture was taken from **Publication 5**.

recorded at selected temperatures are shown in Figs. 5.7 and 5.8. As seen from Fig. 5.7 the main doublet of the Ba-sample remains asymmetric even at temperatures below ∼270 K, while the Fe_2P impurity undergoes a magnetic transition [91–93], which allows us to exclude the possibility that this phase causes the doublet asymmetry.

At lower temperatures (below ∼140 K) a small broadening of the main doublet of the ^{57}Fe Mössbauer spectra was observed for both the Ba- and the Eu-sample. This broadening remains visible down to 6.1 K (for Ba-sample) and 77 K (for Eu-sample). During the fit procedure, the second component with the small quadrupole splitting value can be fitted by a paramagnetic doublet with a magnetic field distribution whereas the first component of the main phase in the Ba- and Eu-samples is essentially identical to the room temperature cases. It is known that in the parent AFe$_2$As$_2$ compounds spin-density wave (SDW) behavior was observed below ∼140 K and these materials undergo a magnetic transition at this temperature [86, 94]. The presence of SDW behavior below ∼140 K in one of our samples (Ba-sample) is visible in the SQUID data, Fig. 5.3, where the deviation of the ZFC curve from a straight line is observed. The observed SDW behavior also suggests that this spectral component can be assigned to the iron atoms with a pure arsenic surrounding. Also the conclusion about coexistence of magnetism and superconductivity in the BaFe$_2$(As$_{0.68}$P$_{0.32}$)$_2$ as well as EuFe$_2$(As$_{0.8}$P$_{0.2}$)$_2$ samples can be made based on the fact that the broadening of the main component is visible in the spectra down to lowest measuring temperatures (6.1 K for the Ba-sample).

A more detailed explanation of the complex main component of the RT Mössbauer spectra can be constructed from a study of the iron-atom surroundings. As mentioned above, in the parent compound AFe$_2$As$_2$ one iron atom is coordinated by four neighboring arsenic atoms. Therefore in the arsenic-substituted AFe$_2$(As$_{1-x}$P$_x$)$_2$ material one iron atom can have from one to four nearest phosphorus atoms in its surrounding. The number of phosphorus atoms in the iron surrounding influences the hyperfine properties of Fe and, thus, shape of the Mössbauer spectrum. X-ray powder diffraction can not detect this effect because no long-range ordering between P and As occurs.

According to the binomial distribution of the phosphorus atoms the iron environments with 2 or 3 phosphorus atoms also give a contribution to the quadrupole splitting. These contributions were included in the value of the quadrupole splitting (and intensity) for the dominating 1P3As environment. However, due to chemical reasons the possibility for having several phosphorus nearest-neighbors may differ from such a statistic model. This can be reason behind the differences between experimental and binomial calculated values is observed in the Table 5.1.

The dependence of the quadrupole splitting value on the iron surrounding and the number of phosphorus in the surrounding was studied by DFT calculations. The calculations were made using the ORCA program version 3.0.2 [95, 96]. The quadrupole splitting parameter (ΔE_Q) can be calculated using the components of the tensor of the electric field gradient (EFG):

$$\Delta E_Q = \frac{1}{2} e Q V_{zz} \sqrt{1 + \frac{1}{3}\eta^2}, \tag{5.1}$$

where V_{xx}, V_{yy} and V_{zz} are the principal components of the EFG tensor at the iron nuclei, e is the electron charge, Q the nuclear quadrupole moment and η the asymmetry parameter:

$$\eta = \left| \frac{V_{xx} - V_{yy}}{V_{zz}} \right|, \tag{5.2}$$

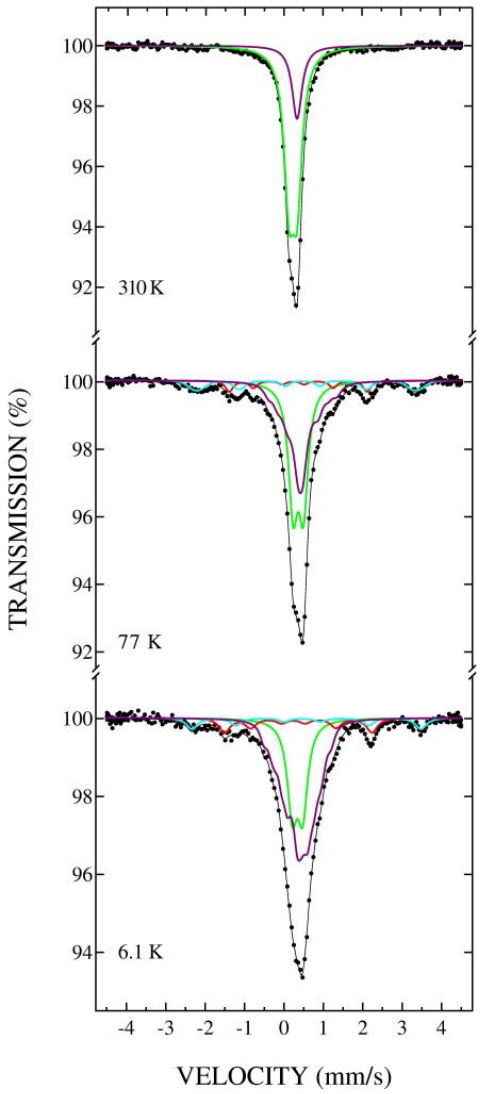

Figure 5.7: ^{57}Fe Mössbauer spectra of BaFe$_2$(As$_{0.68}$P$_{0.32}$)$_2$ recorded at 6.1 K, 77 K and 310 K. Components due to the paramagnetic doublet and the unresolved doublet which broadens magnetically (green and violet, respectively), and the magnetic Fe$_2$P impurity (blue and red) are indicated. This picture was taken from **Publication 5**.

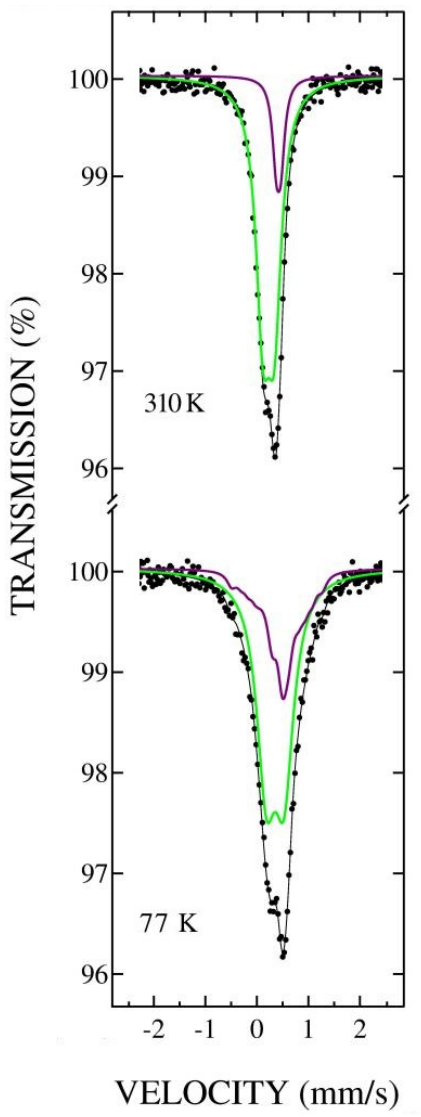

Figure 5.8: ^{57}Fe Mössbauer spectra of $EuFe_2(As_{0.8}P_{0.2})_2$ recorded at 77 K and 310 K. Components due to the paramagnetic doublet and the unresolved doublet which broadens magnetically (green and violet, respectively) are indicated. This picture was taken from **Publication 5**.

where the labeling of the axes are chosen to achieve $|V_{xx}| \leq |V_{yy}| \leq |V_{zz}|$. The EFG tensor was found from the ground state electron density as an expectation value of the field gradient operator [95].

Calculations for a cluster containing one iron atom and four neighbors were made for the five situations with four arsenic (4As), one phosphorus and three arsenic (1P3As), two phosphorus and two arsenic (2P2As), three phosphorus and one arsenic (3P1As), and four phosphorus (4P) which were taken as nearest atoms to the iron atom in the center of the cluster.

During the calculations the B3LYP hybrid density functional in the NORI approximation with a Gaussian-type basis set TZVP of Ahlrichs for the geometry optimizations with "SpecialGrid7" [97] were used. A standard enlarged CP(PPP) basis set for iron atoms was used for the quadrupole-interaction calculation. The experimentally found iron-low-spin-state (S = 0) approximation was taken as a starting point and an increased value of iteration steps (up to 2000) were used in the more difficult cases of 1As3P and 1As2P iron environments. The coordinates of Fe, As and P atoms were taken from the experimental XRD data. Calculated and experimentally found data of quadrupole splitting value are presented in Table 5.2. It is seen that the calculated quadrupole-

Table 5.2: Calculated (using DFT) and experimental quadrupole splitting values. This Table was taken form **Publication 5**.

calc. QS, mm/s					exp. QS, mm/s	
4As	1P3As	2P2As	3P1As	4P	1st comp.*	2nd comp.**
EuFe$_2$(As$_{0.8}$P$_{0.2}$)$_2$						
0.077	0.164	0.383	0.723	0.996	0.119	0.060
BaFe$_2$(As$_{0.68}$P$_{0.32}$)$_2$						
0.041	0.264	−0.207	0.834	−0.211	0.216	0.003
η values for BaFe$_2$(As$_{0.68}$P$_{0.32}$)$_2$						
0.057	0.069	0.844	0.235	0.344	–	–

* assigned to 1P3As; ** assigned to 4As.

splitting values for iron atom that has one phosphorus, three arsenic (1P3As) and four arsenic (4As) in the environment are in good agreement with the experimental values. The obtained calculation results confirm the preferred formation of iron atom surrounding with 1P3As and 4As neighbors in AFe$_2$(As$_{1-x}$P$_x$)$_2$ (A =Ba, Eu) compounds during the substitution process and confirm a distinct difference in hyperfine-parameter values.

CHAPTER VI

Conclusions

Chalcogenide- and pnictide-based polycrystalline samples of iron-based superconductors were successfully synthesized by solid-state reaction and the properties of these samples were studied.

Polycrystalline samples of Fe-chalcogenide $FeTe_{1-x}S_x$ with x = 0.05, 0.10 and 0.20 were synthesized by a vacuum solid-state reaction method. The purity of the synthesized samples was checked by powder X-ray diffraction. Mössbauer spectroscopy gave also additional information about phase content in the samples. The superconducting transition temperature $T_c \approx 8\ K$ was found by SQUID measurements for all obtained samples, excluding the sample having $x = 0.05$. The influence of the number of sintering times on the phase content and superconductivity properties of obtained materials was studied. Improvement of superconductivity transition using oxygen post-annealing was achieved for $FeTe_{0.8}S_{0.2}$. Mössbauer spectroscopy data obtained below and above T_c showed the creation of a low-temperature (below ∼77 K) magnetic ordering of a part of the main phase. The temperature dependence of this internal magnetic field was studied. An unusual behavior of the hyperfine field for the Fe atoms belonging to the antiferromagnetic regions was observed and the evolution of the magnetic hyperfine field for samples $FeTe_{1-x}S_x$, x = 0.05 to 0.20, was reported.

For the non-superconducting sample (x = 0.05) the temperature dependence of the average internal magnetic field shows a straight line which increases from ∼77 K to the lowest measured temperature of 6.8 K. For the superconducting samples $FeTe_{0.8}S_{0.2}$ and $FeTe_{0.9}S_{0.1}$ the internal field depended on the superconductivity transition temperature. The internal field value increases up to T_c and then drops below T_c. This result, as well as the observed temperature dependencies of the magnetic fraction in the sample $FeTe_{0.8}S_{0.2}$ and the intensity ratio in the $FeTe_{0.8}S_{0.2}$ (S2), indicates the existence of a competition between magnetism and superconductivity in $FeTe_{1-x}S_x$ and the suppression of the magnetic ordering by the emerging superconductivity.

Fe-chalcogenide $FeSe_{1-x}$ samples were synthesized by a vacuum solid-state reaction method. An evasive secondary phase with a large quadrupole splitting value of ∼1.7 mm/s was the object of our study. It was found that this secondary phase appears in the sample along with the main paramagnetic phase only after the second synthesis step. A quench into a liquid nitrogen or cold water was used during the synthesis. Optimization of the synthesis conditions employing a higher synthesis temperature of 750°C, gave more intensive Mössbauer resonance lines for the secondary phase.

Polycrystalline samples $FeSe_{1-x}$ with $(1 - x)$ = 0.6, 0.75, 0.82 and 0.9 were synthesized by a two-step reaction with a quench of the ampule into water or liquid N_2, yielding samples exhibiting

presence of the secondary phase. X-ray diffraction data couldn't be matched to any known phase from PDF4 database; the XRD data refinement in compatible with an orthorhombic phase with lattice parameters $a \approx 8.52$ Å, $b \approx 6.96$ Å, and $c \approx 4.90$ Å.

A superconductivity transition at $\sim$8 K for the main phase was found in the samples $FeSe_{0.82}$ and $FeSe_{0.9}$ by SQUID measurements of the temperature dependence of the magnetic susceptibility.

The hyperfine interactions in the obtained $FeSe_{1-x}$ samples were studied by Mössbauer spectroscopy. The isomer shift value of the secondary phase is compatible with high-spin state divalent iron while the main phase iron atoms are in a divalent low-spin state. According to the Mössbauer spectroscopy data taken at various temperatures this secondary phase undergoes a magnetic transition at $T_m \approx$104 K.

Polycrystalline phosphorus-substituted samples $A Fe_2(As_{1-x}P_x)_2$ with A =Ba and Eu were synthesized by a solid-state reaction method in an Ar atmosphere. Sample stoichiometries correspond to $BaFe_2(As_{0.68}P_{32})_2$ and $EuFe_2(As_{0.8}P_{0.2})_2$. The obtained samples were examined by XRD, SQUID, and ^{57}Fe, ^{151}Eu Mössbauer spectroscopy. For both the Ba- and Eu-samples two different Fe environments contribute to the ^{57}Fe Mössbauer spectra. Isomer shifts values indicate a trivalent high-spin state iron and divalent low-spin state iron in these components. The isomer shift of -12 mm/s confirms the +2 valence state of Eu atoms. Two observed components in the spectra were assigned to the iron tetrahedral coordinations of 4As and 1P3As. Binomial distribution and DFT calculations confirm this assignment.

Low-temperature Mössbauer spectroscopy results show a broadening of the component assigned to 4As down to 6 K, suggesting a magnetic ordering of iron atoms coordinated to four As atoms in the main phase. Below the transition temperature of T_c = 30 K magnetic ordering coexists with superconductivity for the Ba-sample.

[1] S. Uchida, J. Phys. Soc. Jpn. **77**, 9 (2008).

[2] H. Hosono, J. Phys. Soc. Jpn. **77**, 1 (2008)

[3] F.-Ch. Hsu, J.-Y. Luo, K.-W. Yeh, T.-K. Chen, T.-W. Huang, Ph. M. Wu, Y.-Ch. Lee, Y.-L. Huang, Y.-Y. Chu, D.-Ch. Yan, and M.-K. Wu, Proc. Natl. Acad. Sci. U.S.A. **105**, 14262 (2008).

[4] G. E. Grechnev, A. S. Panfilov, V. A. Desnenko, A. V. Fedorchenko, S. L. Gnatchenko, D. A. Chareev, O. S. Volkova and A. N. Vasiliev, J. Phys.: Condens. Matter **25** 046004 (2013).

[5] Y. Kamihara, T. Watanabe, M. Hirano, and H. Hosono, J. Am. Chem. Soc. **130**, 3296 (2008).

[6] K. Jin, N. P. Butch, K. Kirshenbaum, J. Paglione and R. L. Greene, Nature **476**, 73 (2011).

[7] I. Felner, U. Asaf, Y. Levi, and O. Millo, Phys. Rev. B **55** R3374 (1997).

[8] S. Malo, D. Ko, J. T. Rijssenbeek, A. Maignan, D. Pelloquin, V. P. Dravid, K. R. Poeppelmeier, Int. J. Inirg. Mater. **2**, 601 (2000).

[9] Z. A. Ren, G. C. Che, H. Xiong, K. Q. Li, Y. S. Yao, D. N. Zheng, Y. M. Ni, S. L. Jia, C. Dong, H. Chen, J. L. Shen, Z. X. Zhao, Solid State Commun. **119**, 579 (2001).

[10] J. Lindén, M. Karppinen, I. Grigoravičiūtė, H. Yamauchi, Phys. Rev. Lett. **98**, 067001 (2007).

[11] S. V. Chong, S. Hashimoto and K. Kadowaki, Solid State Commun. **150**, 1178 (2010).

[12] Z. Gao, Y. Qi, L. Wang, Ch. Yao, D. Wang, X. Zhang, Y. Ma, Physica C: Supercond. **492**, 18 (2013).

[13] D. J. Singh, Sci. Technol. Adv. Mater. **13**, 054304 (2012).

[14] J. Wen, PhD thesis, Stony Brook University, (2010).

[15] J. Wen, G. Xu, G. Gu, J. M. Tranquada and R. J. Birgeneau, Rep Prog. Phys. **74**, 124503 (2011).

[16] D. K. Pratt, W. Tian, A. Kreyssig, J. L. Zarestky, S. Nandi, N. Ni, S. L. Bud'ko, P. C. Canfield, A. I. Goldman, and R. J. McQueeney, Phys. Rev. Lett. **103**, 087001 (2009).

[17] J.-Q. Yan, S. Nandi, J. L. Zarestky, W. Tian, A. Kreyssig, B. Jensen, A. Kracher, K. W. Dennis, R. J. McQueeney, A. I. Goldman, R. W. McCallum, and T. A. Lograsso, Appl. Phys. Lett. **95**, 222504 (2009).

[18] D. Mendoza, J. L. BenItez, F. Morales, R. Escudero, Solid State Commun. **150**, 1124 (2010).

[19] A. S. Sefat, Curr. Opin. Solid State Mat. Sci. **17**, 59 (2013).

[20] S. W. Kim, Y. Kamihara, S.-G. Yoon, H.-S. Han, T. Nomura, S. Matsuishi, K. Nakao, K. Tanabe, M. Hirano, and H. Hosono, J. Phys. Soc. Jpn. Supplement C **77**, 23 (2008).

[21] P. C. Canfield and I. R. Fisher, J. Crystal Growth **225**, 155 (2001).

[22] P. C. Canfield and Z. Fisk, Philos. Mag. B **65**, 1117 (1992).

[23] X. L. Shen, J. At. Mol. Sci. **3**, 89 (2012).

[24] J. Rodriquez-Carvajal, Physica B **192**, 55 (1993).

[25] Y. Mizuguchi, F. Tomioka, S. Tsuda, T. Yamaguchi, and Y. Takano, Appl. Phys. Lett. **94**, 012503 (2009).

[26] Y. Mizuguchi and Y. Takano, J. Phys. Soc. Jpn. **79**, 102001 (2010).

[27] R. Hu, E. S. Bozin, J. B. Warren, and C. Petrovic, Phys. Rev. B **80**, 214514 (2009).

[28] P. Zajdel, P.-Y. Hsieh, E. E. Rodriguez, N. P. Butch, J. D. Magill, J. Paglione, P. Zavalij, M. R. Suchomel, M. A. Green, J. Am. Chem. Soc. **132** 13000 (2010).

[29] Y. Mizuguchi, T. Furubayashi, K. Deguchi, S. Tsuda, T. Yamaguchi, Y. Takano, Physica C **470**, S338 (2010).

[30] K. Deguchi, Y. Takano and Y. Mizuguchi, Sci. Technol. Adv. Mater. **13**, 054303 (2012).

[31] M. K. Wu, F. C. Hsu, K. W. Yeh, T. W. Huang, J. Y. Luo, M. J. Wang, H. H. Chang, T. K. Chen, S. M. Rao, B. H. Mok, C. L. Chen, Y. L. Huang, C. T. Ke, P. M. Wu, A. M. Chang, C. T. Wu, T. P. Perng, Physica C **469**, 340 (2009).

[32] Y. Qiu, W. Bao, Y. Zhao, C. Broholm, V. Stanev, Z. Tesanovic, Y. C. Gasparovic, S. Chang, J. Hu, B. Qian, M. Fang, and Z. Mao, Phys. Rev. Lett. **103**, 067008 (2009).

[33] H. Shi, Z.-B. Huang, J. S. Tse, and H.-Q. Lin, J. Appl. Phys. **110**, 043917 (2011).

[34] M. A. McGuire, A. D. Christianson, A. S. Sefat, B. C. Sales, M .D. Lumsden, R. Jin, E. A. Payzant, D. Mandrus, Y. Luan, V. Keppens, V. Varadarajan, J. W. Brill, R. J. Hermann, M. T. Sougrati, F. Grandjean, G. J. Long, Phys. Rev. B **78**, 094517 (2008).

[35] C. de la Cruz, Q. Huang, J. W. Lynn, J. Y. Li, W. Ratcliff, J. L. Zarestky, H. A. Mook, G. F. Chen, J. L. Luo, N. L. Wang, P. C. Dai, Nature **453**, 899 (2008).

[36] W. Bao, Y. Qiu, Q. Huang, M. A. Green, P. Zajdel, M. R. Fitzsimmons, M. Zhernenkov, S. Chang, Minghu Fang, B. Qian, E. K. Vehstedt, Jinhu Yang, H. M. Pham, L. Spinu, and Z. Q. Mao, Phys. Rev. Lett. **102**, 247001 (2009).

[37] M. J. Han and S. Y. Savrasov, Phys. Rev. Lett. **103**, 067001 (2009).

[38] D. Lumsden, A. D. Christianson, E. A. Goremychkin, S. E. Nagler, H. A. Mook, M. B. Stone, D. L. Abernathy, T. Guidi, G. J. MacDougall, C. de la Cruz, A. S. Sefat, M. A. McGuire, B. C. Sales and D. Mandrus, Nature Phys. **6**, 182 (2010).

[39] L. Zhang, D. J. Singh, and M. H. Du, Phys. Rev. B **79**, 012506 (2009).

[40] Y. Mizuguchi, F. Tomioka, S. Tsuda, T. Yamaguchi, and Y. Takano, Appl. Phys. Lett. **93**, 152505 (2008).

[41] Y. Han, W. Y. Li, L. X. Cao, X. Y. Wang, B. Xu, B. R. Zhao, Y. Q. Guo, and J. L. Yang, Phys. Rev. Lett. **104**, 017003 (2010).

[42] H. Takahashi, H. Okada, H. Takahashi, Y. Mizuguchi, and Y. Takano, J. of Phys.: Conf. Ser. **200**, 012196 (2010).

[43] Ch. Zhang, W. Yi, L. Sun, X.-J. Chen, R. J. Hemley, H.-K. Mao, W. Lu, X. Dong, L. Bai, J. Liu, A. F. Moreira Dos Santos, J. J. Molaison, C. A. Tulk, G. Chen, N. Wang, and Z. Zhao, Phys. Rev. B **80**, 144519 (2009).

[44] K.-W. Yeh, T.-W. Huang, Y.-L. Huang, T.-K. Chen, F.-Ch. Hsu, P. M. Wu, Y.-Ch. Lee, Y.-Y. Chu, Ch.-L. Chen, J.-Y. Luo, D.-Ch. Yan and M.-K. Wu, Europhys. Lett. **84**, 37002 (2008).

[45] M. H. Fang, H. M. Pham, B. Qian, T. J. Liu, E. K. Vehstedt, Y. Liu, L. Spinu, and Z. Q. Mao, Phys. Rev. B **78**, 224503 (2008).

[46] I. Pallecchi, G. Lamura, M. Tropeano, and M. Putti, Phys. Rev. B **80**, 214511 (2009).

[47] H. Okazaki, T. Watanabe, T. Yamaguchi, Y. Kawasaki, K. Deguchi, S. Demura, T. Ozaki, S. J. Denholme, Y. Mizuguchi, H. Takeya, and Y. Takano, J. Phys. Soc. Jpn. **81**, 113707 (2012).

[48] T. Taen, Y. Tsuchiya, Y. Nakajima, and T. Tamegai, Phys. Rev. B **80**, 092502 (2009).

[49] D. J. Gawryluk, J. Fink-Finowicki, A. Wisniewski, R. Puzniak, V. Domukhovski, R. Diduszko, M. Kozlowski and M. Berkowski, Supercond. Sci. Technol. **24**, 065011 (2011).

[50] A. S. Sefat, R. Jin, M. A. McGuire, B. C. Sales, D. J. Singh, and D. Mandrus, Phys. Rev. Lett. **101**, 117004 (2008).

[51] Yu. D. Tretyakov, Soros Educ. Journal, 35 (1999).

[52] K. Deguchi, Y. Mizuguchi, Y. Kawasaki, T. Ozaki, S. Tsuda, T. Yamaguchi and Y. Takano, Supercond. Sci. Technol. **24**, 055008 (2011).

[53] W. A. Dollase, J. Appl. Crystallogr. **19**, 267 (1986).

[54] Y. Mizuguchi, K. Deguchi, T. Ozaki, M. Nagao, S. Tsuda, T. Yamaguchi, and Y. Takano, IEEE T. Appl. Supercon. **21**, 2866 (2011).

[55] V. P. S. Awana, A. Pal, A. Vajpayee, B. Gahtori,Kishan H., Physica C **471**, 77 (2011).

[56] A. Błachowski, K. Ruebenbauer, P. Zajdel, E. E. Rodriguez and M. A. Green, J. Phys.: Condens. Matter. **24**, 386006 (2012).

[57] V. Fano and I. Ortalli, Phys. Stat. Sol. (a) 10 (1972) K121.

[58] K. V. Reddy and S. C. Chetty, Phys. Stat. Sol. (a) **37**, 687 (1976).

[59] J. B. Ward and V. H. McCann, J. Phys. C: Solid State Phys. **12**, 873 (1979).

[60] K. W. Lodge, J. Phys. F: Met. Phys. **9**, 2035 (1979).

[61] G. Hägg and A. L. Kindström, Z. Phys. Chem B **22**, 453 (1933).

[62] H. Okamoto, J. Phase Equilib. **12**, 383 (1991).

[63] S. Margadonna, Y. Takabayashi, M. T. McDonald, K. Kasperkiewicz, Y. Mizuguchi, Y. Takano, A. N. Fitch, E. Suard, K. Prassides, Chem. Commun., 5607 (2008).

[64] T. Imai, K. Ahilan, F. L. Ning, T. M. McQueen, and R. J. Cava, Phys. Rev. Lett. **102**, 177005 (2009).

[65] S. Medvedev, T. M. McQueen, I. A. Troyan, T. Palasyuk, M. I. Eremets, R. J. Cava, S. Naghavi, F. Casper, V. Ksenofontov, G. Wortmann and C. Felser, Nature Mater. **8**, 630 (2009).

[66] M. de Souza, A.-A. Haghighirad, U. Tutsch, W. Assmus, and M. Lang, Eur. Phys. J. B **77**, 101 (2010).

[67] T. M. McQueen, Q. Huang, V. Ksenofontov, C. Felser, Q. Xu, H. Zandbergen, Y. S. Hor, J. Allred, A. J. Williams, D. Qu, J. Checkelsky, N. p Ong, and R. J. Cava , Phys. Rev. B **79**, 014522 (2009).

[68] M. Bendele, A. Amato, K. Conder, M. Elender, H. Keller, H.-H. Klauss, H. Luetkens, E. Pomjakushina, A. Raselli, and R. Khasanov, Phys. Rev. Lett. **104**, 087003 (2010).

[69] J.-P. Libäck, Master's Thesis, Åbo Akademi, (2010).

[70] H. H. Hamdeh, M. M. El-Tabey, R. Asmatulu, J. C. Ho, T. W. Huang, K. W. Yeh and M. K. Wu, Eur. Phys. Lett. **89**, 67009 (2010).

[71] J. L. Pimentel Jr, F. C. Serbena, A. R. Jurelo, J. Supercond. Nov. Magn. **24**, 1437 (2011).

[72] Ch.-M. Yang, P.-W. Chen, J.-Ch. Kou, P. Diko, I.-G. Chen, and M.-K. Wu, IIEEE T. Appl. Supercon. **21**, 2845 (2011).

[73] J. Lindén, E.-L. Rautama, M. Karppinen, H. Yamauchi, Hyperfine Interact. **208**, 133 (2012).

[74] G. Cao, S. Xu, Z. Ren, S. Jiang, C. Feng and Z. Xu, J. Phys.: Condens. Matter. **23**, 464204 (2011).

[75] T. Iye, Y. Nakai, S. Kitagawa, K. Ishida, S. Kasahara, T. Shibauchi, Y. Matsuda, and T. Terashima, J. Phys. Soc. Jpn. **81**, 033701 (2012).

[76] Z. Ren, Z. Zhu, S. Jiang, X. Xu, Q. Tao, C. Wang, C. Feng, G. Cao, and Z. Xu, Phys. Rev. B **78**, 052501 (2008).

[77] S. Ikeda, K. Yoshida, and H. Kobayashi, J. Phys. Soc. Jpn. **81**, 033703 (2012).

[78] A. Błachowski, K. Ruebenbauer, J. Żukrowski, K. Rogacki, Z. Bukowski, and J. Karpinski, Phys. Rev. B **83**, 134410 (2011).

[79] Q. Huang, Y. Qiu, Wei Bao, M. A. Green, J. W. Lynn, Y. C. Gasparovic, T. Wu, G. Wu, and X. H. Chen, Phys. Rev. Lett. **101**, 257003 (2008).

[80] M. Kofu, Y. Qiu, Wei Bao, S.-H. Lee, S. Chang, T. Wu, G. Wu and X. H. Chen, New J. Phys. **11**, 055001 (2009).

[81] S. Jiang, H. Xing, G. Xuan, C. Wang, Z. Ren, C. Feng, J. Dai, Z. Xu and G. Cao, J. Phys.: Condens. Matter **21**, 382203 (2009).

[82] Z. Ren, Q. Tao, S. Jiang, C. Feng, C. Wang, J. Dai, G. Cao, and Z. Xu, Phys. Rev. Lett. **102**, 137002 (2009).

[83] D. Mandrus, A. S. Sefat, M. A. McGuire, and B. C. Sales, Chem. Mater. **22**, 715 (2010).

[84] Y. Tokiwa, S.-H. Hübner, O. Beck, H. S. Jeevan, and P. Gegenwart, Phys. Rev. B **86**, 220505 (2012).

[85] H. S. Jeevan, D. Kasinathan, H. Rosner, and P. Gegenwart, Phys. Rev. B **83**, 054511 (2011).

[86] M. Rotter, M. Tegel, and D. Johrendt, I. Schellenberg, W. Hermes, and R. Pöttgen, Phys. Rev. B **78**, 020503 (2008).

[87] M. M. geb. Rotter, Dissertation zur Erlangung des Doktorgrades der Fakultät für Chemie und Pharmazie der Ludwig-Maximilians-Universität München, (2010).

[88] I. Nowik, I. Felner, Z. Ren, G. H. Cao and Z. A. Xu, J. Phys.: Condens. Matter. **23**, 065701 (2011).

[89] C. Feng, Z. Ren, S. Xu, S. Jiang, Z. Xu, G. Cao, I. Nowik, I. Felner, K. Matsubayashi, and Y. Uwatoko, Phys. Rev. B **82**, 094426 (2010).

[90] H. Raffius, E. Mörsen, B. D. Mosel, W. Müller-Warmuth, and T. Hilbich, M. Reehuis, T. Vomhof and W. Jeitschko, J. Phys. Chem. Solids **52**, 787 (1991).

[91] R. E. Bailey and J. F. Duncan, Inorganic Chemistry **8**, 1444 (1967).

[92] K. Sato, K. Adachi, and E. Ando, J. Phys. Soc. Jpn. **26**, 855 (1969).

[93] T. Ericsson, L. Häggstrom, R. Wäppling and T. Methasiri, Physica Scripta **21**, 212 (1980).

[94] A. Khasanov, J. Jiang, E. E. Hellstrom and A. Nath, J. Phys.: Condens. Matter. **23**, 342201 (2011).

[95] F. Neese, Coord. Chem. Rev. **253**, 526 (2009).

[96] F. Neese, Comput. Molec. Science **2**, 73 (2012).

[97] A. Schäfer, C. Huber, R. Ahlrichs, J. Chem. Phys. **100**, 5829 (1994).

PART II: PUBLICATIONS

PUBL. I

A. Sklyarova, J. Lindén, E.-L. Rautama, and M. Karppinen, A ^{57}Fe Mössbauer study of $FeTe_{1-x}S_x$, *J. Magn. Magn. Matter.*, 329, 129, 2013.

Journal of Magnetism and Magnetic Materials 329 (2013) 129–132

Contents lists available at SciVerse ScienceDirect

Journal of Magnetism and Magnetic Materials

journal homepage: www.elsevier.com/locate/jmmm

A ^{57}Fe Mössbauer study of $FeTe_{1-x}S_x$

A. Sklyarova [a,b], J. Lindén [a,*], E.-L. Rautama [c], M. Karppinen [c]

[a] Department of Physics, Åbo Akademi, FI-20500 Turku, Finland
[b] Lappeenranta University of Technology, Faculty of Physics, Box 20, 53851 Lappeenranta, Finland
[c] Department of Chemistry, Aalto University, FI-00076 Aalto, Finland

ARTICLE INFO

Article history:
Received 18 June 2012
Received in revised form
28 September 2012
Available online 17 October 2012

Keywords:
Chalcogenide superconductor
^{57}Fe Mössbauer spectroscopy

ABSTRACT

A polycrystalline $FeTe_{1-x}S_x$ sample was synthesized using a solid-state reaction method. Magnetization data obtained in the zero-field cooling and field-cooling regimes revealed a superconductivity transition with the critical temperature $T_c \approx 10$ K. ^{57}Fe Mössbauer spectra were recorded in the temperature interval from 5.4 to 300 K in transmission geometry to reveal three components below 77 K: two magnetic and one paramagnetic. One of the magnetic components and the paramagnetic component belong to the $FeTe_{1-x}S_x$ phase. Unusual behavior of hyperfine field for the smaller of the magnetic components was observed, signifying possible competition between antiferromagnetism and superconductivity.

1. Introduction

Three years ago a new type of high-T_c superconducting family containing iron was discovered [1]. Along with iron, elements from the chalcogenide (S, Se or Te) or pnictide (P or As) groups are needed to form the superconducting phase. At the present time, iron-based superconductors are intensively studied owing to the fact that these materials show rather high critical temperatures. Also one reason why iron-based superconductors have recently attracted interest of researchers is the coexistence of superconductivity and magnetism in some of these materials [2,3]. Superconductors with simple structures like the 1:1 composition for FeSe or $FeA_{1-x}B_x$ where A is Te or K, and B is Se or S, are easy to study due to the simplicity of preparation of such samples. Investigating various material properties on either side of the transition temperature may increase our understanding of the mechanism of superconductivity in these materials. The $FeTe_x$ system with different values of x has been studied a lot [4]. It exhibits various structures depending on the Fe–Te ratio [4–6]. An iron excess causes structural transformation. Below 70 K the Fe–Te compounds exhibit an antiferromagnetic ordering and do not show superconducting properties. Superconductivity in these materials starts to appear at the substitution of a part of the tellurium by chalcogenide atoms like Se or S and is sensitive to the amount of substituting atoms [7]. In contrast to the FeSe phase where superconductivity can be enhanced by an applied hydrostatic pressure [8], in $FeTe_{1+x}$ pressure does not bring forth superconductivity. The synthesis of phase pure sulphur substituted samples $FeTe_{1-x}S_x$ is a difficult process because tellurium ions have big radii in comparison with the sulphur ions. With increasing sulphur content in $FeTe_{1-x}S_x$ impurity phases appear due to the solubility limit of sulphur [9]. The coexistence of superconductivity and antiferromagnetism has been reported for $FeTe_{1-x}S_x$ [10–12]. This makes it an interesting object of study as compared to FeSe and Fe(Te,Se) in which the normal state is magnetically unordered. In this work we synthesized a sample with the nominal $FeTe_{0.8}S_{0.2}$ composition and studied the magnetic properties of it using ^{57}Fe Mössbauer spectroscopy.

2. Experimental

A polycrystalline $FeTe_{1-x}S_x$ sample was synthesized using a solid-state reaction method. For production of the TeS precursor material Te (ALDRICH Chemistry, 99.8%) and S (MERCK, DAB 6) powders (1:1) were mixed, sealed in an evacuated quartz tube and annealed at 400 °C for 12 h and furnace cooled to room temperature. The sample was reground, mixed with Fe (Bureau of Analysed Samples, Ltd, nominally 99.95%, but contains traces of oxygen uptake during storage) and Te in appropriate quantities, placed in an evacuated quartz tube and annealed at 600 °C for 12 h. The superconductivity properties were checked with SQUID measurements (Quantum Design, MPMS-XL) in zero-field cooling and field-cooling (10 Oe) regimes using a sample of 30 mg. Phase purity was checked with X-ray diffraction using Cu K α1 radiation (PanAnalytical X'Pert Pro MPD diffractometer) in an ordinary $\theta-2\theta$ geometry. ^{57}Fe Mössbauer spectroscopy was used to investigate the magnetic properties. The sample was reground and

* Corresponding author. Tel.: +358 2 215 4239.
E-mail address: jlinden@abo.fi (J. Lindén).

0304-8853/$ - see front matter © 2012 Published by Elsevier B.V.
http://dx.doi.org/10.1016/j.jmmm.2012.10.013

50 mg of the powder was used for the Mössbauer absorbers. The Mössbauer spectra were measured using a ^{57}Co:Rh source in transmission geometry with Doppler velocities of 8 mm/s, allowing detection of magnetic phases. Measurements were done at selected temperatures between 5.4 and 300 K. The sample was cooled using an Oxford CF506 continuous-flow cryostat with liquid He as a coolant below 77 K and liquid N_2 at and above 77 K. All spectra were fitted with the following Mössbauer parameters: hyperfine field for magnetic components, quadrupole splitting, relative intensity and isomer shift relative to α-Fe. Three components were used in the fitting procedure: one magnetic component (C_1) with a higher hyperfine field (32.6 T at 10 K), a magnetic component (C_2) with a small value of the hyperfine field (9.2 T at 10 K), and a paramagnetic component (C_3). The line widths of components C_2 and C_3 were constrained to be equal. The internal field of the magnetic components exhibited broadening. Therefore, a gaussian distribution of the field with the width ΔB as a fit parameter was included. For the paramagnetic component the angle between wave vector and the z-axis of the electric field gradient was entered as a fit parameter that indicates a crystalline texture for the main phase of our sample. The angle was fixed to the room temperature value at temperatures below 77 K.

3. Results and discussion

The phase composition of the $FeTe_{1-x}S_x$ sample was checked by X-ray powder diffraction, Fig. 1. The XRD pattern revealed that the sample consists of $FeTe_{1-x}S_x$ as a majority phase but shows also presence of FeS and $FeTe_2$. It was also observed that the $FeTe_{1-x}S_x$ phase has a strong preferred orientation along 00l direction. To obtain the fractional amounts of each phase, the pattern was refined using the Rietveld method and the program FullProf [13]. To take the preferential orientation into account, the modified March function (integrated in the software package) was applied. This led to satisfactory fit result, as presented in Fig. 1. The refined texture parameter indicated plate-type crystals, consistent with visual observation. The refined fractional portions of each phase were ca. 93%, 2% and 5% for FeTe, FeS and $FeTe_2$, respectively. Sulphur atoms can replace a part of the tellurium atoms and the value of the c parameter will reveal the S concentration [14]. The c lattice parameter was fitted to 6.275 Å

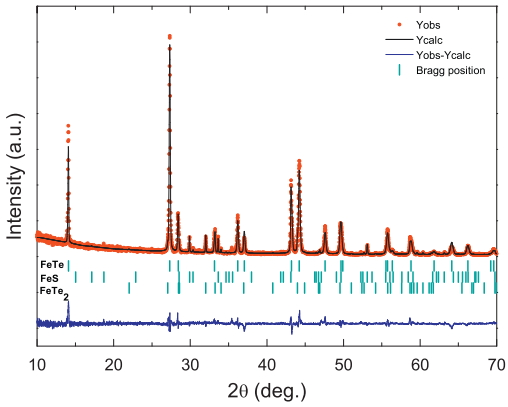

Fig. 1. X-ray powder diffraction pattern and Rietveld refinement profile of $FeTe_{1-x}S_x$. Minority phases are indicated below the main phase. Tetragonal P4/nmm space group was used in the refinement for the main phase.

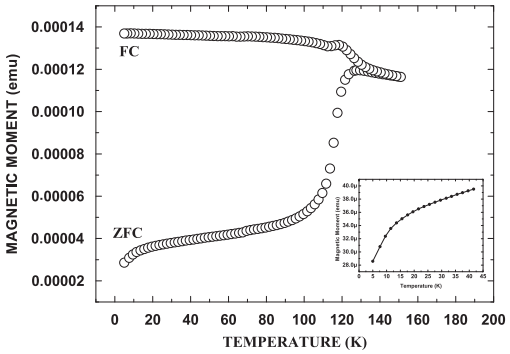

Fig. 2. Magnetic moment vs. temperature obtained in field-cooling (FC) and zero-field-cooling (ZFC) regimes of the SQUID measurements. The inset shows the transition region in more detail.

indicating a 3.9% uptake of S. SQUID data obtained in the ZFC regime reveal the onset of a superconductivity transition with the critical temperature $T_c \approx 10$ K, Fig. 2. From studies of similar compounds it is known that the superconducting fraction in $FeTe_{1-x}S_x$ increases with exposure of the sample to air, annealing in an oxygen atmosphere or by immersing the sample in water [6,15]. Due to using as-synthesized sample – without any additional procedures – the magnetic moment in the FC regime does not show a proper superconducting transition and the magnetization curve in ZFC regime only starts to show a down turn. Such behavior indicates that the superconductivity volume fraction is very small. At 125 K the magnetic moment curve shows an anomaly. It coincides with the Verwey transition of magnetite. The Mössbauer spectra do not show presence of magnetite as the high-velocity spectra were not measured to high enough statistics.

Selected Mössbauer spectra are shown in Fig. 3. Up to 77 K all spectra were fitted by two magnetic components (C_1) and (C_2) and one paramagnetic doublet (C_3). One of the magnetic components in the spectra – C_1 – can be attributed to an impurity phase. The impurity magnetic component covers $\sim$40% at 5.4 K and $\sim$30% of the total spectrum area at 300 K. The magnetic hyperfine field ($\sim$32.5 T at 5.4 K) exhibits a weak temperature dependence between 5.4 and 300 K, indicating a high Néel temperature. Using the XRD data and the internal field value component C_1 can be ascribed to the FeS phase. The value of Néel temperature for FeS phase is around 600 K [16]. However, the XRD pattern and the Mössbauer spectra give rather different values for the FeS concentration. Probably, there is a certain amount of FeS hidden inside the FeTe structure invisible in the XRD characterization. $FeTe_2$ is paramagnetic down to 77 K [4,5]. It has an internal field which is less than 30 T. The magnetic component C_2 may be attributed to FeTe or $FeTe_{1-x}S_x$ with low sulphur content. Both these phases have a magnetic ordering. Thus the sulphur substitution does not fully destroy the antiferromagnetic ordering of the FeTe structure and superconductivity coexists with antiferromagnetism in $FeTe_{1-x}S_x$ at low temperatures. Component C_2 is observed only at temperatures below 77 K. Above 70 K which is the Néel temperature for FeTe [17] the magnetic ordering of C_2 disappears and the Mössbauer spectra show only two components, C_1 and C_3. Component C_3 is the main component and is associated with paramagnetic FeTe and $FeTe_{1-x}S_x$. Upon increasing the temperature from 5.4 K to room temperature the area of paramagnetic doublet increases and its percentage changes from 25% of the total area at 5.4 K to

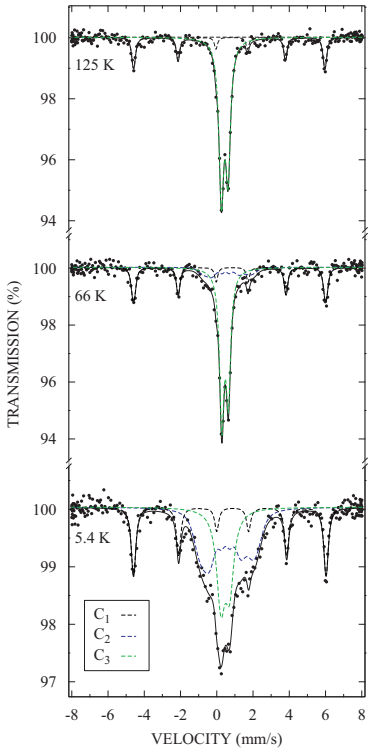

Fig. 3. ^{57}Fe Mössbauer spectra of $FeTe_{0.8}S_{0.2}$ recorded at 5.4 K, 66 K and 125 K.

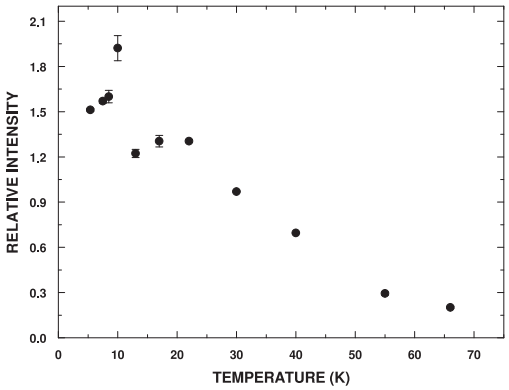

Fig. 4. Intensity ratio between magnetic component C_2 and paramagnetic doublet C_3 vs. temperature.

71% at 300 K. In Fig. 4 the intensity ratio of C_3 and C_2 is plotted. A peak-like kink at 10 K in the intensity ratio may be related to the competition between antiferromagnetism and superconductivity. The temperature dependence of the internal magnetic field of component C_2 is shown in Fig. 5. The behavior of the curve is atypical. The value of $B(T)$ grows with decreasing temperature but

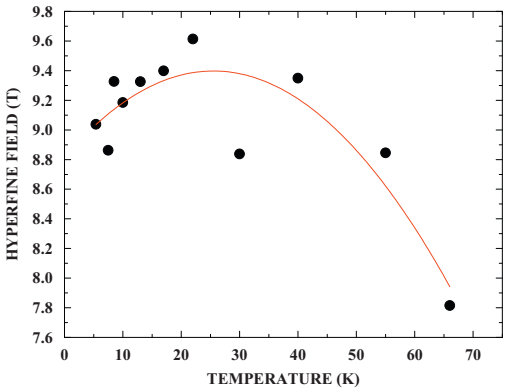

Fig. 5. Internal field vs. temperature for component C_2. The line is a guide for the eye.

at 25 K the curve reaches a maximum and starts to decrease upon further decreasing the absorber temperature. The down-turn of the hyperfine field may again be a consequence of the competition between superconductivity and antiferromagnetism. The two structures that form the magnetically ordered component C_2 in our spectra FeTe and $FeTe_{1-x}S_x$ are intertwined judging by the c lattice parameter. "Islands" of paramagnetic sulphur-rich areas are surrounded by the FeTe main phase. Upon lowering the temperature "islands" shrink and the antiferromagnetically ordered "sea" between the paramagnetic "islands" grows in size, until close to T_c an opposite trend sets in. The superconductivity properties of our sample probably originate from the small sulphur-rich fractions that are distributed over the sample.

4. Conclusions

A $FeTe_{1-x}S_x$ polycrystalline sample was synthesized. SQUID data give a weak superconductivity transition at the critical temperature $T_c \approx 10$ K. The Mössbauer spectra recorded below liquid-nitrogen temperatures were fitted by three components: one paramagnetic doublet which was ascribed to $FeTe_{1-x}S_x$ and two magnetic sextets. The FeS impurity gives rise to one sextet with a $\sim$32.5 T internal field. Above 70 K the magnetic ordering of the second sextet is destroyed and only two components: the magnetic sextet for FeS and the paramagnetic doublet are present in the Mössbauer spectra. Two phases contribute to the doublet and the second magnetic component: $FeTe_{1-x}S_x$ and FeTe. Below 10 K superconducting "islands" of the $FeTe_{1-x}S_x$ phase are distributed over the sample and are separated by thick antiferromagnetic regions of FeTe and $FeTe_{1-x}S_x$ with a low S content. There is an unusual behavior of the hyperfine field for the Fe atoms belonging to the antiferromagnetic regions, indicating that close to the superconductivity transition there is a probable competition between superconductivity and antiferromagnetism.

References

[1] Y. Kamihara, T. Watanabe, M. Hirano, H. Hosono, Journal of the American Chemical Society 130 (2008) 3296.
[2] Chiheng Dong, Hangdong Wang et al., cond-mat.str-el arXiv:1012.5188 (Physical Review B: Accepted Monday November 21, 2011).
[3] Jinsheng Wen, Guangyong Xu, et al., Physical Review B 80 (2009) 1.
[4] V. Fano, I. Ortalli, Physica Status Solidi (a) 10 (1972) K121.
[5] K.V. Reddy, S.C. Chetty, Physica Status Solidi (a) 37 (1976) 687.

[6] Yoshikazu Mizuguchi, Yoshihiko Takano, Journal of the Physical Society of Japan 79 (2010) 102001-1.
[7] Y. Mizuguchi, F. Tomioka, S. Tsuda, T. Yamaguchi, Y. Takano, Journal of the Physical Society of Japan 78 (2009) 074712.
[8] M.H. Fang, B. Qian, et al., cond-mat.str-el arXiv:0811.3021v2.
[9] Y. Mizuguchi, F. Tomioka, et al., Applied Physics Letters 93 (2008) 152505.
[10] R. Khasanov, M. Bendele, et al., Physical Review B 80 (2009) 140511(R).
[11] Rongwei Hu, Emil S. Bozin, J.B. Warren, C. Petrovic, Physical Review B 80 (2009) 214514.
[12] Jinsheng Wen, Guangyong Xu, Genda Gu, J.M. Tranquada, R.J. Birgeneau, Reports on Progress in Physics 74 (2011) 124503.
[13] J. Rodriquez-Carvajal, Physica B 192 (1993) 55.
[14] Y. Mizuguchi, K. Deguchi, T. Ozaki, et al., IEEE Transactions on Applied Superconductivity 21 (2011) 2866.
[15] Y. Mizuguchi, K. Deguchi, et al., Physical Review B 81 (2010) 214510.
[16] F. Li, H.F. Franzen, Journal of Alloys and Compounds 238 (1996) 73.
[17] M.H. Fang, et al., Physical Review B 78 (2008) 224503.

PUBL. II

A. Sklyarova, G. C. Tewari, J. Lindén, H. Yamauchi, and M. Karppinen, Evidence of magnetic broadening in Mössbauer spectra of superconducting $FeTe_{0.8}S_{0.2}$, *Hyperfine Interact.*, 221, 15, 2013.

Hyperfine Interact (2013) 221:15–21
DOI 10.1007/s10751-012-0669-5

Evidence of magnetic broadening in Mössbauer spectra of superconducting $FeTe_{0.8}S_{0.2}$

A. Sklyarova · G. C. Tewari · J. Lindén · H. Yamauchi · M. Karppinen

Published online: 1 November 2012

Abstract Magnetic properties of the $FeTe_{0.8}S_{0.2}$ superconductor were studied by Mössbauer spectroscopy. Low-velocity Mössbauer spectra that were recorded in the temperature range from 5.7 K up to 300 K show a paramagnetic doublet with a broadening at temperatures below 77 K. The broadening can be explained by the appearance of a distribution of hyperfine magnetic fields due to the magnetic ordering of a part of the sample. The magnetically ordered fraction starts to decrease at temperatures below 20 K indicating a possible competition with the onsetting superconductive state.

Keywords ^{57}Fe Mössbauer spectroscopy · Chalcogenide superconductivity · Magnetic properties

1 Introduction

Chalcogenide superconductors are a relative newly discovered type of superconductors that contain iron [1] and exhibit rather high critical temperatures surpassed only by the Cu-based perovskites [2]. Their structures vary from very simple to complex. The most simple 11-structured FeTe exhibits an antiferromagnetic ordering

A. Sklyarova ( ) · J. Lindén
Physics Department, Åbo Akademi University, 20500 Turku, Finland
e-mail: asklyaro@abo.fi

A. Sklyarova
Lappeenranta University of Technology, Faculty of Physics, Box 20, 53851 Lappeenranta, Finland

G. C. Tewari · H. Yamauchi · M. Karppinen
Department of Chemistry, Aalto University, 00076 Aalto, Finland

at low temperatures and does not show superconducting properties even under an applied hydrostatic pressure as FeSe does. FeTe is a parent compound for $FeTe_{1-x}S_x$ that shows a superconducting transition below ∼10 K [3–5]. At the substitution of a part of tellurium by sulphur or another chalcogenide superconductivity arises in these materials. Superconductivity properties of $FeTe_{1-x}S_x$ are sensitive to the concentration of substituting atoms [6] and the synthesis process. The superconductivity transition temperature T_c increases when increasing the portion of substituting atoms and reaches a maximum at $x = 0.2$. Due to the difference between the radii of tellurium and sulphur the synthesis of the pure $FeTe_{0.8}S_{0.2}$ phase is a dificult process. With increasing sulphur content increasing amounts of FeS impurity phase appear [7]. The method of synthesis is also important for the superconductivity properties. The melting method yields samples with a transition temperature of 7.8 K and 20 % of superconducting volume fraction [8]. Using the solid-state reaction method it is possible to obtain purer samples with a higher T_c. Although $FeTe_{1-x}S_x$ does not have a very high critical temperature, the interesting magnetic properties at temperatures below 70 K in these materials attract attention. Coexistence of superconductivity and antiferromagnetism has been reported for $FeTe_{1-x}S_x$ [9–11]. Also in the cuprate superconductors signatures of antiferromagnetism has been reported [12, 13]. In this work the hyperfine fields around T_c were studied using ^{57}Fe Mössbauer spectroscopy.

2 Experimental

A superconducting $FeTe_{0.8}S_{0.2}$ sample was prepared using a solid-state reaction method. Stoichiometric quantities of Fe (99.99 %), Te (99.999 %) and S (99.99 %) powders were mixed, sealed in an evacuated quartz tube, slowly heated up to 1050 °C and annealed for 30 h. The resulting sample powder was reground inside an Ar-filled glove box, pressed into pellets at 10 kbars, annealed again at 800 °C for 20 h and slowly cooled to room temperature in 5 h. After that the sample was annealed in oxygen gas at 200 °C for 12 h. The superconductivity properties were checked with resistivity measurements using a home-build four-probe setup. The purity of the sample was checked with X-ray diffraction using Cu $K\alpha 1$ radiation (PanAnalytical X'Pert Pro MPD diffractometer) in $\theta - 2\theta$ geometry. The magnetic propeties of the $FeTe_{0.8}S_{0.2}$ sample were characterized using ^{57}Fe Mössbauer spectroscopy in transmission geometry. The Mössbauer spectra were measured using a ^{57}Co:Rh source with maximum Doppler velocities of 1.70 mm/s or 2.0 mm/s at temperatures between 5.7 and 300 K. Additional high-velocity Mössbauer spectra at 7 K, 77 K, and 300 K recorded at 10 mm/s allowed checking of impurity phases. The sample was cooled using an Oxford continuous-flow cryostat with liquid He as a coolant below 77 K and liquid N_2 at and above 77 K. The spectra were fitted with the following Mössbauer parameters: asymmetric quadrupole doublet for the main paramagnetic component, relative intensity, isomer shift relative to α-Fe and magnetic hyperfine field for the FeS impurity phase. For the main component the angle between the wave vector and the z-axis of the electric field gradient was entered as a fit parameter that indicates a crystalline texture. Magnetic lines of FeS were fixed according to the high-velocity spectra when analyzing the low-velocity spectra.

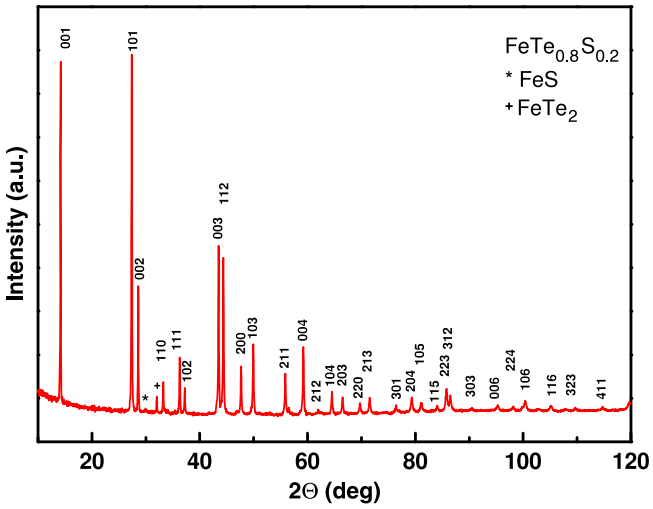

Fig. 1 X-ray powder diffraction pattern for $FeTe_{0.8}S_{0.2}$. Impurities due to FeS and $FeTe_2$ are indicated with ⋆ and +, respectively

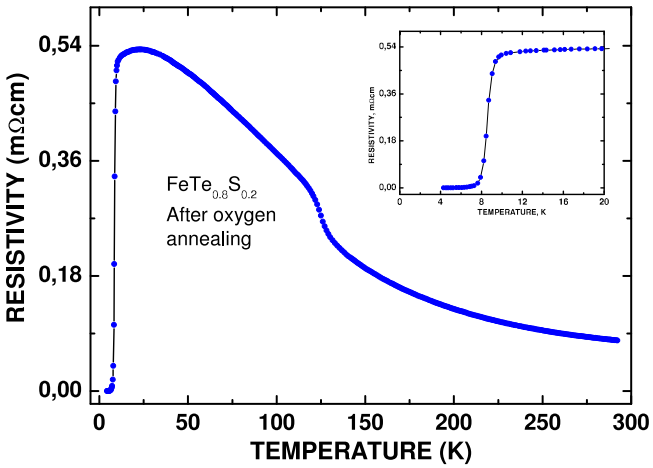

Fig. 2 Electrical resistivity vs. temperature. The *inset* shows the transition region in more detail

3 Results

The XRD pattern for our $FeTe_{0.8}S_{0.2}$ sample shows presence of FeS and traces of $FeTe_2$ along with the main phase of $FeTe_{0.8}S_{0.2}$ (Fig. 1). The superconductivity transition was observed using a resistivity measurement. The temperature dependence of electrical resistivity shows a sharp transition at 9 K (Fig. 2). The anomaly around 120 K is possibly related to the Verwey transition of magnetite.

High-velocity (10 mm/s) Mössbauer spectra detected the presence of 11.4 % FeS (IS = 0.77 mm/s at 300 K) and 4.7 % Fe_3O_4 (IS = 0.19 mm/s at 300 K) which is in accord with the XRD-data, but $FeTe_2$ was not detected. All Mössbauer spectra show a main component consisting of an asymmetric quadrupole doublet assigned to the superconducting $FeTe_{0.8}S_{0.2}$ phase (Fig. 3). The isomer shift that equals 0.44 mm/s at 300 K is compatible with intermediate spin (S = 1) Fe^{2+}. The temperature dependence of the second-order Doppler shift data was fitted to a

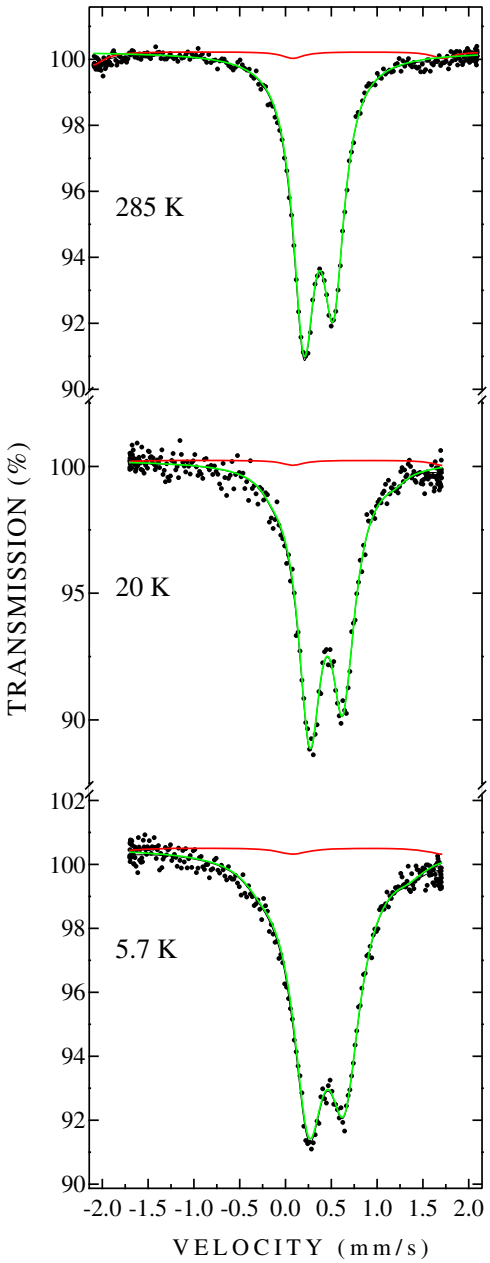

Fig. 3 Mössbauer specta of $FeTe_{0.8}S_{0.2}$ recorded at indicated temperatures. Components due to the broadened paramagnetic doublet (*green*) and central lines of the magnetic FeS impurity (*red*) are indicated

Debye temperature of 405 K above T ≈ 77 K. Below that temperature the Debye model failed, probably due to elastic changes in the lattice. In the spectra recorded above 77 K purely paramagnetic behavior is observed for the main component. The asymmetry of this doublet is due to crystalline texture and the angle between the wave vector and the z-axis of the main component of the electric field gradient was found to differ from the powder-absorber value of 54.74° and instead be a constant of ∼39.5° in all spectra recorded between 77 and 300 K. It was fixed at

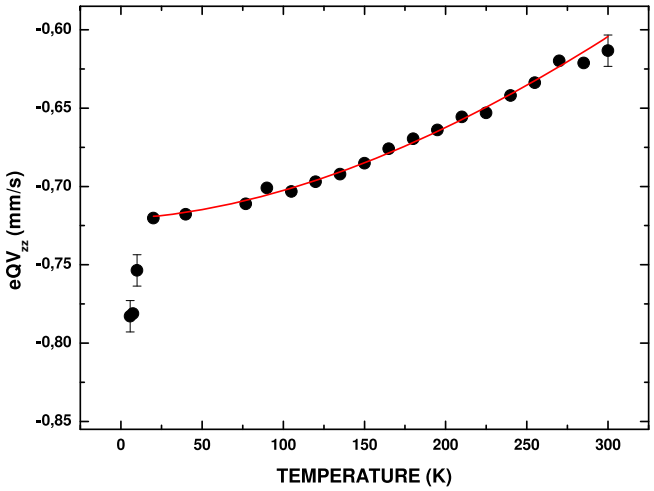

Fig. 4 Quadrupole coupling constant eQV_{zz} vs. temperature for $FeTe_{0.8}S_{0.2}$ with a power law fitting, at temperatures above 20 K, see text

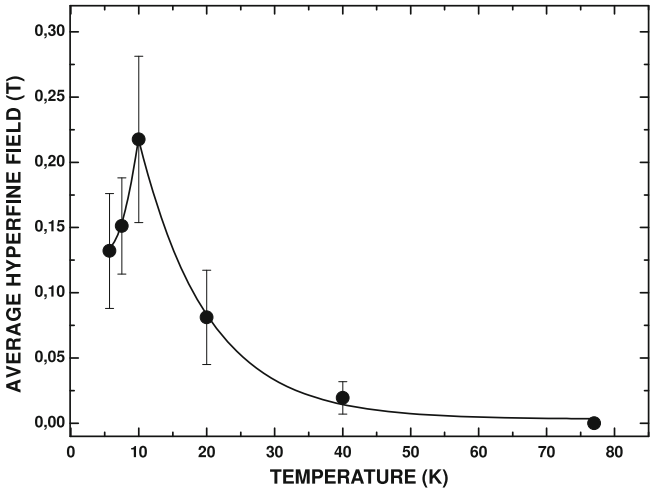

Fig. 5 Temperature dependence of the average magnetic hyperfine field for $FeTe_{0.8}S_{0.2}$. The line is a guide for the eye

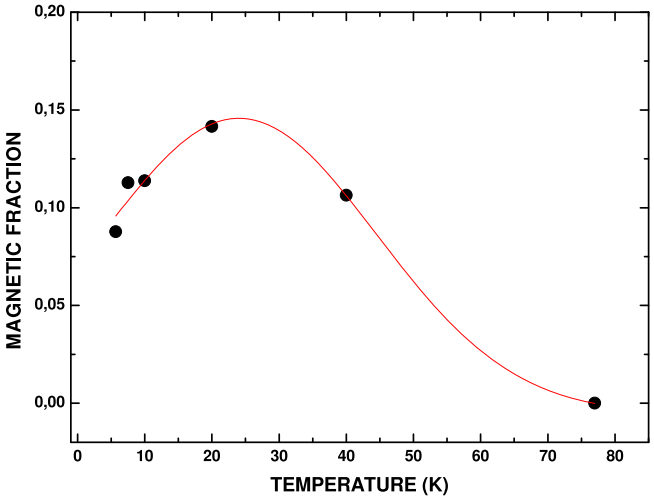

Fig. 6 The fraction of magnetically ordered Fe vs. temperature. The line is a guide for the eye

this value when fitting the spectra recorded below 77 K. The quadrupole splitting of the main component has a negative sign and equals to $eQV_{zz} = -0.71$ mm/s at 77 K. The eQV_{zz} vs. temperature data follow a $(1 - aT^{3/2})$ [14] dependence with $a = 3.2 \cdot 10^{-5}$ (Fig. 4). Below ~20 K the data undergo a sharp drop which roughly coincides with the decline of the internal field, *vide infra*. Also in $FeTe_{0.5}Se_{0.5}$ a change in eQV_{zz} about T_c was reported [15]. The fast decline in eQV_{zz} is probably not associated with a change in the local lattice structure. Instead a minor change in the non-spherical electronic structure of this Fe^{2+} state is a more probable explanation. Below 77 K the spectra display a distinct broadening of the asymmetric doublet. This broadening changes with the temperature, reaching a maximum around 10 K. A similar picture was reported earlier [16, 17]. The broadened doublet was fitted with a histogram distribution of hyperfine magnetic fields. The temperature dependence of the average hyperfine field is shown in Fig. 5. The average field peaks at ~10 K, declining upon further cooling of the sample. The declining section coincides with the onset of superconductivity.

The overall portion of magnetically-ordered Fe is shown in Fig. 6. It peaks at ~20 K. The evolution of the magnetic portion with temperature indicates that a possible competition between the paramagnetic fraction which is associated with superconductivity and the magnetically ordered fraction may take place. Coexistence of magnetism and superconductivity in pnictide FeAs-based superconductors and strong evidence of this phenomenon in $Cs_{0.8}(FeSe_{0.98})_2$ are in accordance with our suggestion [18, 19].

4 Conclusions

Mössbauer spectra from 5.7 K up to room temperature revealed an asymmetric quadrupole doublet assigned to the superconducting $FeTe_{0.8}S_{0.2}$ phase. At temperatures below 77 K the paramagnetic doublet exhibits a broadening that can be attributed to a weak magnetic ordering in the sample. The peaks in the temperature dependences of the magnetically-ordered fractions of Fe and the average magnetic field suggest that a competition between magnetism and superconductivity may occur.

References

1. Kamihara, Y., Watanabe, T., Hirano, M., Hosono, H.: J. Am. Chem. Soc. **130**, 3296 (2008)
2. Bednorz, J.G., Müller, K.A.: Z. Physik **B 64**, 189 (1986)
3. Awana, V.P.S., Pal, A., Vajpayee, A., Gahtori, B., Kishan, H.: Physica C **471**, 77 (2011)
4. Mizuguchi, Y., Tomioka, F., Tsuda, S., Yamaguchi, T., Takano, Y.: Appl. Phys. Lett. **94**, 012503 (2009)
5. Zajdel, P., Hsieh, P.-Y., Rodriguez, E.E., Butch, N.P., Magill, J.D., Paglione, J., Zavalij, P., Suchomel, M.R., Green, M.A.: J. Am. Chem. Soc. **132**, 13000 (2010)
6. Mizuguchi, Y., Tomioka, F., Tsuda, S., Yamaguchi, T., Takano, Y.: J. Phys. Soc. Jpn. **78**, 074712 (2009)
7. Mizuguchi, Y., Tomioka, F., Tsuda, S., Yamaguchi, T., Takano, Y.: Appl. Phys. Lett. **93**, 152505 (2008)
8. Mizuguchi, Y., Deguchi, K., Tsuda, S., Yamaguchi, T., Takano, Y.: Eur. Phys. Lett. **90**, 57002 (2010)

9. Khasanov, R., Bendele, M., Amato, A., Babkevich, P., Boothroyd, A.T., Cervellino, A., Conder, K., Gvasaliya, S.N., Keller, H., Klauss, H.-H., Luetkens, H., Pomjakushin, V., Pomjakushina, E., Roessli, B.: Phys. Rev. B **80**, 140511(R) (2009)
10. Hu, R., Bozin, E.S., Warren, J.B., Petrovic, C.: Phys. Rev. B **80**, 214514 (2009)
11. Wen, J., Xu, G., Gu, G., Tranquada, J.M., Birgeneau, R.J.: Rep. Prog. Phys. **74**, 124503 (2011)
12. Lake, B., Ronnow, H.M., Christensen, N.B., Aeppli, G., Lefmann, K., McMorrow, D.F., Vorderwisch, P., Smeibidl, P., Mangkorntong, N., Sasagawa, T., Nohara, M., Takagi, H., Mason, T.E.: Nature **415**, 299 (2002)
13. Lindén, J., Karppinen, M., Grigoravičiūtė, I., Yamauchi, H.: Phys. Rev. Let. **98**, 067001 (2007)
14. Lodge, K.W.: J. Phys. F: Met. Phys. **9**, 2035 (1979)
15. Lindén, J., Rautama, E.-L., Karppinen, M., Yamauchi, H.: Hyperfine Interact. **208**, 133 (2012)
16. Yadav, C.S., Paulose, P.L.: J. Appl. Phys. **107**, 083908 (2010)
17. Sklyarova, A., Lindén, J., Rautama, E.-L., Karppinen M.: J. Magn. Magn. Mater. (2012). doi:10.1016/j.jmmm.2012.10.013
18. Pratt, D.K., Tian, W., Kreyssig, A., Zarestky, J.L., Nandi, S., Ni, N., Bud'ko, S.L., Canfield, P.C., Goldman, A.I., McQueeney, R.J.: Phys. Rev. Lett. **103**, 087001 (2009)
19. Shermadini, Z., Krzton-Maziopa, A., Bendele, M., Khasanov, R., Luetkens, H., Conder, K., Pomjakushina, E., Weyeneth, S., Pomjakushin, V., Bossen, O., Amato, A.: Phys. Rev. Lett. **106**, 117602 (2011)

PUBL. III

A. Sklyarova, G. C. Tewari, J. Lindén, E.-L. Rautama, and M. Karppinen, Evolution of the internal magnetic field in chalcogenide superconductors $FeTe_{1-x}S_x$ for various x values, *J. Magn. Magn. Matter.*, 357, 82, 2014.

Journal of Magnetism and Magnetic Materials 357 (2014) 82–86

Contents lists available at ScienceDirect

Journal of Magnetism and Magnetic Materials

journal homepage: www.elsevier.com/locate/jmmm

Evolution of the internal magnetic field in chalcogenide superconductors $FeTe_{1-x}S_x$ for various x values

A. Sklyarova [a,b,c], G.C. Tewari [d], J. Lindén [a,*], E.-L. Rautama [d], M. Karppinen [d]

[a] Department of Physics, Åbo Akademi, FI-20500 Turku, Finland
[b] Lappeenranta University of Technology, Faculty of Physics, Box 20, 53851 Lappeenranta, Finland
[c] St. Petersburg State University, Faculty of Physics, Ulyanovskaya Str. 1, Petrodvorets, St. Petersburg 198504, Russia
[d] Department of Chemistry, Aalto University, FI-00076 Aalto, Finland

ARTICLE INFO

Article history:
Received 1 October 2013
Received in revised form
10 January 2014
Available online 27 January 2014

Keywords:
Chalcogenide superconductor
^{57}Fe Mössbauer spectroscopy

ABSTRACT

The behavior of the internal magnetic field in $FeTe_{1-x}S_x$ was studied using Mössbauer spectroscopy in the temperature range from 6.8 K up to 300 K. Spectra of samples with $x=0.05$, 0.10 and 0.20 were recorded and the obtained hyperfine parameters were compared with the superconductivity properties. A dependence of the internal field on the x value and the superconductivity transition temperature was found.

1. Introduction

Chalcogenide superconductors belong to a very suitable class among the iron-based superconductors for studying hyperfine interactions. Effects like the coexistence of magnetism and superconductivity, presence of spin density waves make these materials attractive for various kinds of investigations [1–5].

Superconductivity in the simple unsubstituted FeTe phase cannot be achieved even if an external pressure is applied as in FeSe [6,7]. Iron telluride shows an antiferromagnetic ordering with a Néel temperature around 70 K, but by using substituting elements a suppression of the magnetic ordering occurs. Substitution of tellurium by sulphur or selenium can be used to induce superconductivity. Depending on the concentration of the substituting atom superconductivity will appear and develop into filamentary or bulk type and finally disappear for exceeding quantities of the substituent [8–10]. Earlier studies of Fe-based superconductors indicate that the enhancement of T_c is related to changes in the crystal lattice or magnetic properties of the material. In $FeTe_{1-x}S_x$ the sulphur atoms occupy the sites of tellurium and create a chemical pressure in the lattice owing to the difference in the atomic sizes.

Although bulk superconductivity in conducting materials usually develops from paramagnetic parent phases, studies of the new Fe-based superconductors reveal coexistence of antiferromagnetic ordering and superconductivity [11,12]. Previously it was believed that by substituting a part of tellurium by sulphur the magnetic ordering is completely suppressed and superconductivity is induced but later the presence of a hyperfine magnetic field in superconducting $FeTe_{1-x}S_x$ was observed [1,10]. The addition of sulphur atoms to FeTe makes the magnetic ordering at low temperatures incommensurate even for a very small concentration of substituents [10]. Also in $Fe_{1+y}Te_{1-x}Se_x$ with $y=0.03$ and $x=0.40$–0.5 a magnetic ordering at low temperatures was found [5,24]. It was experimentally found that at temperatures below $\sim$80 K (the exact ordering temperature depends on the substitution level) magnetically ordered fractions appear and below the superconducting transition temperature coexistence of magnetism and superconductivity is observed [5]. In contrast, $Fe_{1+x}Te$ has an commensurate magnetic structure [25]. In the bulk superconductor $FeTe_{0.5}Se_{0.5}$ only paramagnetic iron was observed at all temperatures [5,26].

In $FeTe_{1-x}S_x$ the maximum for the superconducting transition temperature T_c is reached at $x\approx0.2$. For other sulphur concentrations the superconducting volume fraction is smaller and can exhibit filamentary structure. An enhancement of the superconducting volume fraction can be achieved by changing the sulphur content, but also by applying additional procedures during or after the final step of synthesis [13–17]: it has been shown that an oxygen annealing leads to a sharper superconductivity transition and increases the transition temperature. Air-exposure of the materials also shows a good result for improving superconductivity in $FeTe_{1-x}S_x$. The solubility limit of sulphur atoms causes some obstacles for choosing an optimal synthesis method [6]. Several ways of synthesis are used for producing $FeTe_{1-x}S_x$: melting method, Bridgman method and solid-state reaction [20,21].

* Corresponding author.
E-mail address: jlinden@abo.fi (J. Lindén).

0304-8853/$ - see front matter © 2014 Elsevier B.V. All rights reserved.
http://dx.doi.org/10.1016/j.jmmm.2014.01.037

Apparently, a solid-state reaction method gives a better combination for the desired properties in the synthesized materials, however, it also leads to a broadening of the superconductivity transition to zero resistivity, but at the same time a reduced presence of impurity phases is observed.

Owing to the simple process of synthesis we focus our attention on the Fe(Te,S) system for studies on the incipient hyperfine magnetic effects at temperatures around the superconductivity transition. Sulphur-substituted iron telluride samples were produced and the development of superconductivity properties and behavior of the hyperfine magnetic field below 77 K were studied and compared with the earlier results obtained for an optimally substituted sample [18,19].

2. Experimental

For studies of the magnetic properties of superconducting $FeTe_{1-x}S_x$ samples with $x=0.05$, $x=0.10$ and $x=0.20$ were synthesized using a solid-state reaction scheme. Stoichiometric mixtures of iron (99.99%), tellurium (99.99%) and sulphur (99.99%) powders were sealed into quartz tubes under vacuum and slowly heated from room temperature to 1050 °C for 20 h and kept at this temperature for 30 h. The obtained samples were reground inside a glove box with an inert Ar atmosphere, pressed into pellets at 10 kbars, sealed into evacuated quartz tubes and sintered again at 800 °C for 20 h. The oxygen-annealing was used as an additional synthesis step for the synthesis of the $FeTe_{0.8}S_{0.2}$ sample [19].

The superconductivity properties were checked with resistivity measurements using a home-built four-probe setup and with magnetic measurements in zero-field cooling and field-cooling regimes using a SQUID magnetometer (Quantum Design, MPMS-XL). According to the literature $FeTe_{0.95}S_{0.05}$ is not superconducting, $FeTe_{0.9}S_{0.1}$ starts to show superconductivity properties. The samples purity was characterized with an X-ray powder diffractometer (PanAnalytical X'pert Pro MPD, CuK α1 radiation) and the data were analyzed by the Rietveld method using the software program FullProf [27].

Mössbauer spectra were recorded in the temperature range from 6.8 K up to 300 K in transmission geometry using maximum Doppler velocities of 1.70 mm/s and 10.00 mm/s. High-velocity spectra were used for checking the presence of impurity phases. Low-velocity spectra were used for extracting the hyperfine interactions of the main phase. A 25 mCi Cyclotron Co. ^{57}Co:Rh source was used for producing the gamma quanta. For low-temperature measurements an Oxford continuous-flow cryostat with liquid He as a coolant below 77 K and liquid N_2 at and above 77 K was used. The spectra of $FeTe_{0.9}S_{0.1}$ were fitted using a model that includes one paramagnetic doublet from the main phase and

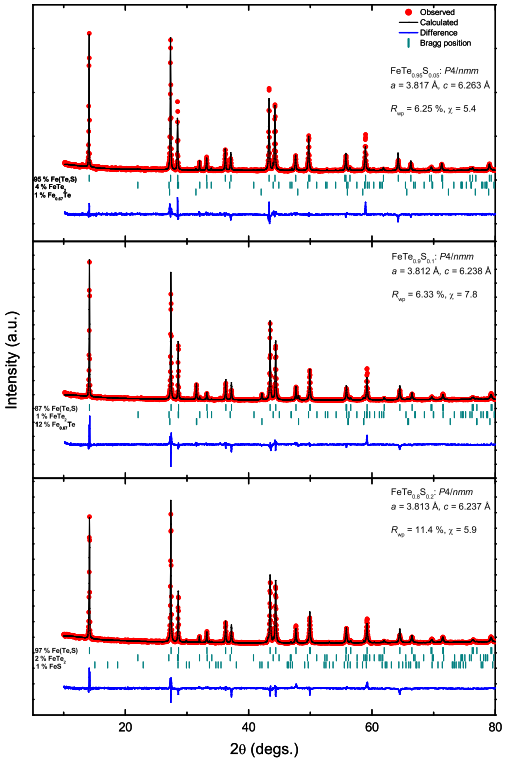

Fig. 1. X-ray powder diffraction patterns for the $FeTe_{0.95}S_{0.05}$, $FeTe_{0.9}S_{0.1}$ and $FeTe_{0.8}S_{0.2}$ samples.

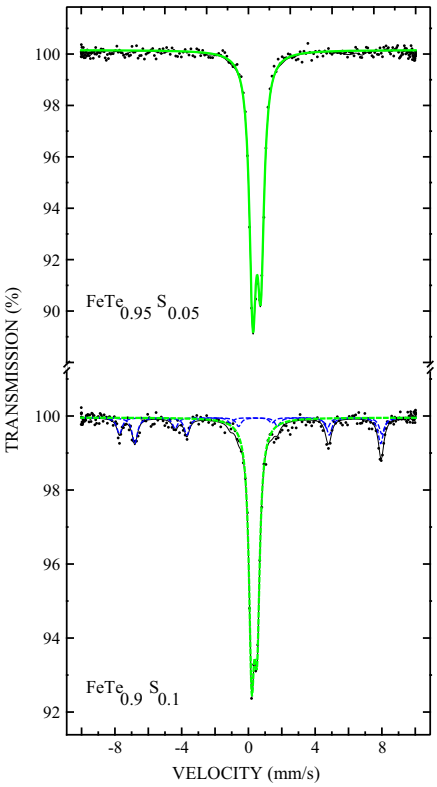

Fig. 2. ^{57}Fe high-velocity Mössbauer spectra of $FeTe_{0.95}S_{0.05}$ (upper panel) and $FeTe_{0.9}S_{0.1}$ (lower panel) recorded at room temperature. Components due to the paramagnetic doublet (green solid) and the magnetic Fe_3O_4 impurity (blue dashed) are indicated. (For interpretation of the references to color in this figure caption, the reader is referred to the web version of this paper.)

two magnetic sextets from magnetic impurities. For fitting the spectra that were recorded below 77 K three singlets and one doublet were used. Two of the three singlets can be associated with the third lines of the magnetic sextets with high internal fields. The third singlet was used for fitting the paramagnetic main component together with a broadened doublet. For $FeTe_{0.95}S_{0.05}$ the fitting model includes only one paramagnetic doublet at all temperatures. All spectra of the investigated materials exhibit a texturized structure and the angle between the wave vector and the principal axis of the electric field gradient was entered as a free fit parameter. Isomer shift values were taken relative to α-Fe at room temperature.

Obtained hyperfine parameters for 0.05 and 0.10 sulphur-substituted samples were compared with properties of the sample with $x=0.20$ reported earlier [18,19].

3. Results and discussion

The XRD analyses showed Fe(Te,S) as the main phase but other phases were also observed. They were identified as $FeTe_2$, $Fe_{0.67}Te$ and FeS and their amounts were found to be dependent on the substitution level of sulphur. The results of the multiphase Rietveld refinements are presented in Fig. 1. The main phase Fe(Te,S) is strongly c-axis oriented and this was taken into account to enable the quantification of the fractional phases. A March–Dollase function was applied to account for the orientation effect and the resulting refined value ($G=0.57<1$) suggests a plate-like texture in the present samples. No sulphur-containing impurities were observed for the $x=0.05$ and 0.10 samples and only 1% of the FeS impurity phase was detected for the $x=0.20$ sample. This indicates that the S-for-Te substitution is rather successful. This is supported by the lattice parameter behavior: the cell volume decreases with increasing x. As the X-ray scattering power is different enough for Te and S, we also studied the fractional occupancies in their crystallographic positions. This was done at the final stage of the refinement so that the chemically fixed occupancy of S was released. This somewhat improved the results and gave 1.8, 6.1 and 9.9% as the actual amount of S in the $x=0.05$, 0.10 and 0.20 samples, respectively. Comparison of the c-axis value for the chemically analyzed samples would give slightly different results (4.9, 7.6 and 7.8%) [28]. This is probably explained by the fact that some of the Fe and Te is bonded in the parasitic phases but the reality should be something in between. The high-velocity Mössbauer spectrum recorded at room temperature revealed also the presence of Fe_3O_4 in the $FeTe_{0.9}S_{0.1}$ sample (Fig. 2). But this impurity was not observed in the $FeTe_{0.95}S_{0.05}$ sample. Paramagnetic $FeTe_2$ and $Fe_{0.67}Te$ impurities were not detected in the high-velocity Mössbauer spectra. The much more intensive main doublet probably masks these two phases in the Mössbauer spectra, as both these impurities are paramagnetic at room temperature [22,23,29]. The isomer shift and quadrupole coupling constant of the main phase were $IS=0.44$ mm/s and $eQV_{zz}=-0.78$ mm/s at 77 K for $x=0.10$ and $IS=0.45$ mm/s and $eQV_{zz}=-0.83$ mm/s at 77 K for $x=0.05$. For the $FeTe_{0.8}S_{0.2}$ sample these values were $IS=0.52$ mm/s and $eQV_{zz}=-0.71$ mm/s at 77 K [19].

The $FeTe_{0.95}S_{0.05}$ sample did not show any superconducting transition in the magnetization nor the resistivity data. In $FeTe_{0.9}S_{0.1}$ the zero-field cooling (ZFC) magnetization measurement shows a broad drop at ~ 10 K (Fig. 3). As expected, the $x=0.20$ sample shows bulk superconductivity: a sharp drop of the magnetization curve is observed at ~ 9 K (Fig. 3). This value of the transition temperature is confirmed by the resistivity measurement. The hump in the susceptibility observed at 125 K on the field-cooling curve is compatible with the Verwey transition in magnetite. A sharper superconducting transition is seen on the resistivity versus temperature curve, Fig. 3, with $T_c \sim 8$ K. The resistivity curve also shows a weak Verwey transition at ~ 125 K.

Low-velocity Mössbauer spectra of the $FeTe_{0.95}S_{0.05}$ and $FeTe_{0.9}S_{0.1}$ samples (Fig. 4) were recorded in the temperature range from room temperature to 6.8 K. The spectra exhibit a broadening of the line width of the main components with decreasing temperature, in particular in the range from 77 K to 6.8 K. The broadened doublets were fitted with a histogram distribution of hyperfine magnetic fields. The temperature dependencies of the

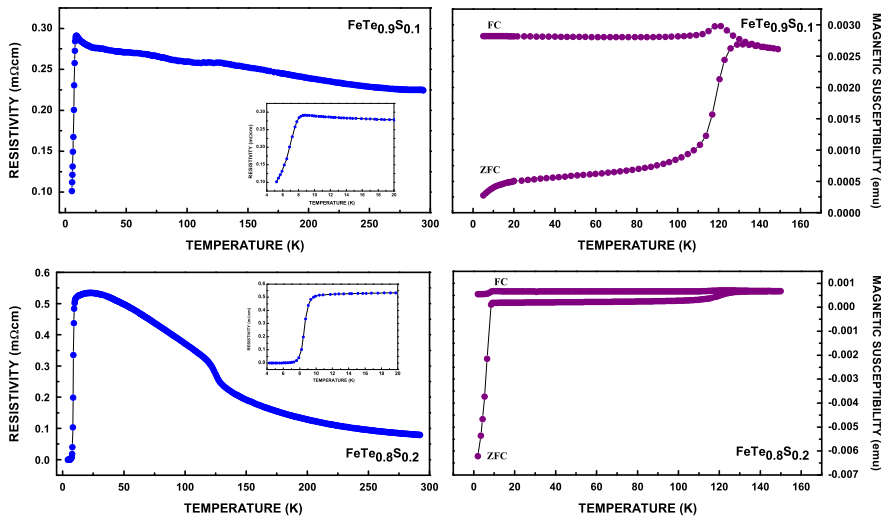

Fig. 3. Resistivity vs. temperature for $FeTe_{0.9}S_{0.1}$ and $FeTe_{0.8}S_{0.2}$ samples. The insets show the transition regions in more detail. Magnetic susceptibility vs. temperature for $FeTe_{0.9}S_{0.1}$ and $FeTe_{0.8}S_{0.2}$ obtained in field-cooling (FC) and zero-field-cooling (ZFC) regimes of the SQUID measurements.

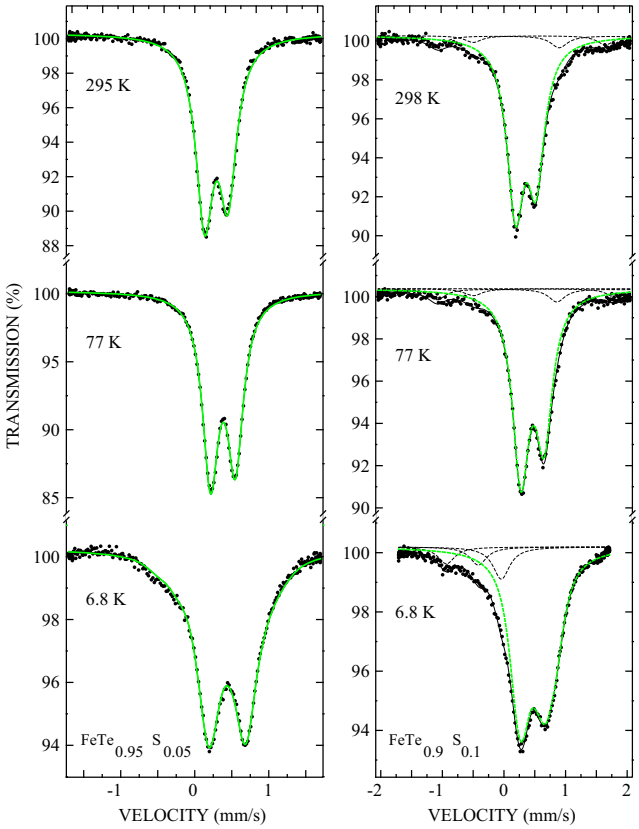

Fig. 4. Left panel: ^{57}Fe Mössbauer spectra of $FeTe_{0.95}S_{0.05}$ recorded at indicated temperatures. Right panel: ^{57}Fe Mössbauer spectra of $FeTe_{0.9}S_{0.1}$ recorded at indicated temperatures. Components due to the broadened paramagnetic doublet (green thick) are indicated. (For interpretation of the references to color in this figure caption, the reader is referred to the web version of this paper.)

hyperfine fields for the $FeTe_{0.95}S_{0.05}$ and $FeTe_{0.9}S_{0.1}$ samples are presented in Fig. 5. In the upper panel of Fig. 5 an increase of the magnetic field with decreasing temperature continues down to the lowest temperature. In $FeTe_{0.9}S_{0.1}$ the magnetic field of the main component grows up to approximately 8.5 K and drops upon further decreasing temperature. A similar behavior was also observed in the $FeTe_{1-x}S_x$ samples with a higher content of sulphur ($x \approx 0.20$) [18,19] and is presented for comparison in Fig. 5. The obtained dependencies of the hyperfine magnetic fields agree with the concept of a competition between magnetism and superconductivity in the $FeTe_{1-x}S_x$ system for the samples which exhibit various degrees of superconductivity. Also, there seems to be a relationship between the peak of the hyperfine magnetic field and the value of the superconductivity transition temperature.

By comparing the average internal fields of the $x=0.05$ and $x=0.10$ samples and the earlier investigated optimally substituted sample with $x=0.20$ it is noticed that in the non-superconducting $FeTe_{0.95}S_{0.05}$ sample the magnetic volume fraction linearly grows with the decreasing temperature, whereas for the two superconducting samples the curves show a faster than linear growth up to the superconducting transition temperature and a sharp down turn at temperatures below T_c. Also, it was observed for the earlier studied sample [19] that the increase of the hyperfine magnetic field has a weaker character and the maximum value of the hyperfine magnetic field is considerably lower than that for the $FeTe_{0.9}S_{0.1}$ sample.

A conclusion that superconductivity in the $FeTe_{1-x}S_x$ system suppresses the magnetic ordering below transition temperature can be drawn which is in contrast to the results for $Fe_{1+y}Te_{1-x}Se_x$ where the volume of the region with the coexistence of the magnetic ordering and superconductivity is increasing even below the superconductivity transition. Therefore in $FeTe_{1-x}S_x$ rather a competition and suppression of the magnetic ordering by superconductivity takes place in agreement with our previous results for the bulk superconductor [19].

4. Conclusions

The evolution of the magnetic hyperfine field for $FeTe_{1-x}S_x$ samples with various x has been studied. The temperature dependencies of the internal field for a non-superconducting sample and the samples that show a superconducting transition were obtained. The sharp drop of the magnetic field value below

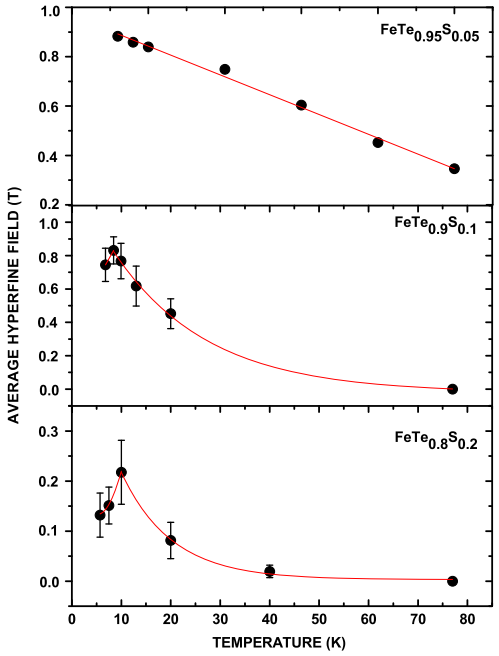

Fig. 5. Average internal fields vs. temperature for $FeTe_{0.95}S_{0.05}$ (upper panel), $FeTe_{0.9}S_{0.1}$ (middle panel), and $FeTe_{0.8}S_{0.2}$ (lower panel) [19]. The lines are guides for the eye.

the superconducting transition temperature suggests a suppression of the magnetic ordering by the emerging superconductivity. This is in contrast to the reported mutual coexistence of magnetic ordering and superconductivity in some Fe-based superconductors.

References

[1] Rongwei Hu, Emil S. Bozin, J.B. Warren, C. Petrovic, Phys. Rev. B 80 (2009) 214514.
[2] Jinsheng Wen, Guangyong Xu, Genda Gu, J.M. Tranquada, R.J. Birgeneau, Rep. Prog. Phys. 74 (2011) 124503.
[3] J. Lindén, M. Karppinen, I. Grigoravičiūtė, H. Yamauchi, Phys. Rev. Lett. 98 (2007) 067001.
[4] B. Lake, H.M. Ronnow, N.B. Christensen, G. Aeppli, K. Lefmann, D.F. McMorrow, P. Vorderwisch, P. Smeibidl, N. Mangkorntong, T. Sasagawa, M. Nohara, H. Takagi, T.E. Mason, Nature 415 (2002) 299.
[5] R. Khasanov, M. Bendele, A. Amato, P. Babkevich, A.T. Boothroyd, A. Cervellino, K. Conder, S.N. Gvasaliya, H. Keller, H.-H. Klauss, H. Luetkens, V. Pomjakushin, E. Pomjakushina, B. Roessli, Phys. Rev. B 80 (2009) 140511 (R).
[6] T.J. Liu, M.H. Fang, B. Qian, E.K. Vehstedt, J.H. Yang, H.M. Pham, L. Spinu, Z.Q. Mao, Bull. Am. Phys. Soc. 54 (2009).
[7] K. Miyoshi, Y. Takaichi, E. Mutou, K. Fujiwara, J. Takeuchi, J. Phys.: Conf. Ser. 200 (2010) 012126.
[8] V.P.S. Awana, A. Pal, A. Vajpayee, B. Gahtori, H. Kishan, Physica C 471 (2011) 77.
[9] Y. Mizuguchi, F. Tomioka, S. Tsuda, T. Yamaguchi, Y. Takano, Appl. Phys. Lett. 94 (2009) 012503.
[10] P. Zajdel, P.-Y. Hsieh, E.E. Rodriguez, N.P. Butch, J.D. Magill, J. Paglione, P. Zavalij, M.R. Suchomel, M.A. Green, J. Am. Chem. Soc. 132 (2010) 13000.
[11] D.K. Pratt, W. Tian, A. Kreyssig, J.L. Zarestky, S. Nandi, N. Ni, S.L. Bud'ko, P.C. Canfield, A.I. Goldman, R.J. McQueeney, Phys. Rev. Lett. 103 (2009) 087001.
[12] Z. Shermadini, A. Krzton-Maziopa, M. Bendele, R. Khasanov, H. Luetkens, K. Conder, E. Pomjakushina, S. Weyeneth, V. Pomjakushin, O. Bossen, A. Amato, Phys. Rev. Lett. 106 (2011) 117602.
[13] Y. Mizuguchi, F. Tomioka, S. Tsuda, T. Yamaguchi, Y. Takano, J. Phys. Soc. Jpn. 78 (2009) 074712.
[14] Yoshikazu Mizuguchi, Yoshihiko Takano, J. Phys. Soc. Jpn. 79 (2010) 102001–1.
[15] Y. Mizuguchi, K. Deguchi, S. Tsuda, T. Yamaguchi, Y. Takano, Phys. Rev. B 81 (2010) 214510.
[16] K. Deguchi, T. Okuda, H. Hara, S. Demura, T. Watanabe, H. Okazaki, M. Fujioka, S.J. Denholme, T. Ozaki, T. Yamaguchi, H. Takeya, F. Saito, M. Hisamoto, Y. Takano, Physica C 487 (2013) 16.
[17] Z.T. Zhang, Z.R. Yang, L. Li, L. Pi, S. Tan, Y.H. Zhang, J. Appl. Phys. 111 (2012) 07E118.
[18] A. Sklyarova, J. Lindén, E.-L. Rautama, M. Karppinen, J. Magn. Magn. Mater. 329 (2013) 129.
[19] A. Sklyarova, G.C. Tewari, J. Lindén, H. Yamauchi, M. Karppinen, Hyperfile Int. 221 (2013) 15.
[20] Y. Mizuguchi, F. Tomioka, S. Tsuda, T. Yamaguchi, Y. Takano, Appl. Phys. Lett. 93 (2008) 152505.
[21] Y. Mizuguchi, K. Deguchi, S. Tsuda, T. Yamaguchi, Y. Takano, Eur. Phys. Lett. 90 (2010) 57002.
[22] V. Fano, I. Ortalli, Phys. Status Solidi (a) 10 (1972) K121.
[23] K.V. Reddy, S.C. Chetty, Phys. Status Solidi (a) 37 (1976) 687.
[24] P. Dai, J. Hu, E. Dagotto, Nat. Phys. 8 (2012) 709.
[25] Wei Bao, Y. Qiu, Q. Huang, M.A. Green, P. Zajdel, M.R. Fitzsimmons, M. Zhernenkov, S. Chang, Minghu Fang, B. Qian, E.K. Vehstedt, Jinhu Yang, H.M. Pham, L. Spinu, Z.Q. Mao, Phys. Rev. Lett. 102 (2009) 247001.
[26] J. Lindén, J.-P. Liböck, M. Karppinen, E.-L. Rautama, H. Yamauchi, Solid State Commun. 151 (2011) 130.
[27] J. Rodriquez-Carvajal, Physica B 192 (1993) 55.
[28] Y. Mizuguchi, K. Deguchi, T. Ozaki, M. Nagao, Sh. Tsuda, T. Yamaguchi, Y. Takano, IEEE Trans. Appl. Supercond. 21 (2011) 2866.
[29] J.B. Ward, V.H. McCann, J. Phys. C: Solid State Phys. 12 (1979) 873.

PUBL. IV

A. Sklyarova, J. Lindén, G. C. Tewari, E.-L. Rautama, and M. Karppinen, ^{57}Fe Mössbauer study of a secondary phase in $FeSe_{1-x}$ with a large quadrupole splitting, *Hyperfine Interact.*, 226, 341, 2014.

Hyperfine Interact (2014) 226:341–349
DOI 10.1007/s10751-013-1007-2

^{57}Fe Mössbauer study of a secondary phase in $FeSe_{1-x}$ with a large quadrupole splitting

A. Sklyarova · J. Lindén · G. C. Tewari · E.-L. Rautama · M. Karppinen

Published online: 23 January 2014

Abstract We have studied the hyperfine interactions in samples belonging to the Fe-Se system. Several samples with various concentrations of selenium were synthesized and investigated. The objective was to find synthesis conditions increasing the concentration of a secondary Fe-Se phase with a rather large quadrupole splitting of ∼1.7 mm/s. At $T_m \approx 104$ K this secondary phase undergoes a magnetic ordering.

Keywords ^{57}Fe Mössbauer spectroscopy · Chalcogenide superconductivity · Magnetic properties

1 Introduction

FeSe forms in a simple structure that exhibits superconducting properties at an optimal 1:1 stoichiometric composition of Fe and Se [1]. The transition temperature of this material

Proceedings of the 32nd International Conference on the Applications of the Mössbauer Effect (ICAME 2013) held in Opatija, Croatia, 1–6 September 2013

A. Sklyarova (✉) · J. Lindén
Physics Department, Åbo Akademi University, FI-20500 Turku Finland
e-mail: asklyaro@abo.fi

J. Lindén
e-mail: jlinden@abo.fi

A. Sklyarova
Faculty of Physics, Lappeenranta University of Technology, Box 20, 53851 Lappeenranta, Finland

A. Sklyarova
Faculty of Physics, St. Petersburg State University, Ulyanovskaya Str. 1, Petrodvorets, St. Petersburg, 198504 Russia

G. C. Tewari · E.-L. Rautama · M. Karppinen
Department of Chemistry, Aalto University, FI-00076 Aalto, Finland

is low (∼8 K) but it can be raised e. g. by applying an external pressure [2, 3]. During the synthesis mixtures of Fe and Se can form various phases: α-FeSe, β-FeSe and γ-FeSe [1, 4]. The composition of the phases obtained and their structures (tetragonal, hexagonal NiAs-type) depend on the selenium content and the temperature of the synthesis [5]. Superconductivity in this compound can exists only in the tetragonal phase below $T_c \approx 8$ K [1, 5].

All phases which FeSe can form show a magnetically ordered structure, except the phase with a tetragonal structure, which at room temperature resides in a paramagnetic state. Upon cooling this material undergoes a tetragonal-to-orthorhombic structural transition at ∼90 K. The temperature of this structural transition depends on the exact stoichiometry of the material. Under an applied hydrostatic pressure a magnetic ordering of non-stoichiometric superconducting $FeSe_{1-x}$ ($x = 0.02 - 0.06$) has been reported [6, 7].

Due to paramagnetism ^{57}Fe Mössbauer spectra of pure FeSe with tetragonal structure consist of a single doublet at room temperature. In $FeSe_{0.82}$ prepared by solid-state reaction by quenching from 650 °C to room temperature an additional paramagnetic doublet in the Mössbauer spectrum was observed [8]. This doublet, characterized by a high quadrupole splitting of ∼1.7 mm/s, was assigned to an impurity phase but its origin was not known. This doublet was also observed by another group and two possible origins of its were discussed but the exact nature of this impurity phase was not determined [9].

The purpose of this work was to prepare and investigate this secondary phase that appears in compounds with a selenium deficiency. Several samples with various concentrations of selenium were synthesized and investigated by Mössbauer spectroscopy. Optimizing the conditions for the secondary phase required some efforts because the exact preparation route was not known from the literature.

2 Experimental

It was found that in our samples the second paramagnetic doublet becomes visible only after a second synthesis step. Two different temperature were used for samples preparation: 650 °C [8, 10] and 750 °C.

Two series of samples with stoichiometries of $FeSe_{0.6}$, $FeSe_{0.75}$, $FeSe_{0.82}$, and $FeSe_{0.9}$ were prepared at 750 °C and investigated. Stoichiometric ratios of iron (99.99 %) and selenium (99.99 %) powders were mixed, sealed in evacuated quartz tubes and annealed at 750 °C for 20 h and quenched into cold water. The obtained samples were denoted series I. Thereafter, a portion of the powders of series I were reground in a mortar, pressed into pellets and sintered again at the same synthesis conditions. After 20 h the samples were quickly taken out of the furnace and quenched into cold water. These samples were denoted series II.

The phase and structure determination were carried out by X-ray powder diffraction (PanAnalytical X'Pert Pro MPD diffractometer). ^{57}Fe Mössbauer spectra were recorded with Doppler velocities of 8.04 mm/s and 2.53 mm/s in transmission geometry in the temperature interval 77−300 K using an Oxford CF506 continuous-flow cryostat and a year-old Cyclotron Co, ^{57}Co:Rh source. The spectra were fitted using the following parameters: line width (Γ) was fixed for all components to be equal excluding the 2^{nd} (M) component (the secondary component which undergoes a magnetic ordering and exhibits a rather broad

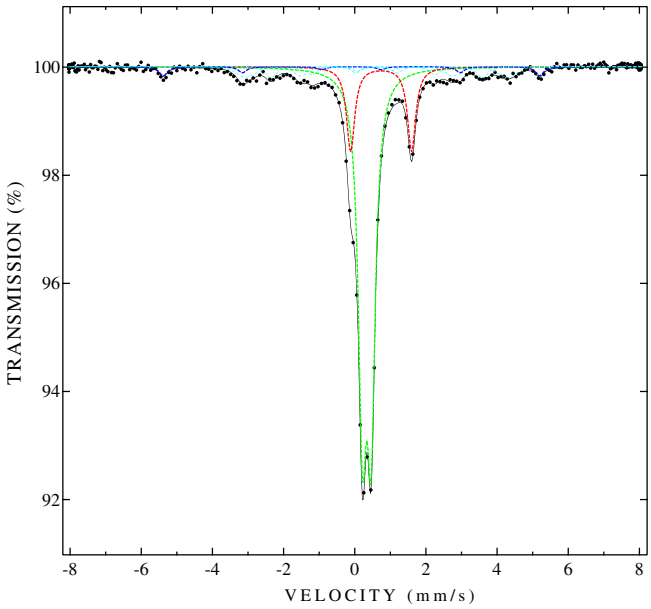

Fig. 1 High-velocity Mössbauer spectrum of the series II $FeSe_{0.9}$ sample recorded at 300 K. Doublets due to the main phase, the secondary phase, and sextets due to elementary iron, and Fe_7Se_8 are drawn in *green*, *red*, *blue*, and *cyan*, respectively

sextet), quadrupole splitting ($QS = eQV_{zz}/2$), isomer shift (δ), component intensities (I), and magnetic hyperfine field (B_{eff}) for magnetically-split components. Isomer shift values are quoted relative to α-Fe at room temperature.

3 Results and discussion

In Fig. 1 a high-velocity Mössbauer spectrum for $FeSe_{0.9}$ of series II is shown. A large portion of a secondary Fe phase is seen with its characteristic large quadrupole splitting. Certain amounts of elementary iron (around 3 % for $FeSe_{0.9}$) were observed. The iron impurity was found in all recorded spectra, most intense in the compound with lowest Se content: 33 % Fe in FeSe0.6 (see Table 1 presented below).

Experimental XRD data for samples $FeSe_{0.6}$ $FeSe_{0.9}$ of series I and II were fitted using the Rietveld method and the program FullProf [11]. The patterns revealed the presence of the FeSe main phase, an unknown Fe-Se phase, Fe_7Se_8 and elementary Fe. The Bragg peaks due to the unknown phase are significantly sharper than the ones coming from the main FeSe phase and the observed Fe_7Se_8 phase. This is a strong indicator that these unidentified reflections are not related to these compositions e.g. in a way of distortion. Despite of a careful and extensive search of the diffraction database, including possible reaction with silica, no match was found for the unaccounted reflections in the XRD pattern. As the heat-treatments clearly increased the intensities of all these unidentified reflections, we suspect that they are coming from one phase. To provide some information of this, we have attempted to find its unit cell by indexing all the reflections that cannot be explained by β-

Table 1 Parameters of the $FeSe_{1-x}$ Mössbauer spectra at RT and around T_m. For the secondary component P denotes paramagnetic and M magnetic

Origin	T, K	Γ, mm/s	δ, mm/s	QS, mm/s	B_{eff}, T	A^1, %	T_m, K
$FeSe_{0.6}$							
FeSe	298	0.276(5)	0.458(5)	0.25(5)	–	42(2)	101
2^{nd} (P)		0.276(5)	0.853(5)	1.69(5)	–	12(2)	
FeSe	102	0.298(5)	0.549(5)	0.29(5)	–	43(2)	
2^{nd} (P)		0.298(5)	0.884(5)	1.61(5)	–	4(2)	
2^{nd} (M)		0.517(9)	0.90(9)	0.19(9)	12.3(7)	10(2)	
FeSe	98	0.311(5)	0.551(5)	0.30(5)	–	42(2)	
2^{nd} (P)		–	–	–	–		
2^{nd} (M)		0.811(7)	0.90(5)	0.08(8)	11.9(9)	13(2)	
$FeSe_{0.75}$							
FeSe	298	0.301(5)	0.495(5)	0.25(5)	–	53(2)	101.5
2^{nd} (P)		0.301(5)	0.886(5)	1.71(5)	–	18(2)	
FeSe	102	0.291(5)	0.555(5)	0.28(5)	–	50(2)	
2^{nd} (P)		0.291(5)	0.982(5)	1.71(5)	–	8(2)	
2^{nd} (M)		0.605(9)	0.812(7)	0.056(9)	10.1(8)	10(2)	
FeSe	101	0.298(5)	0.548(5)	0.29(5)	–	49(2)	
2^{nd} (M)		1.03(9)	0.841(9)	−0.27(7)	9.8(9)	23(2)	
$FeSe_{0.82}$							
FeSe	298	0.361(5)	0.491(5)	0.24(5)	–	64(2)	103
2^{nd} (P)		0.361(5)	0.901(5)	1.72(5)	–	15(2)	
FeSe	104	0.316(5)	0.548(5)	0.29(5)	–	63(2)	
2^{nd} (P)		0.316(5)	0.951(5)	1.80(5)	–	14(2)	
FeSe	102	0.299(5)	0.541(5)	0.291(5)	–	56(2)	
2^{nd} (M)		0.697(8)	0.955(9)	0.12(9)	7.5(9)	17(2)	
$FeSe_{0.9}$							
FeSe	298	0.278(5)	0.445(5)	0.25(5)	–	67(2)	104
2^{nd} (P)		0.278(5)	0.851(5)	1.71(5)	–	17(2)	
FeSe	106	0.291(5)	0.547(5)	0.29(5)	–	63(2)	
2^{nd} (P)		0.291(5)	0.957(5)	1.74(5)	–	18(2)	
FeSe	102	0.290(5)	0.551(5)	0.29(5)	–	63(2)	
2^{nd} (P)		0.290(5)	0.953(5)	1.76(5)	–	6(2)	
2^{nd} (M)		0.688(9)	0.719(9)	0.063(8)	10.7(7)	16(2)	
FeSe	77	0.323(5)	0.554(5)	0.30(5)	–	62(2)	
2^{nd} (M)		0.441(7)	0.935(7)	0.058(9)	16.3(8)	21(2)	

1 Metallic Fe portions of ∼33 %, ∼17 %, ∼12 % and ∼3 % at all indicated temperatures were found for samples with $x = 0.4$, 0.25. 0.18 and 0.1, respectively. Fe_7Se_8 portions of ∼12 %, ∼13 %, ∼16 % and ∼14 % at all indicated temperatures were found for samples with $x = 0.4$, 0.25. 0.18 and 0.1, respectively

FeSe, Fe_7Se_8 and Fe. This was done with the programs integrated in the FullProf software package [11]. A good match was found using an orthorhombic system with lattice parameters a ≈ 8.52 Å, b ≈ 6.96 Å, and c ≈ 4.90 Å(in Pmmm), covering even the tiniest reflections

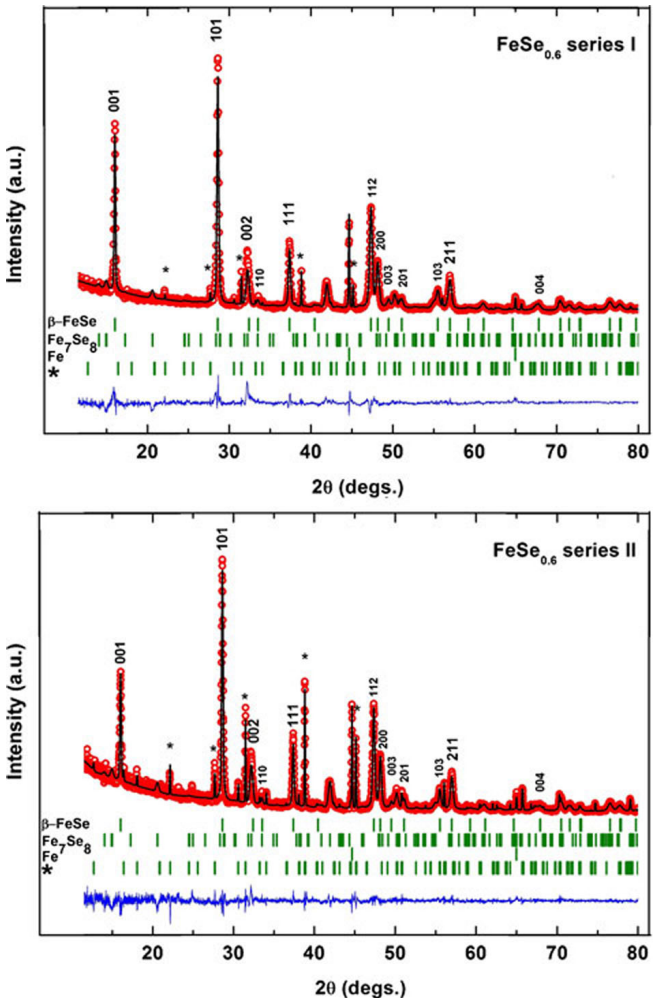

Fig. 2 X-ray powder diffraction patterns for series I and series II $FeSe_{0.6}$ samples. Main peaks of the secondary phase component are denoted by *asterisks*. Indices concern the main β-FeSe phase

left in the XRD pattern. This unit cell is included as a Le Bail fit in the Rietveld refinements shown in Figs. 2 and 3.

Based on the refinements, the ratio of the known components β-FeSe, Fe_7Se_8 and Fe is 9.4:1.4:1 and 3.5:0.8:1 for $FeSe_{0.9}$ and $FeSe_{0.6}$, respectively. The amount of the unknown phase cannot be determined without knowing the crystal structure but by comparing intensities, it can be said that $FeSe_{0.6}$ and $FeSe_{0.9}$ both contain substantial amount of the secondary phase after the second sintering.

These additional XRD peaks were observed also for FeSe single crystals that were grown using the Bridgman method with controlled cooling rate [12], but the phase that gives rise to these peaks was not determined. Upon examining the powder XRD data of the original work [1] it becomes evident that the secondary phase was encountered but left unidentified by the authors.

Mössbauer spectra obtained from samples of series I exhibit only the paramagnetic doublet of the main phase and magnetic Fe_7Se_8 and elementary iron as impurities, with the

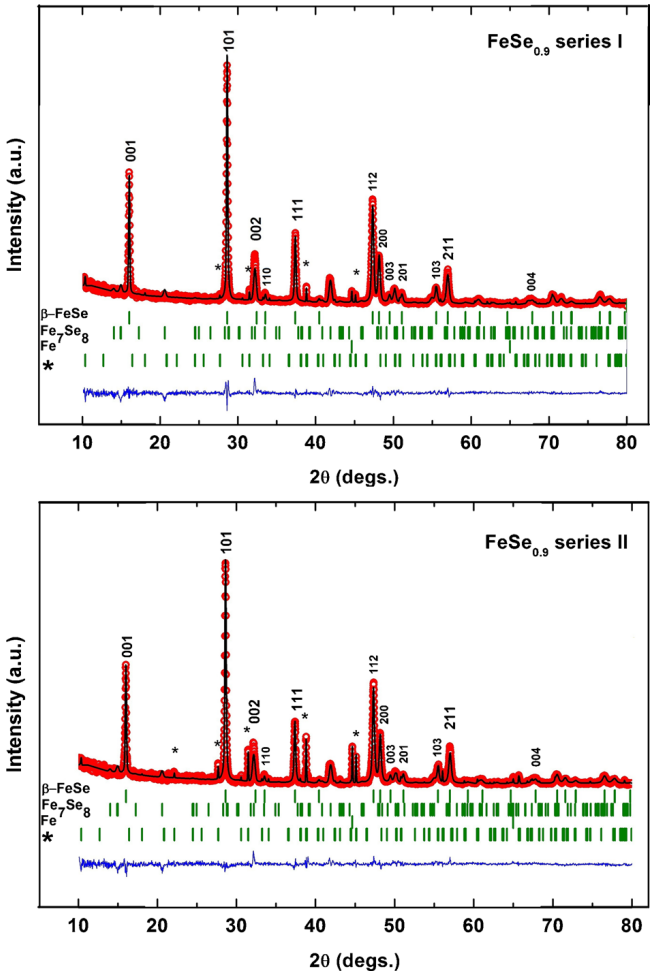

Fig. 3 X-ray powder diffraction patterns for series I and series II $FeSe_{0.9}$ samples. Main peaks of the secondary phase component are denoted by *asterisks*. Indices concern the main β-FeSe phase

secondary FeSe phase barely exceeding the detection limit. The Mössbauer spectra of all investigated samples of series II show the presence of the secondary phase doublet at room temperature, some quantities of Fe_7Se_8 and metallic Fe, Fig. 4. The hyperfine parameters of the main FeSe component and for the secondary phase are given in Table 1. For Fe_7Se_8 literature values of the hyperfine parameters for the corresponding temperatures, quite complex with 3 magnetic subspectra [13], were used. Volume fraction for all components are presented in Table 1.

The main phase has a paramagnetic doublet with $\delta = 0.44$ mm/s and $eQV_{zz}/2 \approx 0.25$ mm/s at room temperature. These parameter values coincide with β-FeSe which has a tetragonal structure and the isomer shift indicates a low-spin state of divalent iron in this material [14]. For the secondary component the isomer shift ($\delta = 0.85$ mm/s) indicates Fe^{2+} in a high-spin state in agreement with earlier data for a similar compound [9]. Presence of interstitial iron a singlet corresponding to trivalent Fe [15] was not observed in the present Mössbauer data. From measurements of Fe(Te,Se) it is known that such Fe species strongly overlap with the percentage main component. Analysis

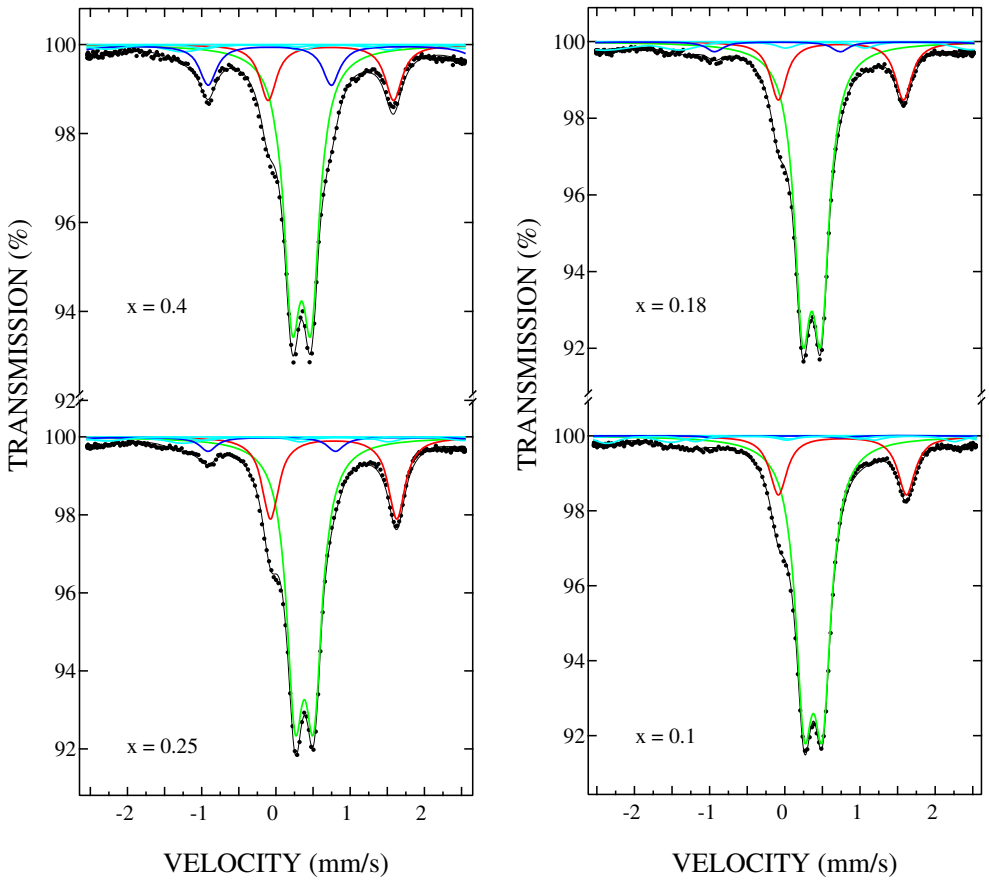

Fig. 4 Mössbauer spectra of $FeSe_{1-x}$ ($x = 0.4, 0.25, 0.18, 0.1$) series II samples at room temperature. *Green*, *blue* and *red lines* indicate the main paramagnetic doublet, elementary iron and secondary phase, respectively. *Lines* (cyan) due to magnetic Fe_7Se_8 are visible in the background

of the XRD data suggests that the possible concentration of interstitial Fe is below a few percents.

The volume fraction of the secondary component depends on the selenium content in the $FeSe_{1-x}$ spectra, Fig. 4. The $FeSe_{0.75}$ compound shows the highest concentration of it, despite the presence of other iron impurities.

The secondary phase undergoes a magnetic transition upon decreasing the temperature. The transition temperature is readily observed in Mössbauer spectra recorded with a temperature step of 0.5 - 1 K, Fig. 5. Similar results were obtained for all investigated samples. For $x = 0.1$ a transition temperature of $\sim$105 K was detected. The transition temperatures for the series II samples are given in Table 1.

From the Mössbauer spectra recorded above and around transition temperature of the secondary phase no changes are observed for the component from the main phase. This also indicates that the main phase and the secondary phase in investigated samples are well separated.

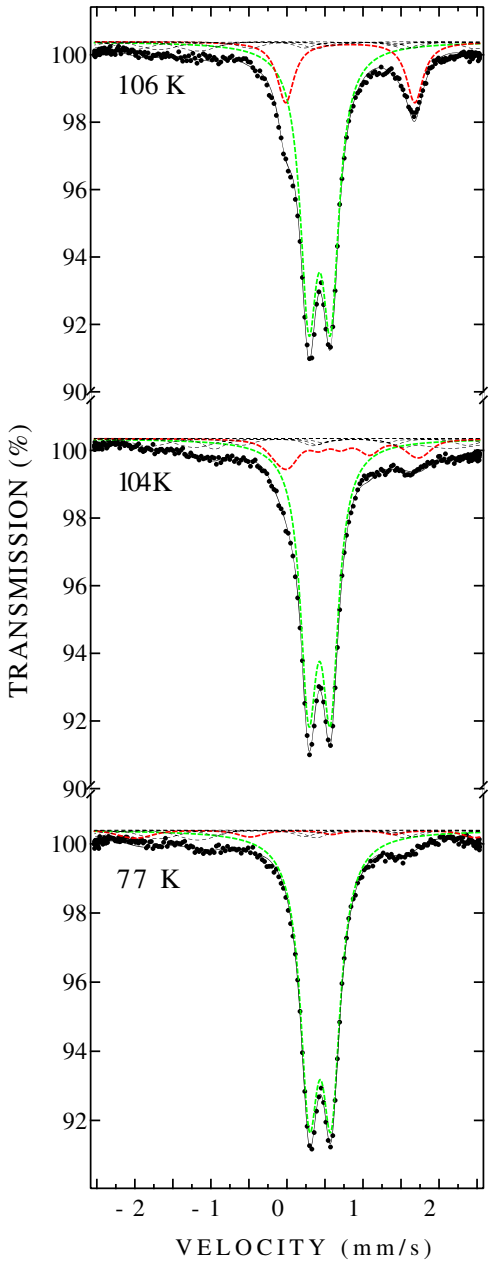

Fig. 5 Mössbauer spectra of the $FeSe_{0.9}$ series II sample recorded at temperatures around the magnetic transition temperature of the secondary phase Fe. *Green* and *red lines* are due to the main phase and secondary phase, respectively. *Weak lines* due to metallic Fe and magnetic Fe_7Se_8 are visible in the background

4 Conclusions

The synthesis conditions for promoting the concentration of a secondary Fe-Se phase in β-FeSe were optimized. A two-step solid-state reaction at 750 °C gives the highest volume fraction of this secondary phase. Mössbauer spectra for all samples obtained by the two step synthesis show the presence of the second paramagnetic doublet with a high quadrupole splitting (∼1.7 mm/s), assigned to the emerging phase. Mössbauer spectra of samples obtained using only one synthesis step did not exhibit the secondary component.

The presence of the secondary phase in the samples after two synthesis was also confirmed by XRD measurements. Secondary phase Fe has valence 2+ and a high-spin state while the main phase Fe atoms are in a divalent low-spin state. The secondary phase Fe atoms undergo a magnetic transition at ∼104 K and the behavior of the Mössbauer spectra recorded at this transition region indicate a spatial separation of the main phase and the secondary phase atoms. Determination of space group and exact stoichiometry of the secondary phase requires further studies.

References

1. Hsu, F.-C., Luo, J.-Y., Yeh, K.-W., Chen, T.-K., Huang, T.-W., Wu, P.M., Lee, Y.-C., Huang, Y.-L., Chu, Y.-Y., Yan, D.-C., Wu, M.-K.: Proc. Natl. Acad. Sci. U.S.A. **105**, 14262 (2008)
2. Imai, T., Ahilan, K., Ning, F.L., McQueen, T.M., Cava, R.J.: PRL **102**, 177005 (2009)
3. Medvedev, S., McQueen, T.M., Troyan, I.A., Palasyuk, T., Eremets, M.I., Cava, R.J., Naghavi, S., Casper, F., Ksenofontov, V., Wortmann, G., Felser, C.: Nat. Mater. **8**, 630 (2009)
4. de Souza, M., Haghighirad, A.-A., Tutsch, U., Assmus, W., Lang, M.: Eur. Phys. J. B **77**, 101 (2010)
5. McQueen, T.M., Huang, Q., Ksenofontov, V., Felser, C., Xu, Q., Zandbergen, H., Hor, Y.S., Allred, J., Williams, A.J., Qu, D., Checkelsky, J., Ong, N.P., Cava, R.J.: Phys. Rev. B **79**, 014522 (2009)
6. Bendele, M., Amato, A., Conder, K., Elender, M., Keller, H., Klauss, H.-H., Luetkens, H., Pomjakushina, E., Raselli, A., Khasanov, R.: PRL **104**, 087003 (2010)
7. Grechnev, G.E., Panfilov, A.S., Desnenko, V.A., Fedorchenko, A.V., Gnatchenko, S.L., Chareev, D.A., Volkova, O.S., Vasiliev, A.N.: J. Phys. Condens. Matter. **25**, 046004 (2013)
8. Libäck, J.-P.: Master's Thesis, Åbo Akademi (2010)
9. Hamdeh, H.H., El-Tabey, M.M., Asmatulu, R., Ho, J.C., Huang, T.W., Yeh, K.W., Wu, M.K.: Eur. Phys. Lett. **89**, 67009 (2010)
10. Pimentel Jr, J.L., Serbena, F.C., Jurelo, A.R.: J. Supercond. Nov. Magn. **24**, 1437 (2011)
11. Rodriquez-Carvajal, J.: Physica B **192**, 55 (1993)
12. Yang, C.-M., Chen, P.-W., Kou, J.-C., Diko, P., Chen, I.-G., Wu, M.-K.: IEEE Trans. Appl. Supercond. **21**, 2845 (2011)
13. Ok, H.N., Lee, S.W.: Phys. Rev. B **8**, 4267 (1973)
14. Lindén, J., Rautama, E.-L., Karppinen, M., Yamauchi, H.: Hyperfine Interact. **208**, 133 (2012)
15. Błachowski, A., Ruebenbauer, K., Zajdel, P., Rodriques, E.E., Green, M.A.: J. Phys. Condens. Matter **24**, 386006 (2012)

PUBL. V

A. Sklyarova, G. C. Tewari, J. Lindén, O. Mustonen, E.-L. Rautama, and M. Karppinen, Mössbauer study of hyperfine interactions in $EuFe_2(As_{1-x}P_x)_2$ and $BaFe_2(As_{1-x}P_x)_2$

J. Magn. Magn. Matter., 378, 327, 2015.

Journal of Magnetism and Magnetic Materials 378 (2015) 327–332

Contents lists available at ScienceDirect

Journal of Magnetism and Magnetic Materials

journal homepage: www.elsevier.com/locate/jmmm

Mössbauer study of hyperfine interactions in $EuFe_2(As_{1-x}P_x)_2$ and $BaFe_2(As_{1-x}P_x)_2$

A. Sklyarova [a,b,c], G.C. Tewari [d,e], J. Lindén [a,*], O. Mustonen [e], E.-L. Rautama [e], M. Karppinen [e]

[a] Department of Physics, Åbo Akademi, FI-20500 Turku, Finland
[b] Lappeenranta University of Technology, Faculty of Physics, Box 20, 53851 Lappeenranta, Finland
[c] St. Petersburg State University, Faculty of Physics, Ulyanovskaya Str. 1, Petrodvorets, St. Petersburg 198504, Russia
[d] Department of Condensed Matter Physics, Weizmann Institute of Science, Rehovot 76100, Israel
[e] Department of Chemistry, Aalto University, FI-00076 Aalto, Finland

ARTICLE INFO

Article history:
Received 15 September 2014
Received in revised form
12 November 2014
Accepted 17 November 2014
Available online 20 November 2014

Keywords:
Pnictide superconductors
Magnetism
Superconductivity
^{57}Fe Mössbauer spectroscopy

ABSTRACT

The magnetic properties of the pnictide superconductors with the nominal composition of $BaFe_2(As_{0.68}P_{0.32})_2$ and $EuFe_2(As_{0.8}P_{0.2})_2$ were studied by ^{57}Fe Mössbauer spectroscopy. A superconducting transition at 30 K was detected and coexistence of magnetism and superconductivity at low temperatures was observed. The Mössbauer spectra show two iron-atom surroundings, which are attributed to undoped AFe_2As_2 and substituted $AFe_2(As_{1-x}P_x)_2$, with at least one phosphorus atom in the tetragonal iron environment, (A = Ba or Eu). These two iron-atom surroundings were attributed to one macroscopic $AFe_2(As_{1-x}P_x)_2$ phase.

1. Introduction

Among iron-based superconducting materials pnictides are most intensively studied due to the variety of physical and chemical properties which these materials have. New pnictide superconductors with various properties are produced using carrier-, hole- or isovalent-doping processes of arsenic in the AFe_2As_2 (A = Ca, Ba, Eu, Sr) parent compound. Two of them are $BaFe_2(As_{1-x}P_x)_2$ and $EuFe_2(As_{1-x}P_x)_2$, the parent materials of which have a layered structure with Ba/Eu atoms between the Fe_2As_2 layers. The properties of these parent compounds are well-known from the literature. Undoped AFe_2As_2 exhibits an anomaly at 140–200 K in the electric resistance, due to a structural phase transition from tetragonal to orthorhombic [1–5]. The structural transition is accompanied by antiferromagnetic, spin-density wave (SDW) transition at the same temperature that was observed by neutron diffraction [4–6]. In substituted pnictides this SDW anomaly shifts to lower temperatures with increasing substitutional-element concentration [7,8]. In Mössbauer spectra the broadening of the spectral lines begins below ~140–200 K and at 77 K a completed magnetic splitting of the main paramagnetic doublet is observed. The value of the hyperfine field is around 5 T [9].

Superconductivity in undoped material can be induced by applying an external pressure. For Ba- or $EuFe_2As_2$ the required external pressure value lies in the range of 20–60 kbar, with a maximum T_c value of ~29 K [10–12]. The most common way to induce superconductivity is hole, electron, and isovalent doping that suppresses the structural and antiferromagnetic transitions and promotes superconductivity [13–19]. In this case the obtained superconducting properties depend on the dopant concentration [7,10,17,19].

By isovalent doping phosphorus atoms are replacing a part of the arsenic atoms. Superconductivity in $AFe_2(As_{1-x}P_x)_2$ appears in the narrow concentration range of x = 0.2–0.6 for A=Ba and x=0.14–0.23 for A= Eu [7,19–23]. The narrowness of the concentration range may be related to the observed overlap of superconductivity and magnetism.

Previously it was thought that the most likely reason for superconductivity arising in these compounds is the chemical pressure due to the difference in radii between dopant and regular atoms, but it has been shown that the presence of a chemical pressure not always leads to superconductivity and the true reason is more complicated [8].

In this paper the hyperfine interactions of $AFe_2(As_{1-x}P_x)_2$ with x = 0.32 for A = Ba and x = 0.20 for A = Eu were examined by

* Corresponding author.
E-mail address: jlinden@abo.fi (J. Lindén).

http://dx.doi.org/10.1016/j.jmmm.2014.11.054
0304-8853/

^{57}Fe Mössbauer spectroscopy. This method is sensitive to the local properties of the investigated nucleus and allows probing of phase composition, magnetic ordering, valence, and spin-state of atoms.

2. Experimental

For the preparation of samples a solid-state reaction method was used. Iron powder (99.99%), barium/europium pieces (99.9%), arsenic pieces (99.999%), and phosphorus powder were directly mixed in stoichiometric ratios and sealed into an evacuated quartz tube. For preventing reactions between barium and the tube wall during the synthesis the mixture of the elements was placed in an alumina crucible, and covered by an another crucible.

The quartz ampule with the Ba-sample mixture was slowly heated up to 600 °C and kept at this temperature for 3 h. After that the temperature was increased and the sample was sintered at 850 °C for 10 h, and slowly cooled to room temperature. The Eu sample was annealed at 1050 °C for 36 h. Both the obtained samples were reground, pressed into pellets, sealed in crucibles in evacuated quartz tubes and sintered again at 950 °C for 25 h. Both the preparation of the mixtures and the grindings were done in a glove box under inert Ar atmosphere.

The superconducting properties were measured using a SQUID magnetometer (Quantum Design, MPMS-XL) in zero-field-cooled (ZFC) and field cool (FC) regimes. The phase contents were checked with X-ray powder diffractometry (PanAnalytical X'pert Pro MPD, Cu $K\alpha 1$ radiation) and the data were analyzed using the software program FullProf [24]. ^{57}Fe Mössbauer spectroscopy was used for the verification of the XRD results and for the investigation of the hyperfine properties.

All Mössbauer measurements were made in transmission geometry with Doppler velocities of 4.50 mm/s and 2.50 mm/s using an approximately one-year old 25 mCi Cyclotron Co. ^{57}Co:Rh source for producing the gamma quanta. Mössbauer spectra were obtained in the temperature range from 6.1 K to 310 K with an Oxford continuous-flow cryostat and coolants of liquid He and liquid N_2 for achieving the temperatures below and above 77 K, respectively.

The recorded spectra were fitted using two components of the paramagnetic main phase and two magnetic components for the impurity. The line intensity, isomer shift, quadrupole splitting, magnetic field and magnetic field distribution were used as fit parameters. Isomer shift values were taken relative to α-Fe at room temperature.

Density functional theory (DFT) calculations of quadrupole splitting were used for the theoretical study of the iron environment influence. Calculations was made with the ORCA 3.0.2 program package [25].

3. Results and discussion

The phase contents in the polycrystalline $BaFe_2(As_{0.68}P_{0.32})_2$ and $EuFe_2(As_{0.8}P_{0.2})_2$ samples were analyzed by XRD and the obtained patterns are presented in Fig. 1.

For both samples the XRD data analysis revealed a tetragonal $ThCr_2Si_2$-type crystal structure ($I4/mmm$) of the main $Ba/EuFe_2(As_{1-x}P_x)_2$ phase and the presence of a preferred orientation along the $00l$ direction. This preferred orientation was taken into account during the fit procedure using the March–Dollase method integrated into the Rietveld program FullProf [24]. The following lattice parameters of the main phase were found: a = 3.928 Å and c=12.824 Å for A=Ba, and a=3.901 Å and c=11.934 Å for A=Eu. Upon comparing obtained unit cell parameters with the ones for undoped samples a shrinkage of the a and c values can be noticed [9]. In the Ba sample, excluding the main phase the presence of two impurities was found. One of them is Fe_2P that is usually included in polycrystalline samples produced by solid-state reaction methods [17,22,26]. Another impurity with a peak close to 2θ=29° was also found. This impurity was observed earlier by another author but it was not possible to determine using the PDF-4 database what phase it is [26,27]. As this impurity does not show up in the ^{57}Fe Mössbauer spectra, it probably does not contain iron. The XRD pattern of Eu sample consists of the main phase and small quantities of the unknown phase.

Superconducting properties were checked using magnetic susceptibility measurements in the temperature range from 4.2 K to RT. Obtained curves show a clear superconductivity transition in the Ba sample: a sharp drop to negative value can be seen in Fig. 2 (a) at 30 K. The Fe_2P magnetic impurity has a ferromagnetic ordering and gives a small positive background on the susceptibility data of curve. This background was subtracted from the data presented in Fig. 2(a). The superconductivity transition of Eu sample is not observed using the SQUID measurements due to the magnetic ordering of the Eu^{2+} atoms at 19 K [18], Fig. 2(b).

The room temperature Mössbauer spectra of the Ba and Eu samples show the presence only of a paramagnetic phase (Fig. 3 (a) and (b) upper panels) with a clear asymmetry of the resonance line. For excluding the texture effect Mössbauer measurements at magic angle were made and only minor changes in the spectra shape were observed, Fig. 3(a) and (b) lower panels.

In measurements below 270 K the $BaFe_2(As_{0.68}P_{0.32})_2$ sample develops magnetic sextets from the Fe_2P impurity proving that it completely overlaps with the paramagnetic main phase at room temperature. Also the literature value for the Curie temperature, $T_C \approx 270$ K [28–30], confirms the assignment of Fe_2P to the sextets. However, despite the splitting of Fe_2P the asymmetry of the main phase remains. The Mössbauer spectra recorded at several selected temperature are shown in Fig. 4.

The literature values of room temperature IS and QS parameters for $Ba/EuFe_2As_2$ and $Ba/EuFe_2P_2$ compounds are IS = 0.31/0.41 mm/s, QS = −0.03/0.07 mm/s, and IS = 0.28/0.28 mm/s, QS = 0.22/0.16 mm/s, respectively [2,9,31–33]. Therefore, at room temperature and above the paramagnetic component of the obtained spectra was fitted using a two component model consisting of an unresolved doublet and a doublet which look very similar to the two extremes of AFe_2As_2 (singlet) and AFe_2P_2 (doublet) phases of $AFe_2(As_{1-x}P_x)_2$ (A = Ba, Eu). The Mössbauer parameters of these paramagnetic components at room temperature are given in Table 1. A similar picture with the presence of two Mössbauer components was already observed recently for the ^{57}Fe Mössbauer study of $EuFe_2(As_{1-x}P_x)_2$ materials [31]. The isomer shift values are compatible with high-spin trivalent iron and low-spin (S = 0) divalent iron. Chemical analysis indicates that Fe is not strongly oxidized, i.e. resides in the +2 oxidation state [34].

At temperatures below ~140 K Mössbauer spectra show a broadening of the central paramagnetic component, that is observed down to the lowest measurement temperature 6.1 K (for Ba sample) and 77 K (for Eu sample), Figs. 4 and 5, respectively. For the fitting procedure of these broad components a magnetic field distribution was added to the fitting parameters for the component, assigned to the AFe_2As_2 surrounding. The spectral shape of the other paramagnetic component remains identical to the room-temperature one. In this temperature region (below 140 K) the parent phase AFe_2As_2 shows a spin-density wave behavior and at 77 K a well resolved magnetic sextet in the Mössbauer spectrum is observed [9,35]. Then, it can be assumed that, as in parent compounds, the unresolved doublet of $Ba/EuFe_2As_2$ in our spectra shows a spin-density wave (SDW) tendency at temperatures below ~140 K although a well-resolved magnetic sextet is not

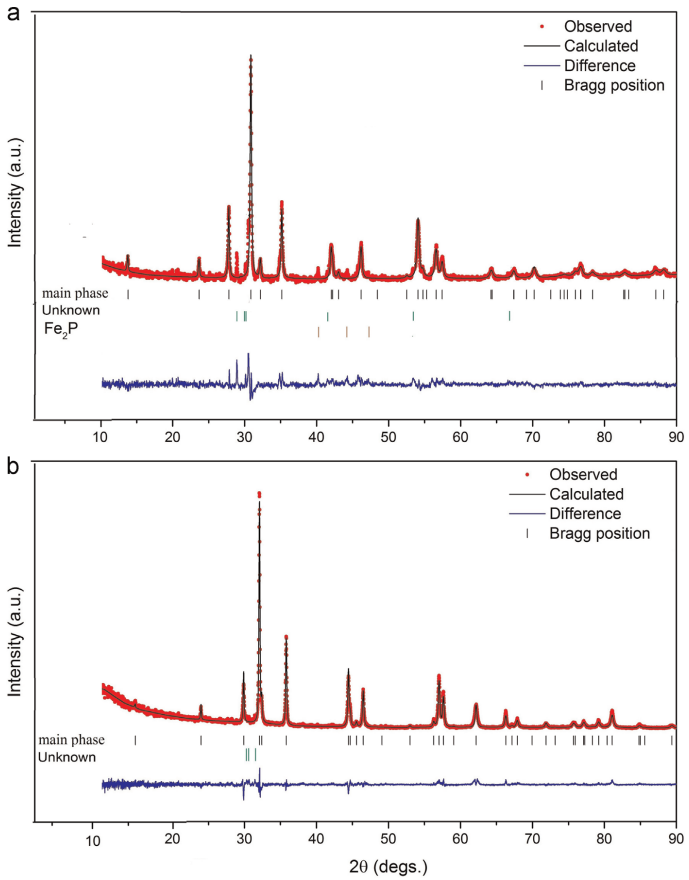

Fig. 1. X-ray powder diffraction pattern for the $BaFe_2(As_{0.68}P_{0.32})_2$ (a) and $EuFe_2(As_{0.8}P_{0.2})_2$ (b) samples. The peaks from Fe_2P and an unknown impurity are indicated.

observed even at very low temperatures. The presence of a SDW in Ba sample is also confirmed by the small deviation from a straight line of the ZFC curve on the magnetic susceptibility picture (see inset in Fig. 2). This deviation remains visible even after removing of the positive background from ferromagnetic Fe_2P. Thus the studied $BaFe_2(As_{0.68}P_{0.32})_2$ as well as $EuFe_2(As_{0.8}P_{0.2})_2$ shows a coexistence between magnetism and superconductivity that is frequently observed for iron-based superconductors [36,37]. Recently a quantum critical point (QCP) at $x \approx 0.3$ was found in the phase diagram of $BaFe_2(As_{1-x}P_x)_2$ [17,38]. The QCP forms a border between two states of superconductivity (SC above QCP) and superconductivity plus SDW (SC+SDW below QCP) [38]. Due to the high (30 K) superconducting T_c value in our Ba-sample and the strong evidence for presence of SDW below T_c, the phosphorus concentration in our Ba sample should be only slightly below 0.3, i.e. on left-hand side of the phase diagram.

The complex Mössbauer spectra obtained at room temperature can be explored by studying the surroundings of the iron atom. In the parent compound AFe_2As_2 (A = Ba, Eu) iron has a tetragonal structure with four neighboring arsenic atoms. During the synthesis process the phosphorus atoms replace arsenic and iron will have from zero to four nearest phosphorus atoms in its surrounding. The number of phosphorus neighbors obviously influences the hyperfine parameters of the iron atoms. XRD is not sensitive to this substitution effect because no long-range ordering between P and As occurs. As Fe_2P orders magnetically below ~270 K, both paramagnetic components can be assumed to belong to the main phase: one of them (with the large quadrupole splitting value) is due to the $AFe_2(As_{1-x}P_x)_2$, and the second (with the small quadrupole splitting value) is due to the pure AFe_2As_2. In AFe_2As_2 one iron atom is tetragonally coordinated by four As nearest neighbors. A calculation using the binomial distribution of phosphorus atoms in substituted compounds indicates that the configurations with 3 As atoms and one P atom (1P3As) (41.16% and 40.96% for the Ba and Eu samples, respectively) and 4 As atoms (4As) (24% and 40.96% for the Ba and Eu samples, respectively) in the iron tetragonal coordination dominate. Environments with more P atoms (2P2As, 3PAs) are lumped together with 1P3As, as they are also expected to exhibit a deformed coordination tetrahedron and hence a non-zero quadrupole splitting. The predictions for component intensities using binomial distribution are given in Table 1. The observed differences between experimental values and binomial prediction may be due to strong overlap between the two paramagnetic components and deviation from a

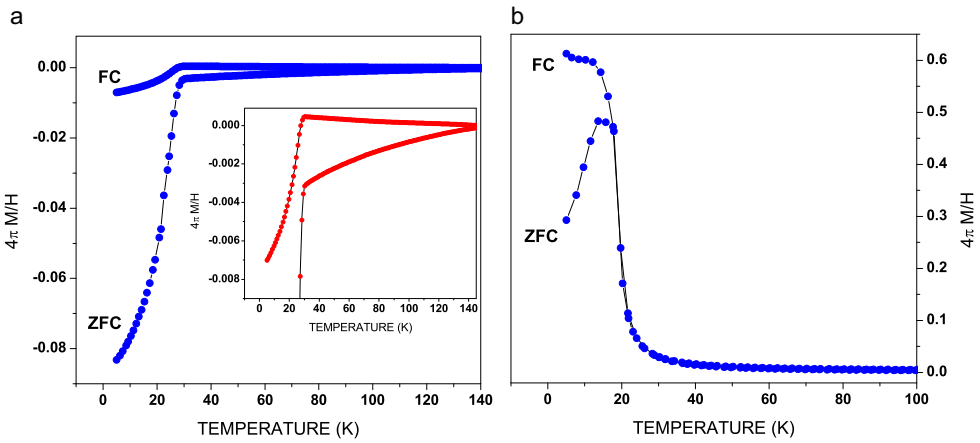

Fig. 2. Magnetic susceptibility vs. temperature for $BaFe_2(As_{0.68}P_{0.32})_2$ (a) and $EuFe_2(As_{0.8}P_{0.2})_2$ (b) obtained in the field-cooling (FC, 10 Oe) and zero-field-cooling (ZFC) regimes of the SQUID measurements. A constant positive ferromagnetic background due to Fe_2P was removed from (a).

true binomial distribution of the environments with more P atoms.

Using DFT calculations estimates for the quadrupole splitting value can be found for the five situations when there are zero, one, two, three or four phosphorus atoms in the tetragonal iron coordination. From one to four phosphorus atoms can replace the positions around iron but these positions are equivalent to each other and it is enough to examine only one of each.

DFT calculations of the quadrupole splitting were made using the ORCA program [25,39]. The quadrupole splitting parameter (ΔE_Q) can be calculated from the electric field gradient (EFG) at the iron nuclei:

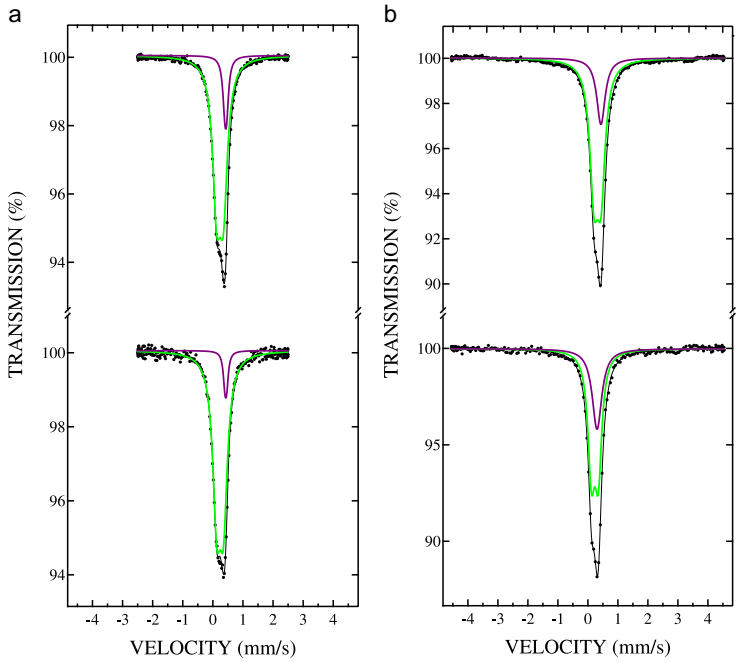

Fig. 3. Room temperature Mössbauer spectra of $EuFe_2(As_{0.8}P_{0.2})_2$ (a) and $BaFe_2(As_{0.68}P_{0.32})_2$ (b) with γ-ray beam parallel to sample normal (upper panels), and in the magic angle (lower panels). Components used in the fit were a paramagnetic doublet (light gray/green online) and an unresolved doublet (dark gray/violet online).

Table 1
Isomer shift and quadrupole splitting values, experimental and calculated (binomial model) values of line intensity of Ba/EuFe$_2$(As$_{1-x}$P$_x$)$_2$ Mössbauer spectra recorded at RT.

	EuFe$_2$(As$_{0.8}$P$_{0.2}$)$_2$		BaFe$_2$(As$_{0.68}$P$_{0.32}$)$_2$	
	1st component	2nd component	1st component	2nd component
IS (mm/s)	0.33	0.56	0.34	0.44
QS (mm/s)	0.119	0.060	0.216	0.003
I(exp) (%)	76	24	79	21
I(binomial) (%)	59	41	76	24
Assignment	1P3As*	4As	1P3As*	4As

* Includes surroundings 2P2As, 3P1As and 4P.

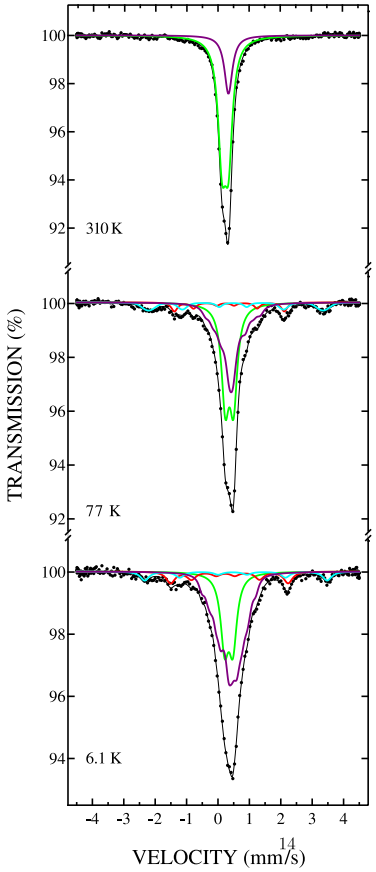

Fig. 4. ^{57}Fe Mössbauer spectra of BaFe$_2$(As$_{0.68}$P$_{0.32}$)$_2$ recorded at 6.1 K, 77 K and 310 K. Components due to the paramagnetic doublet and singlet (light and dark gray/green and violet online, respectively) and the magnetic Fe$_2$P impurity (blue and red online) are indicated.

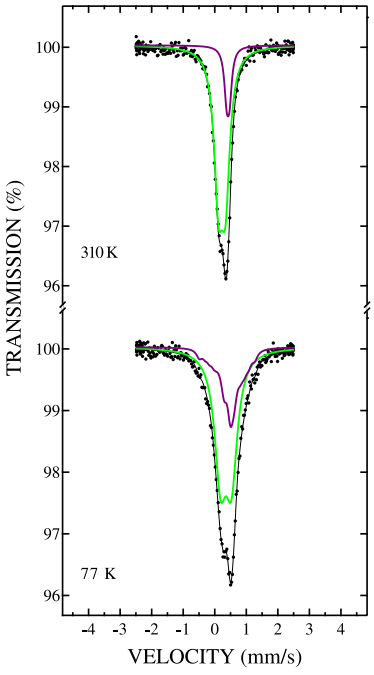

Fig. 5. ^{57}Fe Mössbauer spectra of EuFe$_2$(As$_{0.8}$P$_{0.2}$)$_2$ recorded at 77 K and 310 K. Components due to the paramagnetic doublet and singlet (light and dark gray/green and violet online, respectively) are indicated.

$$\Delta E_Q = \frac{1}{2} eQV_{zz}\sqrt{1+\frac{1}{3}\eta^2}, \tag{1}$$

where V_{xx}, V_{yy} and V_{zz} are the principal components of the EFG tensor, e is the electron charge, Q the nuclear quadrupole moment and η the asymmetry parameter:

$$\eta = \left|\frac{V_{xx}-V_{yy}}{V_{zz}}\right|, \tag{2}$$

where the labeling of the axes is chosen to achieve $|V_{xx}| \le |V_{yy}| \le |V_{zz}|$. The EFG tensor was found from the ground state electron density as an expectation value of the field gradient operator [39].

Calculations were made using the B3LYP hybrid density functional in the NORI approximation with a Gaussian-type basis set TZVP of Ahlrichs for the geometry optimizations with SpecialGrid7 [40]. The isomer shift values of the RT Mössbauer measurement suggest that the calculations should be made in the iron low-spin-state ($S = 0$) approximation. For the calculation of quadrupole interactions on the iron atom the enlarged CP(PPP) basis set was used. The number of iterations was increased to 2000 in the special cases of 1As3P and 1As2P iron environments, which were slow to converge.

Calculations were made using iron, arsenic and phosphorus coordinates which were taken from the room temperature XRD data. The calculated values for the quadrupole splitting are shown in Table 2.

A reasonable agreement between the calculated and experimental data for the quadrupole splitting values of surroundings

Table 2
Calculated (using DFT) and experimental quadrupole splitting values.

Calc. *QS* (mm/s)					Exp. *QS* (mm/s)	
4As	1P3As	2P2As	3P1As	4P	1st comp.*	2nd comp.**
$EuFe_2(As_{0.8}P_{0.2})_2$						
0.077	0.164	0.383	0.723	0.996	0.119	0.060
$BaFe_2(As_{0.68}P_{0.32})_2$						
0.041	0.264	0.207	0.834	0.211	0.216	0.003

* Assigned to 1P3As
** Assigned to 4As.

1P3As and 4As was obtained. Thus, during the substitution process replacement of one arsenic atoms by phosphorus in the tetrahedral iron surrounding seems to be preferred.

4. Conclusions

Polycrystalline $AFe_2(As_{1-x}P_x)_2$ samples with $x = 0.32$ and 0.20 for A = Ba and Eu, respectively, were examined by XRD, SQUID and ^{57}Fe Mössbauer spectroscopy. Two Fe environments giving rise to two ^{57}Fe Mössbauer components were observed and assigned to the pnictide coordinations 4As and 1P3As, respectively. A broadening of the second component down to the 6 K indicates magnetic ordering of iron coordinated by 4As of the main phase. This magnetic ordering coexists with superconductivity below the transition temperature. The coexistence of magnetism and superconductivity suggests that our $BaFe_2(As_{1-x}P_x)_2$ sample is slightly to the left ($x_{QCP} \approx 0.3$) of the recently reported quantum-critical point in this phase.

References

[1] Zhi Ren, Zengwei Zhu, Shuai Jiang, Xiangfan Xu, Qian Tao, Cao Wang, Chunmu Feng, Guanghan Cao, Zhuan Xu, Phys. Rev. B 78 (2008) 052501.
[2] Shugo Ikeda, Kazuki Yoshida, Hisao Kobayashi, J. Phys. Soc. Jpn. 81 (2012) 033703.
[3] A. Błachowski, K. Ruebenbauer, J. Żukrowski, K. Rogacki, Z. Bukowski, J. Karpinski, Phys. Rev. B 83 (2011) 134410.
[4] Q. Huang, Y. Qiu, Wei Bao, M.A. Green, J.W. Lynn, Y.C. Gasparovic, T. Wu, G. Wu, X.H. Chen, Phys. Rev. Lett. 101 (2008) 257003.
[5] M. Kofu, Y. Qiu, Wei Bao, S.-H. Lee, S. Chang, T. Wu, G. Wu, X.H. Chen, New J. Phys. 11 (2009) 055001.
[6] Stephen D. Wilson, Z. Yamani, C.R. Rotundu, B. Freelon, E. Bourret-Courchesne, R.J. Birgeneau, Phys. Rev. B 79 (2009) 184519.
[7] G. Wu, R.H. Liu, H. Chen, Y.J. Yan, T. Wu, Y.L. Xie, J.J. Ying, X.F. Wang, D.F. Fang, X.H. Chen, Europhys. Lett. 84 (2008) 27010.
[8] Marianne Rotter, Christine Hieke, Dirk Johrendt, Phys. Rev. B 82 (2010) 014513.
[9] Marianne Rotter, Marcus Tegel, Dirk Johrendt, Inga Schellenberg, Wilfried Hermes, Rainer Pöttgen, Phys. Rev. B 78 (2008) 020503.
[10] Johnpierre Paglione, Richard L. Greene, Nat. Phys. 6 (2010) 645.
[11] Patricia L. Alireza, Y.T. ChrisKo, Jack Gillett, Chiara M. Petrone, Jacqueline M. Cole, Gilbert G. Lonzarich, Suchitra E. Sebastian, J. Phys.: Condens. Matter 21 (2009) 012208.
[12] C.F. Miclea, M. Nicklas, H.S. Jeevan, D. Kasinathan, Z. Hossain, H. Rosner, P. Gegenwart, C. Geibel, F. Steglich, Phys. Rev. B 79 (2009) 212509.
[13] Dirk Johrendt, Rainer Pöttgen, Physica C 469 (2009) 332.
[14] P.C. Canfield, S.L. Budko, Ni Ni, J.Q. Yan, A. Kracher, Phys. Rev. B 80 (2009) 060501.
[15] C. Lester, Jiun-Haw Chu, J.G. Analytis, S.C. Capelli, A.S. Erickson, C.L. Condron, M.F. Toney, I.R. Fisher, S.M. Hayden, Phys. Rev. B 79 (2009) 144523.
[16] S.R. Saha, T. Drye, K. Kirshenbaum, N.P. Butch, P.Y. Zavalij, Johnpierre Paglione, J. Phys.: Condens. Matter 22 (2010) 072204.
[17] Shuai Jiang, Hui Xing, Guofang Xuan, Cao Wang, Zhi Ren, Chunmu Feng, Jianhui Dai, Zhu'an Xu, Guanghan Cao, J. Phys.: Condens. Matter 21 (2009) 382203.
[18] Zhi Ren, Qian Tao, Shuai Jiang, Chunmu Feng, Cao Wang, Jianhui Dai, Guanghan Cao, Zhuan Xu, Phys. Rev. Lett. 102 (2009) 137002.
[19] David Mandrus, Athena S. Sefat, Michael A. McGuire, Brian C. Sales, Chem. Mater. 22 (2010) 715.
[20] Y. Tokiwa, S.-h. Hübner, O. Beck, H.S. Jeevan, P. Gegenwart, Phys. Rev. B 86 (2012) 220505.
[21] H.S. Jeevan, Deepa Kasinathan, Helge Rosner, Philipp Gegenwart, Phys. Rev. B 83 (2011) 054511.
[22] Guanghan Cao, Shenggao Xu, Zhi Ren, Shuai Jiang, Chunmu Feng, Zhu'an Xu, J. Phys.: Condens. Matter 23 (2011) 464204.
[23] Tetsuya Iye, Yusuke Nakai, Shunsaku Kitagawa, Kenji Ishida, Shigeru Kasahara, Takasada Shibauchi, Yuji Matsuda, Takahito Terashima, J. Phys. Soc. Jpn. 81 (2012) 033701.
[24] J. Rodriquez-Carvajal, Physica B 192 (1993) 55.
[25] F. Neese, Comput. Mol. Sci. 2 (2012) 73.
[26] Veronika Zinth, Dirk Johrendt, Europhys. Lett. 98 (2012) 57010.
[27] Marianne Martin geb. Rotter, Dissertation zur Erlangung des Doktorgrades der Fakultät für Chemie und Pharmazie der Ludwig-Maximilians-Universität München, 2010.
[28] Robert E. Bailey, James F. Duncan, Inorg. Chem. 8 (1967) 1444.
[29] Kiyoo Sato, Kengo Adachi, Eiichi Ando, J. Phys. Soc. Jpn. 26 (1969) 855.
[30] T. Ericsson, L. Häggstrom, R. Wäppling, T. Methasiri, Phys. Scr. 21 (1980) 212.
[31] I. Nowik, I. Felner, Z. Ren, G.H. Cao, Z.A. Xu, J. Phys.: Condens. Matter 23 (2011) 065701.
[32] Chunmu Feng, Zhi Ren, Shenggao Xu, Shuai Jiang, Zhu'an Xu, Guanghan Cao, I. Nowik, I. Felner, Kazuyuki Matsubayashi, Yoshiya Uwatoko, Phys. Rev. B 82 (2010) 094426.
[33] H. Raffius, E. Mörsen, B.D. Mosel, W. Müller-Warmuth, T. Hilbich, M. Reehuis, T. Vomhof, W. Jeitschko, J. Phys. Chem. Solids 52 (1991) 787.
[34] N.N. Greenwood, T.C. Gibb, Mössbauer Spectroscopy, Chapman and Hall Ltd, London, 1971.
[35] Airat Khasanov, Jianyi Jiang, Eric E. Hellstrom, Amar Nath, J. Phys.: Condens. Matter 23 (2011) 342201.
[36] A. Sklyarova, G.C. Tewari, J. Lindén, H. Yamauchi, M. Karppinen, Hyperfine Interactions 221 (2013) 15.
[37] A. Sklyarova, J. Lindén, E.-L. Rautama, M. Karppinen, J. Magn. Magn. Mater. 357 (2014) 82.
[38] T. Shibauchi, A. Carrington, Y. Matsuda, Annu. Rev. Condens. Matter Phys. 5 (2014) 113.
[39] F. Neese, Coord. Chem. Rev. 253 (2009) 526.
[40] A. Schäfer, C. Huber, R. Ahlrichs, J. Chem. Phys. 100 (1994) 5829.

ACTA UNIVERSITATIS LAPPEENRANTAENSIS

590. RUSKOVAARA, ELENA. Entrepreneurship education in basic and upper secondary education – measurement and empirical evidence. 2014. Diss.

591. IKÄHEIMONEN, TUULI. The board of directors as a part of family business governance – multilevel participation and board development. 2014. Diss.

592. HAJIALI, ZUNED. Computational modeling of stented coronary arteries. 2014. Diss.

593. UUSITALO, VILLE. Potential for greenhouse gas emission reductions by using biomethane as road transportation fuel. 2014. Diss.

594. HAVUKAINEN, JOUNI. Biogas production in regional biodegradable waste treatment – possibilities for improving energy performance and reducing GHG emissions. 2014. Diss.

595. HEIKKINEN, JANNE. Vibrations in rotating machinery arising from minor imperfections in component geometries. 2014. Diss.

596. GHALAMCHI, BEHNAM. Dynamic analysis model of spherical roller bearings with defects. 2014. Diss.

597. POLIKARPOVA, MARIIA.Liquid cooling solutions for rotating permanent magnet synchronous machines. 2014. Diss.

598. CHAUDHARI, ASHVINKUMAR. Large-eddy simulation of wind flows over complex terrains for wind energy applications. 2014. Diss.

599. PURHONEN, MIKKO. Minimizing circulating current in parallel-connected photovoltaic inverters. 2014. Diss.

600. SAUKKONEN, ESA. Effects of the partial removal of wood hemicelluloses on the properties of kraft pulp. 2014. Diss.

601. GUDARZI, DAVOOD. Catalytic direct synthesis of hydrogen peroxide in a novel microstructured reactor. 2014. Diss.

602. VALKEAPÄÄ, ANTTI. Development of finite elements for analysis of biomechanical structures using flexible multibody formulations. 2014. Diss.

603. SSEBUGERE, PATRICK. Persistent organic pollutants in sediments and fish from Lake Victoria, East Africa. 2014. Diss.

604. STOKLASA, JAN. Linguistic models for decision support. 2014. Diss.

605. VEPSÄLÄINEN, ARI. Heterogenous mass transfer in fluidized beds by computational fluid dynamics. 2014. Diss.

606. JUVONEN, PASI. Learning information technology business in a changing industry landscape. The case of introducing team entreneurship in renewing bachelor education in information technology in a university of applied sciences. 2014. Diss.

607. MÄKIMATTILA, MARTTI. Organizing for systemic innovations – research on knowledge, interaction and organizational interdependencies. 2014. Diss.

608. HÄMÄLÄINEN, KIMMO. Improving the usability of extruded wood-plastic composites by using modification technology. 2014. Diss.

609. PIRTTILÄ, MIIA. The cycle times of working capital: financial value chain analysis method. 2014. Diss.

610. SUIKKANEN, HEIKKI. Application and development of numerical methods for the modelling of innovative gas cooled fission reactors. 2014. Diss.

611. LI, MING. Stiffness based trajectory planning and feedforward based vibration suppression control of parallel robot machines. 2014. Diss.

612. KOKKONEN, KIRSI. From entrepreneurial opportunities to successful business networks – evidence from bioenergy. 2014. Diss.

613. MAIJANEN-KYLÄHEIKO, PÄIVI. Pursuit of change versus organizational inertia: a study on strategic renewal in the Finnish broadcasting company. 2014. Diss.

614. MBALAWATA, ISAMBI SAILON. Adaptive Markov chain Monte Carlo and Bayesian filtering for state space models. 2014. Diss.

615. UUSITALO, ANTTI. Working fluid selection and design of small-scale waste heat recovery systems based on organic rankine cycles. 2014. Diss.

616. METSO, SARI. A multimethod examination of contributors to successful on-the-job learning of vocational students. 2014. Diss.

617. SIITONEN, JANI. Advanced analysis and design methods for preparative chromatographic separation processes. 2014. Diss.

618. VIHAVAINEN, JUHANI. VVER-440 thermal hydraulics as computer code validation challenge. 2014. Diss.

619. AHONEN, PASI. Between memory and strategy: media discourse analysis of an industrial shutdown. 2014. Diss.

620. MWANGA, GASPER GODSON. Mathematical modeling and optimal control of malaria. 2014. Diss.

621. PELTOLA, PETTERI. Analysis and modelling of chemical looping combustion process with and without oxygen uncoupling. 2014. Diss.

622. NISKANEN, VILLE. Radio-frequency-based measurement methods for bearing current analysis in induction motors. 2014. Diss.

623. HYVÄRINEN, MARKO. Ultraviolet light protection and weathering properties of wood-polypropylene composites. 2014. Diss.

624. RANTANEN, NOORA. The family as a collective owner – identifying performance factors in listed companies. 2014. Diss.

625. VÄNSKÄ, MIKKO. Defining the keyhole modes – the effects on the molten pool behavior and the weld geometry in high power laser welding of stainless steels. 2014. Diss.

626. KORPELA, KARI. Value of information logistics integration in digital business ecosystem. 2014. Diss.

627. GRUDINSCHI, DANIELA. Strategic management of value networks: how to create value in cross-sector collaboration and partnerships. 2014. Diss.